
TRIPLY EXCITED STATES

Correlations in lithium and lithiumlike ions

Lars Bojer Madsen

Department of Physics and Astronomy
University of Aarhus



2003

Knud Taulbjerg - in memoriam

Contents

Preface	v
Acknowledgements	vii
1 Introduction	1
1.1 Brief overview of two-electron atoms	1
1.2 A few central questions	2
2 Resonance parameters	5
3 Experimental results on triply excited states in lithium	9
3.1 Collision or photon excitation	9
3.2 Experiments with collisional excitation	10
3.3 Experiments with photon excitation	12
3.3.1 Photoabsorption experiment	12
3.3.2 Photoion experiments	14
3.3.3 Photoelectron experiments	16
3.4 Parameters for the $\text{Li}(2s2s2p^2P^o)$ resonance	24
4 Theoretical <i>ab initio</i> methods for triply excited lithium	27
4.1 <i>R</i> -matrix calculations	28
4.1.1 <i>R</i> -matrix theory for photoionization	28
4.1.2 <i>R</i> -matrix calculations on triply excited lithium	30
4.2 Saddle-point technique	36
4.2.1 Saddle-point technique: theory	36
4.2.2 Saddle-point technique and complex scaling	38
4.2.3 Saddle-point technique: results on triply excited lithium .	39
4.3 Truncated diagonalization method	41
4.3.1 Truncated diagonalization method: theory	42
4.3.2 Truncated diagonalization method: results	43
4.4 <i>B</i> -splines approach for calculating triply excited states in lithium	43
4.4.1 <i>B</i> -splines approach: theory	44
4.4.2 <i>B</i> -splines: triply excited Rydberg states	46
4.4.3 <i>B</i> -splines and complex rotation	49

4.4.4	<i>B</i> -splines: laser-induced coupling between triply excited states	50
4.4.5	<i>B</i> -splines: partial widths and line shapes in photoexcitation of triply excited states	53
4.5	Analysis of triply excited states in hyperspherical coordinates . .	57
4.5.1	The hyperspherical method	57
4.5.2	Results with the hyperspherical method	59
5	Theoretical models for triply excited lithium	63
5.1	Three-electron ionization ladder	64
5.2	Normal mode analysis of triply excited states	64
5.3	Symmetric rotor model	69
5.3.1	Construction of the symmetric rotor states	70
5.3.2	Classification scheme and configuration mixing	73
5.3.3	Distribution over <i>l</i> quantum numbers	75
5.3.4	Rotational structure in the spectrum of triply excited states?	78
6	Conclusions and outlook	81
7	Dansk resumé	83
	Bibliography	87

Preface

The present dissertation reviews recent work on electron-electron correlations in multiply excited states. In particular it accounts for and puts a perspective on my own work on triply excited states in lithium and lithiumlike atoms.

My research on this topic was initiated during my postdoc period (1998-2000) in the group of Prof. Lambropoulos at the Max Planck Institute for Quantum Optics in Garching by Munich, and continued after my return to the Department of Physics and Astronomy, University of Aarhus.

In the present work I will review experimental results but I will mainly focus on theory. The discussion of the latter will deal with (i) calculational methods and (ii) models for the characterization and understanding of triply excited states. As a computational method the B -splines approach in combination with complex scaling is presented in some detail. This method is very attractive for the calculation of energy positions and total decay widths of resonance states, and its effectiveness will be illustrated by my own calculations on laser-induced transitions between triply excited states.

With respect to the point (ii) above, the characterization in terms of molecular normal modes will be discussed, and a semi-analytical model will be presented which is based on the assumption that the three electrons are arranged in an equilateral triangle with the coplanar nucleus in the centre. These points of view contribute significantly to an improved physical understanding of the electron-electron correlations in three-electron systems. Also a model is introduced for the decay of triply excited Rydberg states.

The points (i) and (ii) supplement each other and illustrate how quantitative calculations may lead to improved qualitative models. Models which, once justified through detailed and critical comparisons with experimental data or *ab initio* calculations, may be used as guidance for the exploration of new regimes of parameter space, and to understand physics in terms of simple pictures.

In connection with my work on electron-electron correlations, the following papers have been published or are about to be published, and they form part of this dissertation. In particular large parts of the present work are contained in the review, paper 13.

1. L. B. Madsen, P. Schlagheck, and P. Lambropoulos,
Laser-Induced Transitions between Triply Excited Hollow States,

- Phys. Rev. Lett. **85**, 42 (2000).
2. L. B. Madsen, P. Schlagheck, and P. Lambropoulos,
Laser-induced transitions between triply excited hollow states,
Phys. Rev. A **62**, 062719 (2000).
 3. L. B. Madsen and P. Lambropoulos,
Line shapes in photoexcitation of triply excited hollow states,
J. Phys. B: At. Mol. Opt. Phys. **34**, 1855 (2001).
 4. L. B. Madsen,
Triply excited Rydberg series and their doubly excited limits in hollow lithium,
J. Phys. B: At. Mol. Opt. Phys. **34**, 2137 (2001).
 5. L. B. Madsen and K. Mølmer,
Correlated Electrons in Lithiumlike Atoms,
Phys. Rev. Lett. **87**, 133002 (2001).
 6. L. B. Madsen and K. Mølmer,
Rotational structure in multiply excited atoms,
Phys. Rev. A **64**, 060501(R) (2001).
 7. P. Lambropoulos, L. A. A. Nikolopoulos, L. B. Madsen and M. G. Makris,
Two- and three-electron atoms in strong laser fields,
in “Super-Intense Laser-Atom Physics” 153 (2001), eds. B. Piraux and K. Rzazewski.
 8. L. B. Madsen and K. Mølmer,
Symmetric rotor of lithiumlike hollow atoms,
Phys. Rev. A **65**, 0225006 (2002).
 9. L. A. A. Nikolopoulos and L. B. Madsen,
Complex-scaled Hartree-Fock wave functions for the frozen core: : A B splines approach,
Comput. Phys. Commun. **151**, 47 (2003).
 10. V. V. Petrunin, M. H. Jacobsen, L. B. Madsen, S. A. Aseyev, and T. Andersen,
Photodetachment of He^- in the vicinity of the two-electron escape threshold,
Phys. Rev. Lett. **90**, 013002 (2003).
 11. L. B. Madsen and K. Mølmer,
Triply excited symmetric rotor states: l distributions,
J. Phys. B: At. Mol. Opt. Phys. **36**, 769 (2003).
 12. L. B. Madsen,
Correlated electrons in multiply excited states at and below threshold,
Physica scripta. To be published.

13. L. B. Madsen,
Triply excited states: electron-electron correlations in lithium,
J. Phys. B: At. Mol. Opt. Phys. (Topical Review) **36**, R223 (2003).

Acknowledgements

Discussions with P. Lambropoulos, K. Mølmer, L. Nikolopoulos, P. Schlagheck, and E. Horsdal-Pedersen are gratefully acknowledged. I thank Grete Flarup for her timely and thorough copy-editing of parts of the manuscript. This work was supported by the Danish Natural Science Research Council (grant no 51-00-0569 and grant no 21-03-0163).

Chapter I

Introduction

1.1 Brief overview of two-electron atoms

For historical and conceptual reasons, it is appropriate to start the presentation with a sketch of the development in the understanding of two-electron atoms. The three-body Coulomb problem as manifested by the correlated motion of two electrons around the atomic nucleus has been at the heart of atomic physics studies ever since the early days of quantum mechanics. Thus, it has played a major role in the development of new theories; not only for electronic ground state properties but also for the treatment of singly and multiply excited states, and the development of the modern quantum mechanical theory (Heisenberg, 1925; Schrödinger, 1926) was to a great extent driven by the failure of the quantum theory by Bohr (1913) to predict the correct ground state energy of helium. Modern quantum theory, however, also faces the problem that the Schrödinger equation cannot be solved in an analytical form for atoms containing more than one electron. Therefore approximate methods for the calculation of atomic spectra are important and already Fock (1930) proposed the 'self-consistent field method', where each electron is considered to be in motion in the self-consistent mean-field generated by the nucleus and all the other electrons. Hartree (1928) had proposed a similar method, but did not include the exchange interaction between the electrons.

The Hartree-Fock theory has been extremely effective for the calculation of the ground state and single-electron excitation part of the spectrum but when atomic states with multiply excited electrons are considered, the electron-electron correlations become increasingly important, and the conventional computational methods do not apply. In fact, one of the main reasons why the atomic physics community is still concerned with the three-body Coulomb problem is that doubly excited states give rise to anomalies in the continuum above the first ionization threshold which cannot be explained in the single-particle Hartree-Fock picture. One of the first key experiments illustrating this feature was due to Madden and Codling (1963) who reported results on photoabsorption in helium to states of $^1P^o$ symmetry below the $\text{He}^+(N = 2)$ threshold,

where N is the principal quantum number. Here the meaning of the symbol $^1P^o$ is $^{2S+1}L^\pi$ with S the total spin, L the total angular momentum, and π the parity of the state. The experiment showed two important things. Firstly, it provided clear evidence of structures in the continuum. These features were associated with doubly excited autoionizing resonance states whose line shape was described by the theory of Fano (1961). For each doubly excited state with configurations of the type, say, $2s2p$ there will always be a degenerate continuum state, $1s\epsilon p$ in the present case. The electron-electron interaction couples these two states and the doubly excited state decays by autoionization. The line shape of the excitation cross-section in the vicinity of resonance depends explicitly on the interplay between the direct coupling to the continuum and the coupling to the continuum via the resonance.

Secondly, the experiment of Madden and Codling showed that the electron-electron correlations in a doubly excited state render impossible a classification in terms of a single electron configuration. For example, in the single-configuration picture one would, due to the degeneracy of the $2s$ and $2p$ levels in the positive helium ion, expect the presence of two separate series of autoionizing resonances converging to the $\text{He}^+(N=2)$ threshold, namely the $|2snp; ^1P^o\rangle$ and $|2pns; ^1P^o\rangle$ series. In the experiment, however, only a single series was observed. In their analysis of the Madden and Codling experiment, Cooper et al. (1963) pointed out that the $|2snp\rangle$ and $|2pns\rangle$ configurations become so strongly mixed that the physical eigenstates are more closely described by the symmetric or antisymmetric linear combinations $(|2snp\rangle \pm |2pns\rangle)/\sqrt{2}$.

The Madden and Codling (1963) experiment and the accompanying theoretical discussions of Fano and co-workers (Fano, 1961; Cooper et al., 1963; Fano and Cooper, 1965) triggered the interest of theoreticians and mark the birth of more than 40 years of intense investigations of electron correlations in multiply excited states. In general, the theoretical studies aimed at precise *ab initio* calculations of the states of interests, but also focused on the question of how to understand and classify the multiply excited states. In this connection the Schrödinger equation has been solved in a variety of refined basis-sets (see, for example, the review by Bachau et al. (2001) and references therein). Also hyperspherical coordinates have been considered (Macek, 1968) as well as the molecular adiabatic approach (Feagin and Briggs, 1986, 1988). Furthermore group theoretical methods (see, for example, the reviews by Rau (1990) and by Herrick (1983)) have been developed and an understanding in terms of approximate quantum numbers associated with the angular and radial correlations has emerged (Lin, 1984, 1986).

For more discussions on helium including semiclassical quantization, the reader is referred to the recent review by Tanner et al. (2000).

1.2 A few central questions

The topic of this work is not the two- but the three-electron atom with lithium as the generic example. We choose to study lithium in detail because it is

the fundamental four-body Coulomb problem, and in a triply excited state, the three electrons move in a highly correlated manner which provides the possibility to test in detail theoretical approximations aiming at a precise description of three-electron dynamics.

It is clear that the two- and the three-electron problems are related. If we look at atomic spectra below the second ionization threshold, a three-electron atom essentially behaves like a two-electron atom, and it can, consequently, be effectively described by the methods developed for the latter systems. It is only as we cross the second ionization threshold that a new regime is encountered. In this spectral region there is the possibility of triply excited states with the inner orbitals all empty, and the three electrons moving around at relatively large distances from the nucleus, that is the configurations are described as $nl n' l' n'' l''$ with n , n' and n'' larger than or equal to two. Such states are referred to as *hollow* states. For these states new decay channels open up. Besides the normal decay modes of autoionization into a state in the ion under the escape of an electron ($1sn'l'e l''$), additionally, a triply excited state will at some point be located above a doubly excited state in the singly charged target ion. Now the decay may occur to such a doubly excited state, which may further decay by autoionization to a state in the doubly charged ion. Of course, also the possibility of radiative decays will be present, but these channels are weak for the lighter (low nuclear charge) systems we shall be concerned with here. Exceptions do occur when the states considered are metastable against autoionization. The $2p2p2p\ ^4S^o$ resonance is one such example which we shall discuss in section 3.2.

Going from the two- to the three-electron problem immediately brings up a series of questions.

1. Is there anything new to be learned about electron-electron correlations if the number of electrons is increased?
2. How does the presence of new decay channels affect the dynamics?
3. Are the methods and concepts developed for two-electron atoms applicable to the three-electron problem?

The answers to these questions (and more) will be discussed in detail in the present work. It should be stressed that the answer to the first, and in a sense the most critical question, is yes - there are things to be learned. Obviously it is interesting in its own right to uncover new layers of the structure of atoms, but it will become clear that the physical pictures developed in the discussion of electron-electron correlations provide a new perspective. For recent reviews on the three-electron problem the reader is referred to the works by Wuilleumier (2000) and Kennedy (2001).

Figure 1.1 summarizes the energy level structure in Li, Li^+ and Li^{++} . In Li we see the triply excited hollow states. These decay to states in Li^+ , and Li^{++} . If the energy of the triply excited state is high enough, the decay may occur

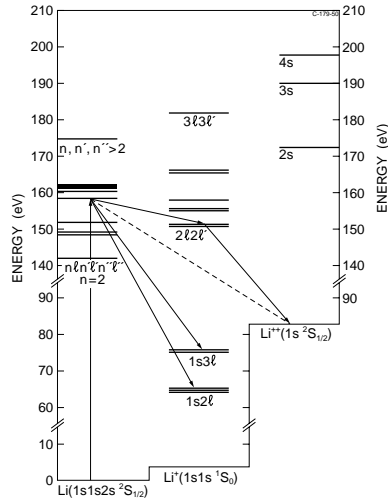


Figure 1.1: Energy level scheme in Li, Li^+ and Li^{++} . Adopted from Wuilleumier et al. (1998).

through a doubly excited state in the Li^+ ion. We shall return to the energy level scheme in subsequent sections.

Although the interaction between highly-charged ions and surfaces will not be discussed in this work, it should be mentioned that hollow states play a key role in the study of such processes (see, for example, the review by Winter and Aumayr (1999)).

Atomic units (au) with $\hbar = m_e = e = 1$ will be used throughout this work unless indicated otherwise.

Chapter II

Resonance parameters

In the discussion of triply excited resonance states, the resonance parameters which are the energy position E_0 and the width Γ of the resonance will be of central importance. Frequently we shall also meet the asymmetry parameter q (Fano, 1961) in the discussion of the shape of the photoexcitation cross-section close to a resonance.

In this chapter we outline a description of photoexcitation from a bound state to the energy range of a single non-degenerate discrete state embedded in a single continuum. This will allow us to introduce q in a simple manner. The present approach is similar to that described by Lambropoulos and Zoller (1981), although in that work the problem was studied within the resolvent operator method. A generalization of the present formalism to the situation of one discrete state embedded in multiple continua was recently presented by Madsen and Lambropoulos (2001) in connection with a detailed study of line shapes in the photoexcitation to triply excited states.

Let $|g\rangle$ denote the ground state, $|a\rangle$ the discrete part of the autoionizing state, and $|E\rangle$ the corresponding continuum. These states are assumed to satisfy $H_0|g\rangle = E_g|g\rangle$, $H_0|a\rangle = E_a|a\rangle$, and $H_0|E\rangle = E|E\rangle$, where H_0 is part of the atomic Hamiltonian $H_a = H_0 + V$, with V the configuration interaction which mixes a configuration belonging to the discrete spectrum with the continuum (Fano, 1961). The discrete states $|g\rangle$ and $|a\rangle$ are orthonormal and the continuum states $|E\rangle$ are energy normalized, $\langle E|E'\rangle = \delta(E - E')$, and orthogonal to the discrete states.

We are interested in probing the autoionizing state with an external interaction which we will consider to be a time-dependent electromagnetic radiation field $F(t)$ linearly polarized along the z axis and of angular frequency ω . We denote the corresponding part of the Hamiltonian by D and write the full Hamiltonian as

$$H = H_a + D = H_0 + V + D. \quad (2.1)$$

For the purpose of analyzing only near-resonant excitation of the autoionizing state, the state vector of the system is expanded in the restricted basis

consisting of $|g\rangle, |a\rangle$ and $|E\rangle$

$$|\Psi(t)\rangle = C_g(t)|g\rangle + C_a(t)|a\rangle + \int dE C_E(t)|E\rangle, \quad (2.2)$$

and inserted into the time-dependent Schrödinger equation

$$i \frac{\partial}{\partial t} |\Psi(t)\rangle = H |\Psi(t)\rangle. \quad (2.3)$$

To proceed, we introduce slowly varying amplitudes, $c_g = C_g \exp(iE_g t)$, $c_a = C_a \exp(i(E_g + \omega)t)$, $c_E = C_E \exp(i(E_g + \omega)t)$, and treat the continuum as a sink, i.e., set the time derivative of the continuum amplitude equal to zero, $\dot{c}_E = 0$. In this way, the continuum is eliminated adiabatically. Finally, we introduce the rotating wave approximation, which means that anti-resonant energy terms in the exponents are neglected.

The above procedure leads to the following set of differential equations for the time-dependent discrete-state amplitudes

$$i\dot{c}_g = \left(\int dE \frac{|\Omega_{gE}|^2}{E_g + \omega - E} \right) c_g + \left(\Omega_{ga} + \int dE \frac{\Omega_{gE} V_{aE}}{E_g + \omega - E} \right) c_a \quad (2.4)$$

$$i\dot{c}_a = \left(\Omega_{ag} + \int dE \frac{V_{aE} \Omega_{Eg}}{E_g + \omega - E} \right) c_g + \left(E_a - E_g - \omega + \int dE \frac{|V_{aE}|^2}{E_g + \omega - E} \right) c_a \quad (2.5)$$

with $V_{aE} = V_{Ea}^*$, $V_{aE} = \langle a|V|E\rangle$ the configuration interaction of the discrete part $|a\rangle$ with the continuum $|E\rangle$, and $\Omega_{gE} = \Omega_{Eg}^*$, $\Omega_{gE} = D_{gE}F(t)/2$ the Rabi coupling between the ground state and the continuum with D_{gE} the dipole matrix element $\langle g|D|E\rangle$ along the z axis. Finally, $\Omega_{ga} = \Omega_{ag}^*$, $\Omega_{ga} = D_{ga}F(t)/2$ denotes the Rabi coupling between the ground state and the discrete state $|a\rangle$, expressed in terms of the dipole matrix element $D_{ga} = \langle g|D|a\rangle$ along the z axis.

In equations (2.4)-(2.5) the integration over energy runs from the lowest threshold of the continuous spectrum and comes from the adiabatic elimination of the continuum. The evaluation of the atomic coupling parameters entering the above equations is simplified by using the following identity for generalized functions (distributions)

$$\lim_{\eta \rightarrow 0^+} \frac{1}{E_0 - E + i\eta} = \mathcal{P} \frac{1}{E_0 - E} - i\pi\delta(E_0 - E), \quad (2.6)$$

where \mathcal{P} denotes the principal value, and δ is the Dirac delta function. By using this relation in equations (2.4)-(2.5) we obtain

$$i\dot{c}_g = \left(S_g - i\frac{\gamma_g}{2} \right) c_g + \tilde{\Omega}_{g,a} \left(1 - \frac{i}{q} \right) c_a, \quad (2.7)$$

$$i\dot{c}_a = \tilde{\Omega}_{a,g} \left(1 - \frac{i}{q} \right) c_g - \left(\delta + i\frac{\Gamma_a}{2} \right) c_a. \quad (2.8)$$

The parameters entering equations (2.7)-(2.8) are the radiation induced energy shift of the ground state (S_g), the ionization rate of the ground state (γ_g), the autoionization width (Γ_a), the effective Rabi coupling ($\tilde{\Omega}_{g,a}$), the asymmetry parameter q and the energy detuning δ (Madsen et al., 2000*a,b*; Madsen and Lambropoulos, 2001). Explicitly these parameters are defined as

$$S_g = \mathcal{P} \int dE \frac{|\Omega_{g,E}|^2}{E_g - \omega - E}, \quad (2.9)$$

$$\gamma_g = 2\pi |\Omega_{g,E}|^2, \quad (2.10)$$

$$\Gamma_a = 2\pi |V_{a,E}|^2, \quad (2.11)$$

$$\tilde{\Omega}_{g,a} = \Omega_{g,a} + \mathcal{P} \int dE \frac{\Omega_{g,E} V_{E,a}}{E_g + \omega - E}, \quad (2.12)$$

$$\frac{1}{q} = \frac{\pi \Omega_{g,E} V_{E,a}}{\tilde{\Omega}_{g,a}}, \quad (2.13)$$

$$\delta = \omega - (E_a^r - E_g), \quad (2.14)$$

with E_a^r the resonance position of the autoionizing state, including the self-energy shift and the laser-induced ac Stark shift. For the radiation intensities which we have in mind in the present work, we may safely neglect the ac Stark shifts. Equations (2.7) and (2.8) allow for the description of a time-dependent coherent pulse interacting non-perturbatively with the system and driving the $|g\rangle \rightarrow |a\rangle$ transition strongly (Lisitsa and Yakovlenko, 1974).

In the weak-probe regime, where only a small percentage of the total population leaves the ground state, we may approximate the ground state amplitude by $c_g \simeq 1$. The rate of decay of the ground state is then obtained from

$$R_{\text{decrease}} = -\partial_t |c_g|^2 = -2\text{Re}(\dot{c}_g). \quad (2.15)$$

In steady state for the discrete part $|a\rangle$, $\dot{c}_a = 0$, we find from equations (2.15) and (2.7)

$$R_{\text{decrease}} = \gamma_g + 2\text{Re} \left(i \tilde{\Omega}_{g,a} \left[1 - \frac{i}{q} \right] c_a \right), \quad (2.16)$$

with

$$c_a = \frac{\tilde{\Omega}_{a,g} (1 - i/q)}{\delta + i\Gamma_a/2}. \quad (2.17)$$

Inserting equation (2.17) into equation (2.16) we obtain

$$R_{\text{decrease}} = \gamma_g + \frac{2\tilde{\Omega}_{g,a}^2}{\delta^2 + \Gamma_a^2/4} \left(\frac{\Gamma_a}{2} - \frac{\Gamma_a}{2q^2} + \frac{2\delta}{q} \right), \quad (2.18)$$

which is equivalent to the result obtained by Fano (1961) as may be seen by scaling the detuning in units of the half width $\epsilon = \delta/(\Gamma_a/2)$ and squaring equation (2.13)

$$\frac{1}{q^2} = \frac{\gamma_g \Gamma_a}{4\tilde{\Omega}_{g,a}^2}, \quad (2.19)$$

to obtain

$$R_{\text{decrease}} = \gamma_g \left(1 + \frac{1}{\epsilon^2 + 1} (q^2 - 1 + 2\epsilon q) \right). \quad (2.20)$$

Equation (2.19) follows from equation (2.13) and the definitions of the ionization and autoionization rates, and we see that $1/q^2$ is related to the ratio between the dipole excitation probability to the continuum at resonance and the quasi-bound state.

If we keep the expression for the line shape in the form of equation (2.18), we immediately extract the resonance position and width. The first term in the parenthesis, in combination with the denominator of the pre-factor, describes a Lorentzian. The second and the last terms describe the asymmetry due to the coherence build up in the excitation step of the autoionizing state. Note that equation (2.18) reduces to the well-known Lorentzian line shape for bound-bound transitions in the limit of a symmetric resonance ($1/q \rightarrow 0$), corresponding to $|\tilde{\Omega}_{a,g}|/\sqrt{\gamma_g \Gamma_a} \gg 1$.

Clearly, the line shape obtained by observing the rate of decrease of the population in the ground state, $|g\rangle$, should equal the shape obtained from the rate of increase in the continuum $R_{\text{decrease}} = R_{\text{increase}}$, with

$$R_{\text{increase}} = \partial_t P = \partial_t \int dE |c_E|^2, \quad (2.21)$$

where P denotes the probability for finding the system in the continuum. It is reassuring to see by the following explicit calculation that this is indeed the case within our approximation scheme. The probability P can be calculated by considering the differential equation for the continuum amplitude C_E ,

$$i\dot{C}_E = \Omega_{E,g} \exp(iEt) c_g + V_{E,a} \exp(iEt) c_a, \quad (2.22)$$

integrating it formally, calculating $|C_E|^2 = |c_E|^2$ and performing the integration over energy noting that $\int dE \exp(iE(t-t')) = 2\pi\delta(t-t')$. At the end of the calculation the rate is obtained by differentiation with respect to time. In the weak-probe and steady state limit we obtain

$$R_{\text{increase}} = \gamma_g + \Gamma_a |c_a|^2 + \frac{4\tilde{\Omega}_{a,g}}{q} \text{Re}(c_a), \quad (2.23)$$

which, by equation (2.17), is seen to be equal to equations (2.18) and (2.20).

Generalizations of the above formalism to multiple continua were given by Madsen et al. (2000*a,b*) and by Madsen and Lambropoulos (2001). In short, the shifts, widths and rates are now incoherent sums of terms pertaining to the different continua involved. The asymmetry parameter, on the other hand, reads

$$\frac{1}{q} = \frac{\pi \sum_j \Omega_{gE_j} V_{E_j a}}{\tilde{\Omega}_{g,a}}, \quad (2.24)$$

where the index j labels the different continua. We see from this expression that $1/q^2$, in this more general case, is not simply related to the ratio between direct ionization and excitation via the quasi-bound state.

Chapter III

Experimental results on triply excited states in lithium

3.1 Collision or photon excitation

Triply excited states in lithium are located above the second ionization limit, that is above the 1s ground state of the Li^{++} ion. To get a feeling of the energies involved, we note, for example, that the lowest triply excited state of $^2\text{P}^o$ symmetry, denoted as the $\text{Li}(2s2s2p\ ^2\text{P}^o)$ resonance by its dominant configuration, is located approximately 142 eV above the $\text{Li}(1s1s2s\ ^2\text{S}^e)$ ground state. Accordingly, to access the states of interest one needs at least around this amount of excitation energy. Figure 1.1 shows a schematic energy level diagram for Li, Li^+ and Li^{++} in the energy region corresponding to triply excited Li and doubly excited Li^+ .

Experimentally, the energy needed to address the triply excited states is mediated either by collisions or by photoexcitation. While the first measurements by collisional excitation were reported in the 1970s (Bruch et al., 1975; Rødbro et al., 1979), only as late as 1994 advances in new light sources made it possible to study the lowest triply excited state in lithium by photoabsorption (Kiernan et al., 1994). In a discussion of which method to use, it is interesting to cite from the paper by Rødbro et al. (1979) where the triply excited states were excited by collisions: "... photon excitation is generally restricted to those excited states which can be populated by electric dipole (E1) transitions. In addition, the E1 transition probability is low if two or more electrons have to be excited simultaneously." and "... heavy-ion collision processes are not restricted by specific selection rules so that optically inaccessible states are strongly populated...". And to compare these statements with the point of view presented in the photoabsorption work by Kiernan et al. (1994): "The primary advantage of the photoabsorption technique is that it is selective and probes the fundamental photon-atom interaction. It produces spectra of less complexity as it accesses only those states which are optically connected to a known ground state; it can also provide sufficient resolution to measure resonance widths and q values".

From these statements it is clear that the two methods supplement each other. In the case of photoabsorption one has more control over the excitation process, on the other hand certain states which are not populated by dipole allowed transitions can only be efficiently investigated by collisional excitation; or alternatively, as proposed in recent works by Madsen et al. (2000*a,b*); Madsen and Lambropoulos (2001), by controlled laser-induced transitions between triply excited states. A point which we shall return to in chapter 4.

3.2 Experiments with collisional excitation

Bruch et al. (1975) used the beam-foil interaction mechanism to populate highly excited states in lithium. In this experiment a beam of ~ 30 keV Li^+ ions were passed through carbon foils and from the back of the foil some Li atoms and Li^+ ions emerged in multiply excited states. Subsequently, the electrons coming from the autoionization decays were detected and a structure occurring in the spectrum at ~ 80 eV was tentatively assigned to be due to autoionization of triply excited states of $^2\text{P}^o$, $^2\text{D}^e$, and $^2\text{S}^e$ symmetry into $1s2s^{1,3}\text{S}\ell$ and $1s2p^{1,3}\text{P}\ell$ continua. The experimental energy resolution of approximately 2 eV was, however, too poor to allow a definite assignment. In particular, the analysis was hampered by the possibility of having, within the resolution of the experiment, a transition in the Li^+ ion coinciding with the energy involved in the decay of the triply excited state.

Rødbro et al. (1979) reported a high resolution Auger spectrum for lithium obtained by using a gaseous target of helium or ethylene (C_2H_4) and a beam of Li^+ ions with energy around 300 keV. Compared with the experiment of Bruch et al. (1975), replacing the foil with a target gas led to an improved energy resolution of only ~ 0.1 eV. By comparison with available theoretical data, this allowed an identification of most of the doubly excited resonances in Li^+ . Some of these are seen in figure 3.1 which shows the high-energy part of the Li autoionizing spectrum. Insert (a) corresponds to 200 keV Li^+ on ethylene and (b) to 300 keV Li^+ on helium. Additionally, there were around 11 spectral lines whose origin was not clear. These were tentatively assigned to be due to the decay of triply excited states with dominant $2s2s2p$ and $2s2p2p$ configurations, and of doublet and quartet spin symmetry, and of total angular momentum from zero to two. Peak number 23 in figure 3.1(a) is one such example. A final assignment of the observed features came three years later when more theoretical information was provided by saddle-point calculations of Chung (1982) (see section 4.2). The lines were due to the decay of the triply excited lithium states $2s2s2p^2\text{P}^o$, $2s2p2p^4\text{P}^e$, $2s2p2p^2\text{P}^e$ and $2p2p2p^2\text{D}^o$. The figure also illustrates that many different symmetries are reached by collisional excitation.

Neither of the experiments mentioned above (Bruch et al., 1975; Rødbro et al., 1979) reported widths of the autoionizing states. As we shall see later, typical widths of the autoionizing triply excited lithium resonances are ~ 0.1 eV, corresponding to a lifetime of ~ 10 fs ($1 \text{ fs} = 10^{-15} \text{ s}$), which is much shorter than

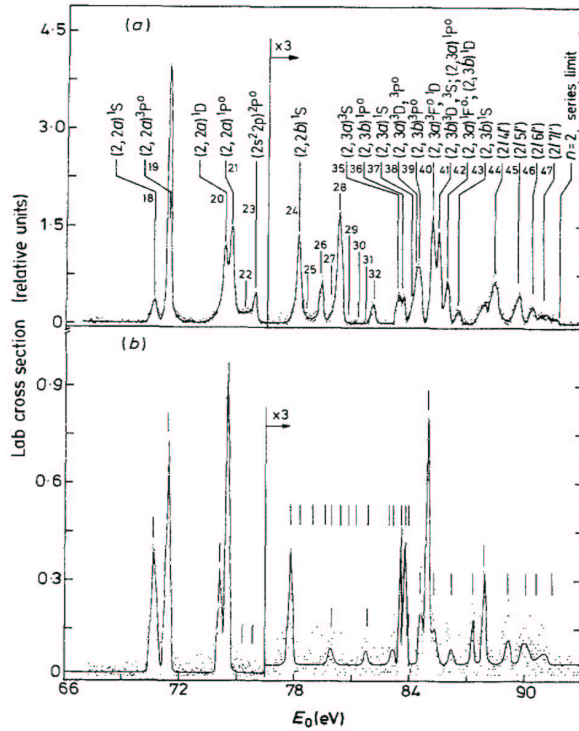


Figure 3.1: The high-energy part of the Li autoionizing spectrum excited in (a) 200 keV Li^+ on ethylene and (b) 300 keV Li^+ on helium. The peaks correspond to doubly excited Li^+ and triply excited Li states. From Rødbro et al. (1979).

what is possible to measure by beam-foil techniques. As discussed, for example, in the review by Martinson and Gaupp (1974), this method is restricted to the study of lifetimes between 10^{-11} s and 10^{-7} s. In this connection it should be mentioned that in the 1980s there were two beam-foil experiments concerned with the position and decay of the $2p2p2p^4S^o$ resonance in lithium (Agentoft et al., 1984; Mannervik et al., 1989). The $2p2p2p^4S^o$ state is metastable against autoionization since no channels are open which leave the total spin, parity and angular momentum unchanged. Thus, even though the $2p2p2p^4S^o$ state is located above the second ionization limit in Li, at about 150 eV above the ground state, the autoionization channel is closed, and the dominant decay is by the radiative dipole allowed transition to the $\text{Li}(1s2p2p^4P^e)$ state. In their measurement Agentoft et al. (1984) found a wavelength of 145.02 ± 0.05 Å for the $2p2p2p^4S^o \rightarrow 1s2p2p^4P^e$ transition. Mannervik et al. (1989) improved the precision on the wavelength measurement and reported the value 145.016 ± 0.006 Å. In the latter experiment also the lifetime of the state was derived, and a value

of 13.5 ± 1.5 ps (1ps = 10^{-12} s) was reported.

Müller et al. (1989) studied electron impact ionization of Li^+ in a crossed-beam experiment. In a scan over 768 equidistant energy points for the electron projectile from 130 eV to 160 eV, the resolution was better than 0.01 % from point to point. Two relatively strong resonances were observed and associated with triply excited $2s2s2p^2P^o$ and $2s2p2p^2D^e$ states of an intermediate lithium atom. The resonances were fitted with Fano profiles (Fano, 1961), and the positions were determined to be at projectile electron energies 137.7 ± 0.1 eV and 140.1 ± 0.1 eV, respectively. When the ionization potential of lithium, 5.39 eV¹, is added, the resonance positions are $E_0(^2P^o) = 143.1 \pm 0.2$ eV and $E_0(^2D^o) = 145.5 \pm 0.2$ eV. These values for the resonance positions will be compared with photoexcitation values in table 3.2.

3.3 Experiments with photon excitation

The current interest in triply excited states in lithium is strongly stimulated by the progress in the means by which these states can be accessed. Developments in bright light sources with high photon energies and high resolution, have made possible photon excitation measurements in which both the positions, the autoionization widths, and in some cases even the asymmetry parameter q of the triply excited resonances are determined. These new possibilities have led to major advances in the experimental study of triply excited states during the last decade.

Photoexcitation of the $\text{Li}(1s1s2s^2S^e)$ ground state to a triply excited state can only proceed via electron-electron correlation. This is due to the one-particle nature of the dipole operator governing the photon absorption process. For example, the dipole matrix element between the dominant configuration of the ground state and that of the lowest-lying triply excited $^2P^o$ resonance $\langle 1s1s2s^2S^e | \mathbf{D} | 2s2s2p^2P^o \rangle$ is zero. From this perspective it is clear that photoexcitation is a very efficient probe of the correlation in the final resonance state (and in the initial ground state), and, hence, such processes challenge our current abilities to characterize highly correlated systems.

3.3.1 Photoabsorption experiment

Kiernan et al. (1994) reported a measurement on the lowest triply excited resonance of $^2P^o$ symmetry. The state was detected by photoabsorption using the dual laser plasma technique for the generation of the radiation. A comparison of the experimental data with theoretical data available at the time (Chung, 1982; Ahmed and Lipsky, 1975; Nicolaides and Beck, 1977; Safronova and Senashenko, 1978; Simons et al., 1979) and a Hartree-Fock configuration-interaction calculation identified the state as the $2s2s2p^2P^o$ state, after its dominant configuration. The position E_0 above the $\text{Li}(1s1s2s^2S^e)$ ground state, the

¹Energy levels are from the NIST database: <http://physics.nist.gov/PhysRefData/>

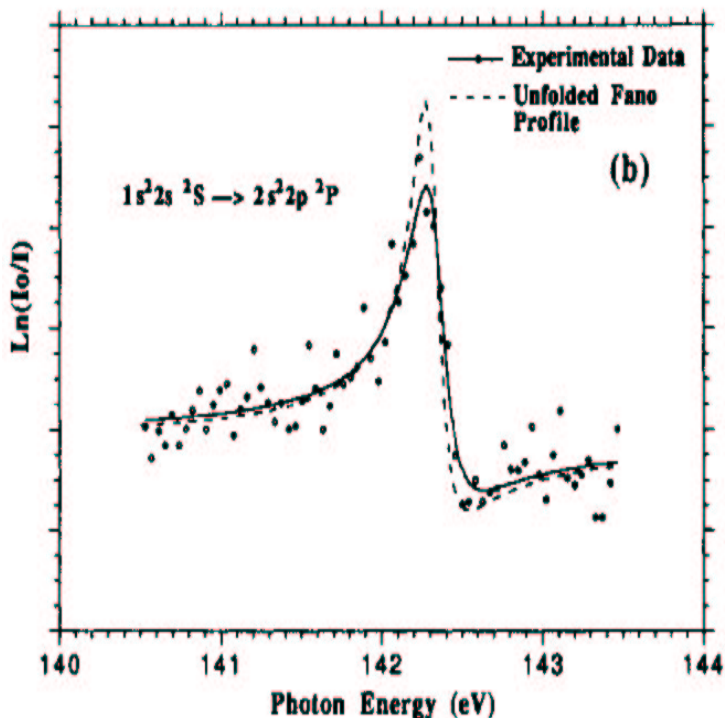


Figure 3.2: Photoabsorption spectrum of atomic lithium near the energy of the main $\text{Li}(1s^2 2s^2 S^e) \rightarrow \text{Li}(2s^2 2p^2 P^o)$ transition. The broken curve represents a fit to the data with a Fano profile after correcting for instrumental broadening. From Kiernan et al. (1994).

total autoionization width Γ , and the asymmetry parameter q were determined by fitting the experimental data with a Fano profile (Fano, 1961). Figure 3.2 shows the photoabsorption spectrum in the vicinity of the resonance. The resonance parameters were determined to be $E_0 = 142.32 \pm 0.05$ eV, $\Gamma = 0.20 \pm 0.04$ eV and $q = -2.2 \pm 0.60$. The values of the energy and the width were in reasonable agreement with theoretical results referred to in the paper by Kiernan et al. (1994). We notice a difference between the energy position measured by Kiernan et al. (1994) and the position reported in the crossed-beam experiment mentioned at the end of section 3.2. (Müller et al., 1989).

The dual laser plasma technique used by Kiernan et al. (1994) could not be readily improved with respect to resolution and tunability range of the photon source. Synchrotron based sources are more flexible and were used in the photoion and photoelectron experiments to be discussed below.

3.3.2 Photoion experiments

Kiernan et al. (1995) used extreme-ultra-violet radiation from the undulator beamline at HASYLAB to measure the photoion yield as a function of photon energy in the spectral region of hollow lithium states. The Li^{++} ion yield was typically two orders of magnitude smaller than the Li^+ ion signal and, as a consequence, only the latter spectrum was used for the determination of the resonances. An improved resolution of ~ 20 meV allowed a more precise determination of the resonance parameters of the $\text{Li}(2s2s2p^2P^o)$ state: $E_0 = 142.32 \pm 0.02$ eV, $\Gamma = 0.14 \pm 0.02$ eV, and $q = -2.0 \pm 0.3$. Within the limits of experimental error these figures lie within the results of the data presented by Kiernan et al. (1994). In addition to the lowest-lying $2P^o$ resonance, a series of triply excited states was observed, and tentatively assigned by Hartree-Fock calculations.

Besides the experiment by Kiernan et al. (1995), three more photoion yield experiments have been reported, all carried out at the Photon Factory in Japan (Azuma et al., 1995, 1997; Wehlitz et al., 1999). In the first experiment Azuma et al. (1995) detected photoion spectra and determined the position and width of the $\text{Li}(2s2s2p^2P^o)$ resonance to an accuracy of 0.1 eV and 0.04 eV, respectively. These values were in agreement with the values in Kiernan et al. (1994, 1995). Also the value of the asymmetry parameter, $q = -2.2 \pm 0.2$, was in agreement with previous results. Table 3.2 presents a compilation of results on the $\text{Li}(2s2s2p^2P^o)$ state.

In the work by Azuma et al. (1995) more resonances were measured and figure 3.3 shows the photoion yield spectrum for photon energies between 140 eV and 165 eV (Azuma et al., 1995). The letters attached to the peaks indicate that the resonances were identified in terms of dominant configurations by multiconfiguration Dirac-Fock calculations. In the experiment also data were recorded in the Li^{++} ion channel. In that channel there was no measurable asymmetry in the resonance profile and by fitting the symmetric structure in the spectrum by a Lorentzian, the position of the $\text{Li}(2s2s2p^2P^o)$ state was determined to be 142.34 eV, which is in agreement with previous data.

Azuma et al. (1995) stressed the striking aspect of the “complete absence of any identifiable Rydberg series structure” in their data. Later Rydberg series of the type $2l2l'n'l''$ were documented in one experiment (Journel et al., 1996), and in a multitude of numerical calculations. We shall return to this point when discussing photoelectron measurements and in chapter 4 when considering different theoretical methods.

Using the same synchrotron radiation and photoion spectroscopy technique, Azuma et al. (1997) measured with an energy resolution of ~ 30 meV the lowest $2P^o$ resonance with completely empty K and L shells. Based on its dominant electron configuration this resonance was labelled $\text{Li}(3s3s3p^2P^o)$ and was referred to as doubly hollow (Diehl, Cubaynes, Chung, Wuilleumier, Kennedy, Bizau, Journel, Blancard, VoKy, Faucher, Hibbert, Berrah, Morgan, Bozek and Schlachter, 1997). The resonance was measured in the Li^{++} ion channel, and

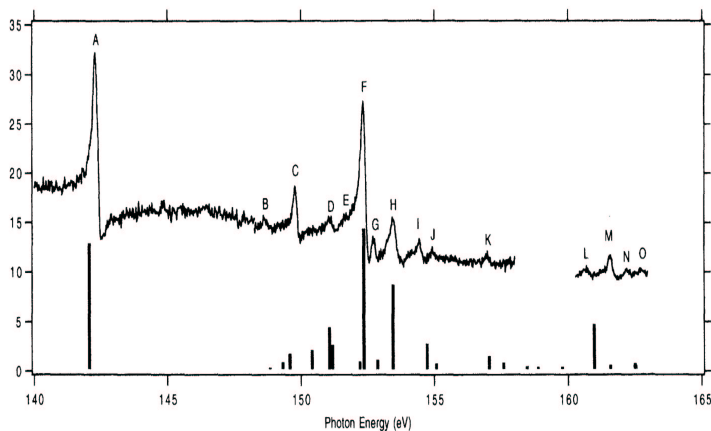


Figure 3.3: Triply excited Li resonances as a function of photon energy. The bar diagram indicates energy positions obtained by multiconfiguration Dirac-Fock calculations. From Azuma et al. (1995).

the decay takes place through two-step autoionization via a doubly excited state in Li^+ . This mechanism was already described by Hansen (1975) in the context of enhanced double ionization in Ba. The structure in the ion yield was fitted with a Fano profile and the resonance parameters were $E_0 = 175.25 \pm 0.10$ eV, $\Gamma = 0.32 \pm 0.01$ eV, and $q = 2.1 \pm 0.1$. As seen from figure 1.1, this energy is indeed above the lowest doubly excited state in the Li^+ ion.

The most recent photoion experiment on hollow lithium was described by Wehlitz et al. (1999). In that experiment the resolution and the signal-to-noise ratio were improved compared with the experiment by Azuma et al. (1995), and the synchrotron radiation was tuned between 141.4 eV and 143.5 eV to scan the energy region of the $2s2s2p^2P^o$ resonance. Photoion spectra were recorded in both the Li^+ and Li^{++} ion channels. As seen from figure 3.4, no two-step sequential autoionization channels, via doubly excited states in the Li^+ ion, are open for the decay of the $2s2s2p^2P^o$ resonance, and the double continuum is populated either via direct double photoionization or via one-step autoionization. Both the photoion spectrum in the Li^+ and in the Li^{++} ion channels showed an asymmetry. The energy of the resonance was measured to be 142.33 eV in the Li^+ ion channel and the value obtained by measuring in the Li^{++} ion channel was the same within 0.004 eV. Within experimental error the measurement of the width gave identical results in the two channels, $\Gamma = 0.124 \pm 0.03$ eV. The modulus square of the asymmetry parameter q is related to the probability of going to the single- or double-electron continuum directly or via the triply excited state, and therefore it is not surprising that different values of q were measured in the two channels. For single ionization the

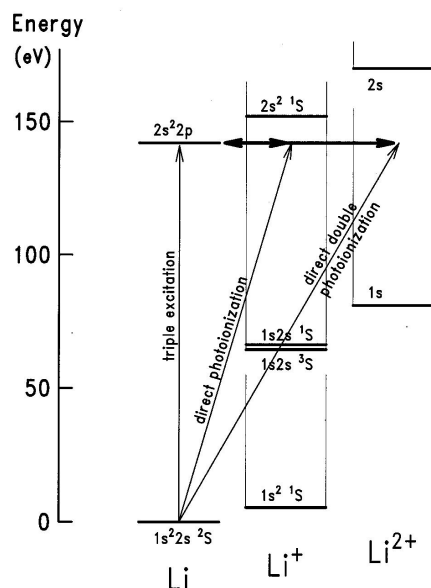


Figure 3.4: Schematic energy-level diagram of some states in Li, Li^+ and Li^{2+} . The transitions involved in the photoionization experiment are indicated by arrows. The lowest autoionization resonance in the Li^+ ion channel is above the $2s2s2p^2P^o$ resonance of interest. From Wehlitz et al. (1999).

result was $q = -1.97 \pm 0.03$, for double ionization the result was $q = 6.9 \pm 0.7$.

3.3.3 Photoelectron experiments

The photoion experiments discussed above are integral measurements in the sense that the total number of ions of a specific charge state is measured as a function of the energy of the photon. Accordingly, such experiments may only provide data on the positions and total autoionization widths of resonances.

Experiments based on photoelectron spectroscopy, on the other hand, allow a determination of partial cross-sections leaving the system in individual final ionic states, to be referred to as target states. For example, the process probing the spectral region of triply excited states $\text{Li}(1s1s2s^2S^e) + \hbar\omega \rightarrow \text{Li}^+(1snl^{1,3}L) + e'$ may, depending on the energy of the intermediate excited Li^* state, leave the target lithium ion in different $\text{Li}^+(1snl^{1,3}L)$ target states. The photon energy, $\hbar\omega$, and the energy of the measured electron, however, uniquely determine the final Li^+ target state.

Photoelectron spectrometry experiments require a photon flux which is orders of magnitude higher than that required with the photoion technique. This makes the demands to the light source higher or forces the experimenter to open

wider the exit slit of the monochromator to increase the flux. This in turn will lead to a poorer resolution as compared to the ion yield measurements.

To date, eight photoelectron experiments concerned with the detection of triply excited states have been performed. The first experiment by Journal et al. (1996) was performed at the synchrotron facility in Orsay. Here the brilliance was moderate, and the experimental resolution was not as good as in the photoion experiments discussed in section 3.3.2 (~ 50 meV). The other photoelectron experiments (Diehl et al., 1996; Cubaynes et al., 1996; Diehl, Cubaynes, Chung, Wuilleumier, Kennedy, Bizau, Journal, Blancard, VoKy, Faucher, Hibbert, Berrah, Morgan, Bozek and Schlachter, 1997; Diehl, Cubaynes, Kennedy, Wuilleumier, Bizau, Journal, VoKy, Faucher, Hibbert, Blancard, Berrah, Morgan, Bozek and Schlachter, 1997; Diehl, Cubaynes, Wuilleumier, Bizau, Journal, Kennedy, Blancard, VoKy, Faucher, Hibbert, Berrah, Morgan, Bozek and Schlachter, 1997; Diehl, Cubaynes, Zhou, VoKy, Wuilleumier, Kennedy, Bizau, Manson, Morgan, Blancard, Berrah and Bozek, 2000; Diehl, Cubaynes, Zhou, VoKy, Wuilleumier, Kennedy, Bizau, Manson, Blancard, Berrah and Bozek, 2000) were performed in Berkeley, where photons from the Advanced Light Source served to photoexcite the resonances. The undulator beamline 9.0.1 provides the most intense light source in the energy range of interest allowing for an improved energy resolution (~ 20 meV). All the experiments were published together with extensive R -matrix calculations which in general agreed satisfactory with the measurements.

Journal et al. (1996) scanned through the energy range around the lowest triply excited $\text{Li}(2s2s2p^2P^o)$ resonance and measured the photoionization cross-section corresponding to the channels $\text{Li}(1s1s2s^2S^e) + \hbar\omega \rightarrow \text{Li}^+(1s2s^1,3S^e) + \epsilon l$ and $\text{Li}(1s1s2s^2S^e) + \hbar\omega \rightarrow \text{Li}^+(1s2p^3,1P^o) + \epsilon l$. In both cases a variation was observed at the position of the resonance whose energy and width were determined to be $E_0 = 142.30 \pm 0.50$ eV and $\Gamma = 0.20 \pm 0.04$ eV. It is interesting that the measurement was able to resolve differences in the effects of interference in different decay channels: the profile in the $^3,1S^e$ -channel was asymmetric, pointing to an interference between direct photoionization, and ionization via the autoionizing triply excited state. The profile in the $^3,1P^o$ -channel, on the other hand, was symmetric, indicating that the amplitude for the direct process was too weak to result in interference with the amplitude for ionization via the triply excited state.

Diehl et al. (1996) measured the photoionization cross-section in the $1s3s^3S^e$ and $1s2p^1,3P^o$ ionic channels in the photon energy range from ~ 140 eV and up to ~ 160 eV. Compared with the Orsay experiment (Journal et al., 1996), the higher brightness of the synchrotron radiation from the Advanced Light Source led to an improved energy resolution of ~ 20 meV. Figure 3.5 shows the experimental and theoretical R -matrix partial photoionization cross-section of Li in the $\text{Li}^+(1s2p^1P^o)$ ionic channel. The high spectral resolution made it possible to obtain a profile-width which was sufficiently accurate to serve as a test of theoretical calculations. As seen from the figure, the theoretical energy differs from the experimental value by around 0.2 eV which is caused

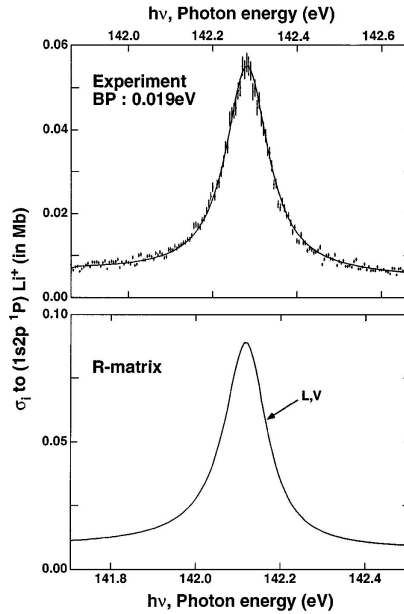


Figure 3.5: Upper part: experimental photoionization cross-section of Li in the $\text{Li}^+(1s2p^1P^o)$ ionic channel in the vicinity of the $\text{Li}(2s2s2p^2P^o)$ triply excited state. Lower part: *ab initio* *R*-matrix calculations. L and V refer to length and velocity gauge calculations, respectively. See text. From Diehl et al. (1996).

by a shift of the theoretical *R*-matrix value of the Li^+ ground state. This shift is common to all the *R*-matrix calculations discussed in this work, and is also visible in the figures below. The theoretical absolute value of the cross-section is about 50 % larger than the measured value which has a total uncertainty close to 35 %. The *R*-matrix calculations in length (L) and velocity (V) gauges are identical on the scale of the figure. The two forms lead to identical cross-sections for exact wave functions, so this is a signature of the high quality of the wave functions used in the calculation. When expressed in terms of the electric dipole operator, the coupling is said to be in the length gauge. When expressed in terms of the vector potential and the momentum operator, a velocity gauge calculation is performed. These forms will be discussed in more detail in section 4.1 (see equations (4.4)–(4.5)). See also the recent work by Madsen (2002) for some general considerations about gauge invariance. The parameters of the $2s2s2p^2P^o$ resonance were determined to be $E_0 = 141.28 \pm 0.03$ eV, and $\Gamma = 0.118 \pm 0.003$ eV. Additionally, five more resonances between 149.98 eV and 153.66 eV were observed and assigned by comparison with *R*-matrix calculations and with photoion data by Azuma et al. (1995).

In an interesting two-colour experiment, Cubaynes et al. (1996) reported

Table 3.1: Energies (E_0 in eV), widths (Γ in meV) and asymmetry parameter (q) for some even-parity triply excited Li states. Numbers in parenthesis indicate the uncertainty in the last digits.

Assignment	E_0^a	Γ^a	q^a	E_0^b	q^b	E_0^c	Γ^c
$2s2p2p^2D^e$	142.92(5)	103(10)	-2.6(2)	142.76	-2.71	142.91	90
$2s2p2p^2S^e$				144.63		144.63	54
$2s2p2p^2S^e$	145.08(5)	47(5)	-2.1(2)	145.00	-2.09	145.07	48

^aExperiment from Cubaynes et al. (1996).

^b R -matrix calculation from Cubaynes et al. (1996).

^cSaddle-point calculation from Chung and Gou (1995, 1996).

the first photoexcitation measurements on even-parity hollow states in Li. A continuous-wave dye laser of photon energy $\hbar\omega_L$ was tuned on the transition from the ground state to the first singly excited state, $\text{Li}(1s1s2s^2S_{1/2}^e) + \hbar\omega_L \rightarrow \text{Li}(1s1s2p^2P_{3/2}^o)$, located at an energy 1.8479 eV above the ground state. This laser coupling transferred a fraction of the Li atoms into the singly excited $2P^o$ state. In the second step, radiation from the Advanced Light Source was scanned through the region of hollow state resonances. The photoionized electrons were detected in the $[1s2p^3P^o + \epsilon p]^2P, ^2S, ^2D$ channels. The resolution was around 40 meV. The experiment resolved energies and widths of the lowest triply excited states of S and D symmetry and even parity. Some of the results are reproduced in table 3.1 which shows that the agreement between theory and experiment is very good. The experiment illustrates how new layers of the spectrum of hollow lithium states may be uncovered in a selective and controlled manner by introducing an additional laser coupling. As will be discussed in section 4, the idea of adding still another coupling, which may be realized by a suitable laser, to induce dipole transitions directly between triply excited states was explored theoretically by Madsen et al. (2000*a,b*); Madsen and Lambropoulos (2001).

Diehl, Cubaynes, Wuilleumier, Bizau, Journal, Kennedy, Blancard, VoKy, Faucher, Hibbert, Berrah, Morgan, Bozek and Schlachter (1997) reexamined the question of the existence of Rydberg series in hollow lithium states. Their study was partly motivated by the need for understanding the correlated three-electron dynamics in more detail and partly by the photoion experiment of Azuma et al. (1995) which did not resolve any Rydberg series. Diehl, Cubaynes, Wuilleumier, Bizau, Journal, Kennedy, Blancard, VoKy, Faucher, Hibbert, Berrah, Morgan, Bozek and Schlachter (1997) succeeded in measuring extended Rydberg series with principal quantum number extending up to 8 by electron spectrometry at the Advanced Light Source. The excitation and decay process is sketched in figure 3.6 and is summarized in the following process: $\text{Li}(1s1s2s^2S^e) + \hbar\omega \rightarrow \text{Li}^+([(2s2p^3P^o)ns]^2P^o) \rightarrow \text{Li}^+(2s2s^1S^e)$ (151.66 eV) $+\epsilon_1p$ and subsequently, $\text{Li}^+(2s2s^1S^e) \rightarrow \text{Li}^{++}(1s1s^2S^e) + \epsilon_2s$ (70.63 eV) (Figure 3.7 right scale). Simultaneously, decay into the ground state or singly excited states in the Li^+ ion is allowed, so states of the type $\text{Li}^+(1snl)$ including the lowest triplet state

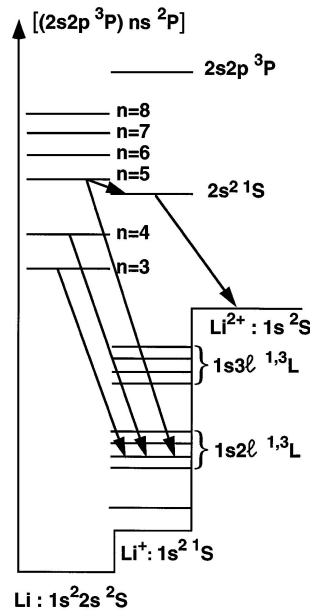


Figure 3.6: Simplified energy-level diagram of Li, Li⁺ and Li²⁺. From Diehl, Cubaynes, Wuilleumier, Bizau, Journel, Kennedy, Blancard, VoKy, Faucher, Hibbert, Berrah, Morgan, Bozek and Schlachter (1997).

Li⁺(1s2s³S^e) tagged experimentally by ~ 87 eV electron emission are also possible target states (Figure 3.7 left scale). The Rydberg states were observed by detecting the intensity of the high-energy electron associated with two-step autoionization via a doubly excited state in Li⁺. This process is energetically allowed when the principal quantum number n of the Rydberg electron is larger than five. The doubly excited Li⁺(2s2s¹S^e) is located 151.66 eV above the ground state. This is still below any excited states in Li²⁺, and the Li⁺(2s2s¹S^e) state will, accordingly, decay with the emission of a characteristic high-energy electron (70.63 eV).

As seen in figure 3.7, a Rydberg series was clearly observed in the Li⁺(2s2s¹S^e) channel. Oppositely, hardly any modification of the spectrum was seen across the Rydberg resonances in the Li⁺(1s2s³S^e) ionic channel. This sensitivity to the decay channel, and the difference in the channel-signals (see left and right scales in figure 3.7), explained why no Rydberg series were observed in the experiment by Azuma et al. (1995) where the *total* photoion yield was recorded. As it was the case in the discussion of figure 3.5, the calculated energies are shifted by ~ 0.2 eV and again the theoretical cross-section is higher than the experimental one.

Triply excited states with not only an empty K -shell but also an empty

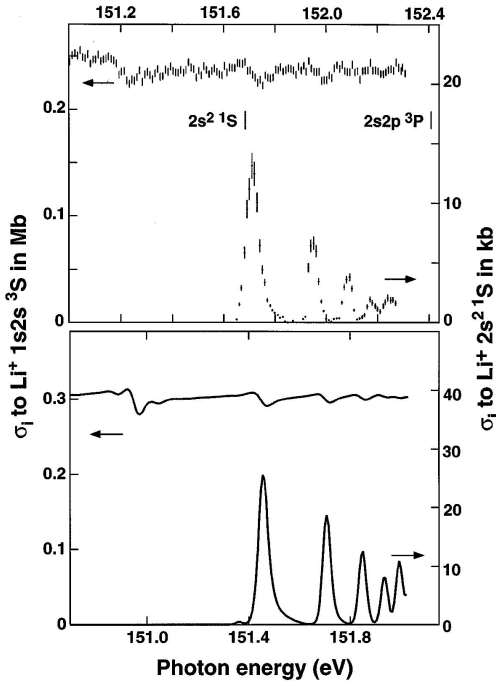


Figure 3.7: Upper part: experimental photoionization cross-section of Li in the $\text{Li}^+(1s2s^3S^e)$ ionic channel (upper curve, left scale) and $\text{Li}^+(2s2s^1S^e)$ channel (lower curve, right scale) as function of the photon energy. The first resonance from the left corresponds to $n = 5$. Lower part: corresponding *ab initio* R -matrix calculations convoluted with the experimental resolution. From Diehl, Cubaynes, Wuilleumier, Bizau, Journal, Kennedy, Blancard, VoKy, Faucher, Hibbert, Berrah, Morgan, Bozek and Schlachter (1997).

L -shell were seen in a photoion experiment by Azuma et al. (1997). Such resonances were also observed in the photoelectron spectrometry experiment by Diehl, Cubaynes, Chung, Wuilleumier, Kennedy, Bizau, Journal, Blancard, VoKy, Faucher, Hibbert, Berrah, Morgan, Bozek and Schlachter (1997). The energy resolution was similar to the one of the other photoelectron experiments, that is around 50 meV. The photoionization cross-section was measured by detecting the Auger electrons from the decay of doubly excited states in the Li^+ ion. In the $\text{Li}^+(2s2s^1S^e)$ channel a symmetric resonance structure was observed at a photon energy of ~ 175 eV, and a comparison with saddle-point and R -matrix calculations allowed the assignment $\text{Li}(3s3s3p^2P^o)$ to this structure. The resonance parameters were determined to be $E_0 = 175.165 \pm 0.050$ eV, and $\Gamma = 250 \pm 50$ meV, in agreement with the values reported by Azuma et al. (1997) ($E_0 = 175.25 \pm 0.10$ eV, $\Gamma = 320 \pm 10$ meV).

The technique based on the measurement of Auger electrons from the decay of doubly excited states in Li^+ , was also used by Diehl, Cubaynes, Kennedy, Wuilleumier, Bizau, Journal, VoKy, Faucher, Hibbert, Blancard, Berrah, Morgan, Bozek and Schlachter (1997) to measure decay routes of triply excited states. Five new resonances between 160 and 163 eV were reported, and the dominant configurations were determined by R -matrix calculations to be of the inter-shell type $2s3l3l'$ and $2s3l4l'$ with l and l' equal to s,p or d.

Angle-resolved photoelectron spectrometry studies

The most recent experiments on triply excited states measured the angle-resolved energy dependence of the photoelectrons emitted over the energy range of the $\text{Li}(2s2s2p^2P^o)$ (Diehl, Cubaynes, Zhou, VoKy, Wuilleumier, Kennedy, Bizau, Manson, Morgan, Blancard, Berrah and Bozek, 2000) and $\text{Li}(2p2p2p^2P^o)$ (Diehl, Cubaynes, Zhou, VoKy, Wuilleumier, Kennedy, Bizau, Manson, Blancard, Berrah and Bozek, 2000) resonances. With a cylindrical mirror analyser the photoelectrons were measured at several different angles with respect to the polarization vector of the photon beam with a spectral resolution of about 40 meV.

The expression for β in the $\text{Li}^+(^3,^1P)$ channel is (Manson and Starace, 1982)

$$\beta(^3,^1P) = \frac{1 - 2\sqrt{2}\rho \cos \Delta}{1 + \rho^2}, \quad (3.1)$$

where $\rho = |S_s|/|S_d|$ is the ratio between the scattering matrix for the s- and d-channels for the out-going electron, and where Δ is the difference between the ϵ_s and ϵ_d phaseshifts. From the expression in equation (3.1), it may be derived by Racah algebra that for independent s and d contributions $\Delta = \pi$ and $\rho^2 = 1/2$ which leads to the value $\beta = 2$. If the probability of the emission of a d-wave is vanishingly small then $\rho \rightarrow \infty$ and the angular parameter β tends to zero. The energy variation of β was measured in the partial $\text{Li}^+(1s2p^1,^3P^o)$ ionic channels where only s- or d-electrons are possible in the final continuum state. In both cases the β value was a little below 2 at energies detuned from resonance. For the $\text{Li}(2s2s2p^2P^o)$ resonance, the minimum in β (0.4 ± 0.1) had shifted ~ 60 meV to the blue compared with the position of the resonance (see figure 3.8). For the $\text{Li}(2p2p2p^2P^o)$ resonance a shift of 10–20 meV to the red was observed and the minimum in β was higher (0.8 ± 0.2) (Diehl, Cubaynes, Zhou, VoKy, Wuilleumier, Kennedy, Bizau, Manson, Blancard, Berrah and Bozek, 2000). The minimum in β was shown to approximately coincide with the maximum in ρ .

It is possible to understand the difference in the absolute values of the minima for the two resonances from simple arguments. For the $\text{Li}(2s2s2p^2P^o)$ resonance the dominant configurations are $2s2s2p$ ($\sim 80\%$) and $2p2p2p$ ($\sim 12\%$) (Azuma et al., 1995; Madsen and Mølmer, 2001a, 2002). Without change in single-electron angular momenta, the $2s2s2p$ configuration can decay to the $\text{Li}^+(1s2p^1,^3P^o) + \epsilon_s$ ionic channel with the emission of an isotropic s-electron. The $\text{Li}^+(1s2p^1,^3P^o) + \epsilon_d$ channel is expected to be less likely since this decay

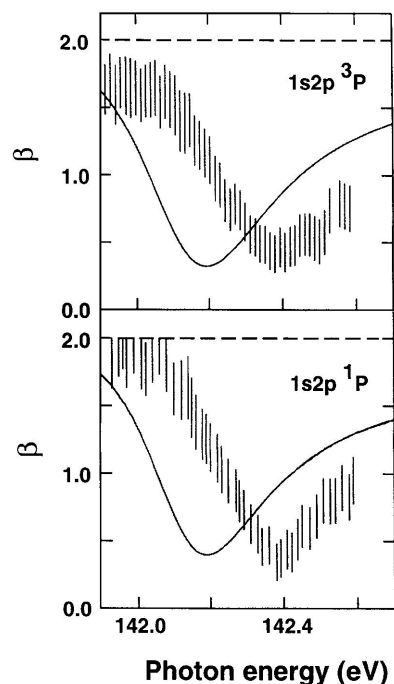


Figure 3.8: Variation of the angular distribution parameter β in the $\text{Li}^+(1s2p^3P\ \epsilon l)$ (upper panel) and $\text{Li}^+(1s2p^1P\ \epsilon l)$ (lower panel) channels in the energy range of the $\text{Li}(2s2s2p^2P^o)$ resonance. Full lines are length and velocity gauge R -matrix calculations which are identical on the scale of the figure. Note the energy shift of ~ 0.2 eV of the theoretical curves (see section 3.3.3). From Diehl, Cubaynes, Zhou, VoKy, Wuilleumier, Kennedy, Bizau, Manson, Morgan, Blancard, Berrah and Bozek (2000).

proceeds via a change in l . This points to the low minimum value of the β parameter for the $\text{Li}(2s2s2p^2P^o)$ resonance. For the $\text{Li}(2p2p2p^2P^o)$ resonance the dominant configurations were estimated by multiconfiguration Dirac-Fock calculations (Azuma et al., 1995): $2p2p2p$ (30%), $2s2s3p$ (15%), $2p2p3p$ (14%), and $2s2p3s$ (14%). Here the $2s2s3p$ and $2s2p3s$ configurations may decay to $\text{Li}^+(1s2p^{1,3}P^o) + \epsilon s$ without change in l . The other configurations, which add up to approximately 45% of the population of the resonance, will have to change l in decaying to both s and d channels and, accordingly, one can not expect the decay to the d-channel to be suppressed to the same extent as was the case for the $\text{Li}(2s2s2p^2P^o)$ resonance. This leads to a more anisotropic distribution or a more anisotropic distribution or a higher minimum value for β .

The differences in the behaviour of the β values for the two resonances show how delicate a measure this parameter is for the correlations in the autoionizing resonances. Apart from an overall energy shift, the overall agreement between

R -matrix calculations and experiments is good.

Recently it was pointed out by Hansen and Verbockhaven (2002) that angle-resolved photoelectron spectra (see figure 1 in (Diehl, Cubaynes, Zhou, VoKy, Wuilleumier, Kennedy, Bizau, Manson, Morgan, Blancard, Berrah and Bozek, 2000)) can be used to obtain a measure for the relative strength in different decay channels. Absolute partial widths can be obtained if the measured angular distributions are absolute. In the case under consideration decay to the $1s2p^3P^o$ and $1s2p^1P^o$ states were measured and a rough value of 4.5 for the ratio $1s2p^3P^o/1s2p^1P^o$ between the intensities of decay into the two channels was obtained. This value was compared with B -spline and saddle-point calculations predicting 3.6 and 3.3 while the R -matrix value was 3.1 (Hansen and Verbockhaven, 2002).

3.4 Parameters for the $\text{Li}(2s2s2p^2P^o)$ resonance

Table 3.2 presents a selection of experimental and theoretical values for the lowest triply excited $^2P^o$ state. In the table experiments which clearly identify the state are listed.

On the theoretical side we have chosen to focus on calculations following the first photoabsorption experiment (Kiernan et al., 1994). For references to earlier work, the reader is referred to table I in the paper by Kiernan et al. (1994) which lists energies from Ahmed and Lipsky (1975), Nicolaidis and Beck (1977), Safronova and Senashenko (1978), Simons et al. (1979), and Chung (1982).

As seen from table 3.2, all the photoexcitation measurements agree on the position of the resonance within the accuracy of the experiment. The most precise experimental value is $142.28 \pm 0.03\text{eV}$. The variation in the values for the width is larger. The first photoabsorption (Kiernan et al., 1994) and the first photoelectron experiment (Journel et al., 1996) agree on the width 200 ± 40 meV which is, within experimental errors, not significantly different from the value reported in the more recent measurements. The latter all agree within the uncertainty. The average experimental value is about $120 - 130$ meV. For the q parameter most experiments point to a value of q around -2 .

The theoretical values for the position agree with the experimental results within the accuracy of the data. Also the values for the width agree with the measured values. The variation in the theoretical q parameter is similar to the variation in the experimental values.

Table 3.2: Selected experimental and theoretical values for the Li(2s2s2p²P^o) resonance. The energies are term energies relative to the Li(1s1s2s²S^e) ground state.

Experimental	E_0 (eV)	Γ (meV)	q
Crossed beam ^a	143.1(1)		
Photoabsorption ^b	142.32(5)	200(40)	-2.2(6)
Photoion ^c	142.32(2)	140(20)	-2.0(3)
Photoion ^d	142.35(10)	150(20)	-2.2(1)
Photoelectron ^e	142.30(5)	200(40)	-1.4(4)
Photoelectron ^f	142.28(3)	118(30)	
Photoion ^g	142.33(10)	124(30)	-1.87(3)
Photoelectron ^h	142.28(3)		
Theoretical			
Saddle-point complex-rotation (SPCR) ⁱ	142.255	117.47	
R -matrix ^e	142.2	132	-1.86
R -matrix ^{f,j}	142.12	130	
R -matrix ^{k,g}	142.30	123	-2.17
Truncated diagonalization method ^l	142.255		
B splines complex-rotation ^m	142.3	131	-2.9
SPCR and K -matrix ⁿ	142.254	116	-2.13
B splines ^o	142.274	115.33	

^aFrom Müller et al. (1989).^bFrom Kiernan et al. (1994).^cFrom Kiernan et al. (1995).^dFrom Azuma et al. (1995).^eFrom Journal et al. (1996).^fFrom Diehl et al. (1996).^gFrom Wehlitz et al. (1999).^hFrom Diehl, Cubaynes, Zhou, VoKy, Wulleumier, Kennedy, Bizau, Manson, Morgan, Blancard, Berrah and Bozek (2000).ⁱFrom Chung and Gou (1995).^jFrom VoKy, Faucher, Zhou, Hibbert, Qu, Li and Bely-Dubau (1998).^kFrom Berrington and Nakazaki (1998).^lFrom Conneely and Lipsky (2000).^mFrom Madsen et al. (2000*a*).ⁿFrom Fang and Chung (2001).^oFrom Hansen and Verbockhaven (2002, 2003).

Chapter IV

Theoretical *ab initio* methods for triply excited lithium

To make a correct interpretation of experimental spectra of the triply excited states in lithium, it is essential to have theoretical predictions for the energy positions and widths of the resonances. For the assignment and understanding of the electron-electron correlations, it is also desirable to be able to calculate other quantities such as, for example, the dominant configurations.

The photoexcitation experiments of section 3.3 gave new stimulus to *ab initio* calculations, aiming not only at the determination of energies and widths, but also at the prediction of the photoionization cross-section. For these purposes different methods have been used. These include the *R*-matrix, the saddle-point, and the truncated diagonalization methods. The latter also in combination with a fully numerical *B*-spline basis and complex scaling.

Basically, all those theories are concerned with the solution of the non-relativistic time-independent Schrödinger equation

$$H\Psi = E\Psi, \quad (4.1)$$

with the Hamiltonian (ignoring spin-dependent terms)

$$H = \sum_{i=1}^3 \left(\frac{\mathbf{p}_i^2}{2} - \frac{1}{r_i} \right) + \sum_{i<j}^3 \frac{1}{|\mathbf{r}_i - \mathbf{r}_j|}. \quad (4.2)$$

If we ignore the electron-electron interaction part, the Hamiltonian is reduced to a sum of independent single-electron interactions $\sum_{i=1}^3 (\mathbf{p}_i^2/2 - 1/r_i)$, the solution of which is a product of three analytically known Coulomb wave functions.

The electron-electron interaction terms introduce tremendous complications for the solution of equation (4.1). Firstly, the electron-electron interaction introduces correlations between the three electrons. The $\sum_{i<j}^3 |\mathbf{r}_i - \mathbf{r}_j|^{-1}$ part of the Hamiltonian (4.2) is, for example, not diagonal in a basis of antisymmetrized products of single-electron hydrogenic configurations. This means that the single-electron quantum numbers are no longer good quantum numbers,

and the eigenfunctions are necessarily represented as superpositions of configurations. Secondly, there is the question of quantum statistics. Electrons are fermions, and, accordingly, the total wave function written as a linear combination of products of space and spin wave functions must be antisymmetric under the exchange of any pair of electrons. The correlation associated with the antisymmetrization of the total wave function is referred to as Pauli correlation. Antisymmetrization of the total wave function is a trivial problem for the two-electron system because, in that case, the four dimensional spin space spanned by two spin 1/2 particles is completely exhausted by states that are either symmetric (the triplet states) or antisymmetric (the singlet state). The symmetry of the spin wave function then dictates the symmetry on the spatial part. For three-electron systems there are spin states without any overall exchange symmetry. Therefore the question of antisymmetrization needs special attention. We will return to this question later (see chapter 5).

4.1 R -matrix calculations

4.1.1 R -matrix theory for photoionization

R -matrix theory is efficient for the study of photoionization of atoms because exchange and correlation effects between the photoelectron and the residual electrons in the ion are confined to a limited volume of configuration space centred around the nucleus. In the R -matrix method, the initial step is to separate this complicated inner interaction region, enclosed within a sphere of radius a , from the outer region where the interaction is a simple function of the radial distance r of the electron from the nucleus. The full many-body problem is only solved “exactly” within the sphere $0 \leq r \leq a$. The R -matrix connects the two regions at the boundary $r = a$, and accounts for the net effect of the interactions in the inner region at the bounding surface. The matching of the inner solution with the solution in the outer region via the R -matrix allows the determination of the K -matrix, S -matrix and cross-section.

Progress in R -matrix theory was reviewed in the monograph edited by Burke and Berrington (1993). Also more recent papers (Quigley and Berrington, 1996; Zatsarinny and Fischer, 2000) provide useful introductions to the theory. For completeness, the main ideas are recalled here.

The differential cross-section for photoionization of an $(N + 1)$ -electron atom with the ejection of an electron in the direction $\hat{\mathbf{k}}$ is, in the dipole approximation, proportional to the modulus square of the matrix element of the dipole operator \hat{O}_d between initial state Ψ_i and final state $\Psi_f^-(\hat{\mathbf{k}})$:

$$\langle \Psi_f^-(\hat{\mathbf{k}}) | \hat{O}_d | \Psi_i \rangle, \quad (4.3)$$

with

$$\hat{O}_d = \sum_{i=1}^{N+1} z_i \quad (4.4)$$

in the length gauge and with

$$\hat{O}_d = \sum_{i=1}^{N+1} \frac{\partial}{\partial z_i} \quad (4.5)$$

in the velocity gauge. Here z is the component of the space vector \mathbf{r} of the photoelectron along the photon polarization vector. Quantum theory is gauge invariant, so the theory formally predicts the same result for the photoionization cross-section with either of the forms (4.4) or (4.5). In practical calculations identical results in the two gauges is a good indication of converged results (Madsen, 2002).

The wave functions Ψ_i and $\Psi_f^-(\hat{\mathbf{k}})$ of equation (4.3) represent the initial bound state of the atom and the final scattering state of the ejected electron plus residual ion, respectively. The boundary condition for $\Psi_f^-(\hat{\mathbf{k}})$ is a plane wave in the direction of the ionized electron $\hat{\mathbf{k}}$ and ingoing waves in all open channels.

In the *R*-matrix method both Ψ_i and $\Psi_f^-(\hat{\mathbf{k}})$ are expanded in the inner region $0 \leq r \leq a$, in terms of energy-independent *R*-matrix basis functions ψ_k ($j = i, f$) (Burke and Taylor, 1975)

$$\Psi_j = \sum_k A_{jk} \psi_k, \quad (4.6)$$

where the A_{jk} expansion coefficients are described below and where the basis functions are expanded as

$$\begin{aligned} \psi_k = \mathcal{A} \sum_{ij} c_{ijk} \bar{\Phi}_i(\mathbf{x}_1, \mathbf{x}_2, \mathbf{x}_3, \dots, \mathbf{x}_N; \hat{\mathbf{r}}_{N+1} \sigma_{N+1}) u_{ij}(r_{N+1}) r_{N+1}^{-1} \\ + \sum_j d_{jk} \phi_j(\mathbf{x}_1, \mathbf{x}_2, \dots, \mathbf{x}_{N+1}). \end{aligned} \quad (4.7)$$

Here \mathcal{A} is the operator which antisymmetrizes the ionized electron coordinate with the N ionic electron coordinates. The quantities $\mathbf{x}_i = \mathbf{r}_i \sigma_i$ represent the space and spin coordinates of the i th electron, and $\bar{\Phi}_i$ are channel wave functions which are eigenstates for parity and of the total angular momentum L and spin S as obtained by coupling the angular momentum and spin of the multi-configuration wave function of the ion with those of the ionized electron. The radial continuum basis functions $u_{ij}(r_{N+1})$, which represent the ionized electron, are non-zero at the surface of the sphere, $r = a$. The functions ϕ_j are quadratically integrable functions which vanish at $r = a$. They are formed by the bound state orbitals describing the atom, and include configuration interactions and ensure the completeness of the basis. Finally, c_{ijk} and d_{jk} are expansion coefficients determined by diagonalization of the $(N + 1)$ -electron Hamiltonian appropriately modified to account for the non-vanishing surface terms at the boundary $r = a$, i.e., in the inner region the *R*-matrix basis functions ψ_k diagonalize the operator $H_{N+1} + L_{N+1}$, with $L_{N+1} = \sum_{i=1}^{N+1} \frac{1}{2} \delta(r_i - a) \left(\frac{d}{dr_i} - \frac{b-1}{r_i} \right)$ the Bloch operator (Bloch, 1957) and b an arbitrary constant.

Now we return to equation (4.6) and project on the channel wave function $\bar{\Phi}_i$. Evaluating on the surface $r = a$ yields the basic equations describing the solution to the photoionization problem in the inner region (Quigley and Berrington, 1996)

$$\mathbf{A}(E) = \epsilon^{-1} \mathbf{w}^T \mathbf{R}^{-1} \mathbf{F} \quad (4.8)$$

$$\mathbf{R}(E) = \mathbf{w} \epsilon^{-1} \mathbf{w}^T + \mathbf{R}_{\text{Buttle}}(E) \quad (4.9)$$

$$\mathbf{F}(E, a) = \mathbf{R} \dot{\mathbf{F}}, \quad \dot{\mathbf{F}} \equiv \left(\frac{d}{dr} - \frac{b}{a} \right) \mathbf{F} |_{r=a} \quad (4.10)$$

Here $\mathbf{A}(E)$ is the matrix of expansion coefficients, $\mathbf{F}(E)$ contains the projections $F_i(r)$ of Ψ on the channel wave function $\bar{\Phi}_i$, $F_i = \langle \bar{\Phi}_i | \Psi \rangle'$ where the prime denotes integration over all space and spin coordinates in the inner region except the relative radial coordinate of the ejected electron, \mathbf{w} consists of the surface amplitudes $a^{-1} w_{ik} = \langle \bar{\Phi}_i | \psi_k \rangle_{r=a}$, $\epsilon(E)$ is a diagonal matrix whose elements are $E_k - E$, $\mathbf{R}_{\text{Buttle}}(E)$ is a diagonal matrix with a correction introduced by Buttle (1967), \mathbf{R} is an $n \times n$ matrix with n the number of channels retained in the close-coupling expansion (4.7). This is the matrix from which the theory derived its name, the R -matrix theory. The matching condition for the radial wave function of the ionized electron is given by equation (4.10).

The amplitudes w_{ik} and poles E_k of the R -matrix are obtained directly from the eigenvectors and eigenvalues of $H_{N+1} + L_{N+1}$. Note that (4.8)–(4.10) are not the same for Ψ_i and $\Psi_f^-(\hat{\mathbf{k}})$ since the wave functions have different angular symmetries due to the absorption of the angular momentum carried by the photon. In the state Ψ_i all channels are closed; in $\Psi_f^-(\hat{\mathbf{k}})$ at least one channel is open. This imposes different boundary conditions on the F_i 's. The solutions to the radial equations satisfied by F_i in the external region $r > a$ were discussed by Burke and Taylor (1975). The total cross-section for photoionization can be expressed in terms of the quantities introduced in equations (4.8)–(4.10) and a matrix containing the matrix elements of the dipole operator between R -matrix basis states ψ_k (see, for example, Burke and Taylor (1975)).

In closing this section, it should be mentioned that the R -matrix approach has been implemented in a series of computer codes for atomic, molecular and optical physics. The method is uniquely effective for the production of interesting scattering data for a wide range of physical processes, and the generality of the method, which was developed for the description of atomic processes, is exemplified by calculations of interest for the modelling of stellar atmospheres (see the monograph of Burke and Berrington (1993) for further details). The precise experimental photoelectron data on hollow Li may be used to test and develop R -matrix computer codes even further.

4.1.2 R -matrix calculations on triply excited lithium

The experimental photoelectron data discussed in section 3.3.3 were published together with R -matrix calculations aiming at the determination of resonance

parameters, and partial and total photoionization cross-sections. The calculations were performed by VoKy, Faucher, Hibbert and collaborators, and the method of the calculations was essentially the same in all the papers. It was discussed in some detail in the paper by Journal et al. (1996), and in greater length by VoKy, Faucher, Hibbert, Li, Qu, Yan, Chang and Bely-Dubau (1998); VoKy, Faucher, Zhou, Hibbert, Qu, Li and Bely-Dubau (1998). The latter works also presented calculations of the angular distribution parameter β (equation (3.1)).

Berrington and Nakazaki also performed *R*-matrix calculations in the energy region of triply excited hollow lithium states (Berrington and Nakazaki, 1998; Wehlitz et al., 1999). As discussed by Berrington and Nakazaki (1998), the accuracy of the method is very sensitive to the choice of target states included in the expansion (see equation (4.7) above). In contrast to VoKy et al. Berrington and Nakazaki (1998) included pseudo-states in their expansion of the core target states that allowed for a representation of the double photoionization channel. Another difference in the two methods was the methods used to determine the resonance positions and widths, and to determine the assignment in terms of the dominant configuration $nl'n'l''$.

Calculations by VoKy and collaborators

In the *R*-matrix calculations of VoKy et al. a good representation of the lithium target ion Li^+ was obtained with 29 target states. The channel states $\bar{\Phi}_i$ of equation (4.7) were subsequently formed by coupling the angular momenta of the target states with the angular momentum of the ejected electron.

VoKy, Faucher, Hibbert, Li, Qu, Yan, Chang and Bely-Dubau (1998); VoKy, Faucher, Zhou, Hibbert, Qu, Li and Bely-Dubau (1998) discussed the choice of basis functions. Hartree-Fock or “spectroscopic” orbitals of the form $1snl$ with $l \leq n \leq 4$ were used to describe the target. Also included were certain correlation orbitals and ten doubly excited target states. The configuration interaction expansion of the target states included 151 basic configurations, giving 369 configuration couplings for the 29 target states. The calculated Li^+ energies were given in table III in the papers by VoKy, Faucher, Hibbert, Li, Qu, Yan, Chang and Bely-Dubau (1998); VoKy, Faucher, Zhou, Hibbert, Qu, Li and Bely-Dubau (1998) and compared with experimental energies. The energy difference between the calculated and the experimental values was almost constant — approximately 0.2 eV, indicating that the ground state energy was too high by this amount. This shift of about 0.2 eV is common to all the *R*-matrix calculations discussed here, and it was touched upon earlier in connection with the experimental results in section 3.3.

The initial bound and final continuum states of the lithium atom were calculated with a *R*-matrix radius of $a = 30.2a_0$, with a_0 the Bohr radius. For each orbital angular momentum of the ejected electron with $l \leq 4$, 38 continuum basis functions were used. The summation over the square integrable $(N + 1)$ -electron basis functions ϕ_j in equation (4.7) included only terms that had parent terms in the first summation of equation (4.7).

For identification purposes VoKy et al. were guided by assignments proposed by multiconfiguration Dirac-Fock (Azuma et al., 1995) and configuration interaction Hartree-Fock (Kiernan et al., 1995). They also adopted the quantum defect approximation (Seaton, 1983) and used

$$\frac{1}{2(n^*)^2} = E_{\text{threshold}}(2l2l' {}^{2S+1}L) - E([2l2l' {}^{2S+1}L]nl'' {}^2P^o) \quad (4.11)$$

with n^* the effective quantum number $n^* = n - \mu_n$, and μ_n the quantum defect. From the fitting of the numerical calculations to the experimental partial photoelectron cross-sections, the positions $E([2l2l' {}^{2S+1}L]nl'' {}^2P^o)$ of the resonances were precisely determined. For a particular target state, equation (4.11) may then be used to identify the resonance. Note in passing that an alternative method based on multichannel quantum defect theory was used by Li et al. (1996, 1997).

A collection of results on the lowest Li(2s2s2p²P^o) resonance is shown in table 3.2. The calculations of VoKy et al. (entries e,j,f in table 3.2) are in good agreement with the other experimental and theoretical results. For example, there is very satisfactory agreement between the calculations and the experimental photoelectron data of Journal et al. (1996). Also, as shown in the table and in figure 3.5, the R -matrix code produced very good agreement, on a relative scale, with the values of the measured partial cross-sections obtained at the Advanced Light Source in Berkely (Diehl et al., 1996). The agreement was good both in the energy range of the Li(2s2s2p²P^o) resonance and at higher energies at around 149–154 eV above the ground state. As exemplified in table 3.1, equally good agreement with theory was observed in the case of photoionization in the region of triply excited $2l2l'2l''$ even parity states (Cubaynes et al., 1996), and also, as shown in figure 3.7, the R -matrix predictions for the photoionization cross-section in the region of $2l2l'n''$, $n = \{3, 4, \dots, 8\}$ Rydberg series were satisfactory (Diehl, Cubaynes, Wuilleumier, Bizau, Journal, Kennedy, Blancard, VoKy, Faucher, Hibbert, Berrah, Morgan, Bozek and Schlachter, 1997).

Most recently the R -matrix method was used in a calculation of the angular distribution parameter β (equation (3.1)) in the vicinity of the Li(2s2s2p²P^o) (Diehl, Cubaynes, Zhou, VoKy, Wuilleumier, Kennedy, Bizau, Manson, Morgan, Blancard, Berrah and Bozek, 2000) and the Li(2p2p2p²P^o) (Diehl, Cubaynes, Zhou, VoKy, Wuilleumier, Kennedy, Bizau, Manson, Blancard, Berrah and Bozek, 2000) resonances. These theoretical calculations were essential in order to understand a shift in the minimum in the β -parameter with respect to the position of the resonance.

In the paper by Diehl, Cubaynes, Kennedy, Wuilleumier, Bizau, Journal, VoKy, Faucher, Hibbert, Blancard, Berrah, Morgan, Bozek and Schlachter (1997), R -matrix calculations were shown to reproduce the photoionization cross-section in the range up to 163 eV above the lithium ground state. However, as the energy increased the calculations became less accurate as, for example, seen from the comparison with the data in the region of the lowest triply excited state within the $n = 3$ manifold (Diehl, Cubaynes, Chung, Wuilleumier,

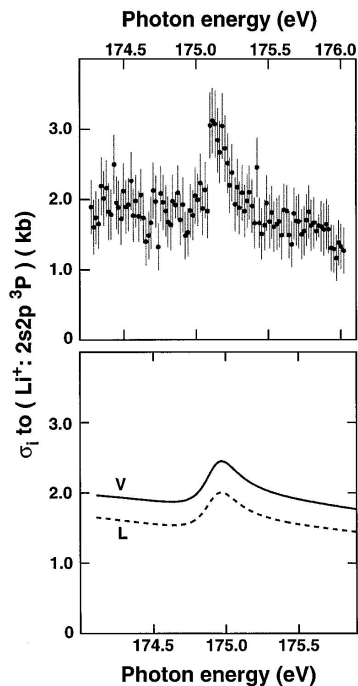


Figure 4.1: Upper part: experimental photoelectron cross-section of Li in the $\text{Li}^+(2s2p^3P^o)$ ionic channel as a function of the photon energy in the vicinity of the $\text{Li}(3s3s3p^2P^o)$ state. Lower part: corresponding *R*-matrix calculations convoluted with the experimental resolution and in velocity (V) and length (L) gauge forms. From Diehl, Cubaynes, Chung, Wulleumier, Kennedy, Bizau, Journal, Blancard, VoKy, Faucher, Hibbert, Berrah, Morgan, Bozek and Schlachter (1997).

Kennedy, Bizau, Journal, Blancard, VoKy, Faucher, Hibbert, Berrah, Morgan, Bozek and Schlachter, 1997). For this higher-lying state, the number of target states in the close-coupling expansion of the *R*-matrix basis states ψ_n (see equation (4.7)) was increased from 29 to 86 to represent the 3s3s, 3s3p, 3p3p and the other $3snl$ configurations for $n \leq 4$. Whereas the length and velocity forms of the photoionization cross-section (see equations (4.3)–(4.5)) gave results that were indistinguishable on the scale of the figures in all of the calculations discussed above, the two forms differed by $\sim 20\%$ for excitation into the doubly excited $\text{Li}^+(2s2p^3P)$ channel at excitation energies between 174 eV and 176 eV. This is shown in figure 4.1. For excitation into the higher channels ($[2s3s^3S + (2s3p^1P, 2p3s^1P)] \text{Li}^+$), the results obtained in the two gauges did not even agree qualitatively. Accordingly, the target orbitals entering the calculation should be improved to describe the higher-energy states accurately. Never-

theless, the R -matrix method gave a prediction of $E(3s3s3p^2P^o) = 174.90$ eV for the resonance position, which is in reasonable agreement with the measured value 175.165 ± 0.050 eV (Diehl, Cubaynes, Chung, Wulleumier, Kennedy, Bizau, Journal, Blancard, VoKy, Faucher, Hibbert, Berrah, Morgan, Bozek and Schlachter, 1997).

Calculations by Berrington and Nakazaki

The method of Berrington and Nakazaki (Berrington and Nakazaki, 1998; Wehlitz et al., 1999) differs somewhat from the calculations discussed above. Firstly, some additional pseudo-states were included in the description of the Li^+ target states. These pseudo-states allowed an approximate description of the double ionization continuum $\text{Li}^{++} + e^- + e^-$. This inclusion made possible a direct comparison with the photoion-yield experiment of Wehlitz et al. (1999) where the Li^{++} yield was monitored as a function of photon energy. Secondly, Berrington and Nakazaki (1998) used the so-called QB method (Quigley and Berrington, 1996) to identify the positions and widths of the resonances. For this latter purpose VoKy et al. fitted their calculated photoionization cross-sections by a Fano profile (Fano, 1961). Thirdly, Berrington and Nakazaki (1998) used the calculated form of the R -matrix wave function in the closed channels, the ϕ_j part of the expansion in equation (4.7), to extract the mixing coefficients d_{jk} in each closed channel. In this way a measure of the amplitude of the resonance state was obtained in each closed channel.

Berrington and Nakazaki (1998) used 25 Li^+ target states to describe total ionization and two additional states, $2s3s^3, ^1S^e$, to ensure convergence in the analysis of resonances. Berrington and Nakazaki (1998) just like VoKy et al. had an upward shift of 0.2 eV in the Li^+ ground state. This shift was accounted for by adding 0.2 eV to the energy scale. 28 continuum terms per channel $\bar{\Phi}_i$ (see equation (4.7)) were included. The R -matrix boundary was $a = 10a_0$.

For the $\text{Li}(2s2s2p^2P^o)$ resonance a position of $E_0 = 142.30$ eV and a width of $\Gamma = 123\text{meV}$ were found. The small quantitative difference with the saddle-point method results (Chung and Gou, 1995) (see table 3.2) was attributed to the fact that the double ionization continuum was neglected in the latter calculation.

The positions of 16 additional hollow states between 142.30 eV and 154 eV were determined and dominant configurations were assigned to some of the resonances. Table 7 in Berrington and Nakazaki (1998) exposes some remaining ambiguities in the identification: the QB method, the R -matrix method (Journal et al., 1996), and the saddle-point technique (Chung and Gou, 1995) did not agree on the assignment of all of the first five $^2P^o$ Li resonances between the $2s2p^3P$ and $2p2p^3P$ thresholds in Li^+ . Of particular interest are the calculations of energies and widths for all the 480 resonances of the type $2l2'l''$ for $n \leq 9$, $l'' \leq 3$ using the QB method (Berrington and Nakazaki, 1998). In section 4.3 we shall return to some of these results, compare them with other results (Verbockhaven and Hansen, 2000a) and discuss them in connection with

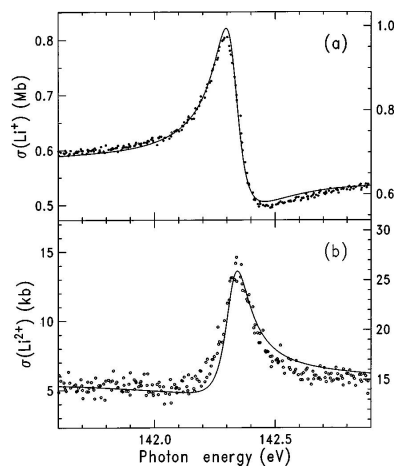


Figure 4.2: (a) Li^+ partial photoelectron cross-section on the vicinity of the $\text{Li}(2s2s2p\ ^2P^\circ)$ resonance. Circles are experimental results. Solid lines are calculations. The scale on the left side is for experimental data and the scale on the right side is for the theoretical curves. (b) Corresponding results for Li^{++} . From Wehlitz et al. (1999).

arguments put forward by Madsen (2001).

Figure 4.2 shows the measured and calculated partial photoionization cross-sections in the (a) Li^+ and (b) Li^{++} channels (Wehlitz et al., 1999). The theoretical profiles were shifted upwards in energy by 0.26 eV to match the experimental data. These were normalized to an absolute measurements by Mehlman et al. (1982) which were reported to have a systematic error of 20 %. Taking this error into account, figure 4.2(a) shows an excellent agreement between the measurements and the *R*-matrix calculations. For the Li^{++} -ion yield, on the other hand, figure 4.2(b) shows a difference in the size of the calculated and measured double-ionization cross-section. Despite this discrepancy, which might be due to the use of a basis which was not fully optimized for the direct double-ionization channel (Wehlitz et al., 1999), the asymmetry and sign of the *q* parameter was predicted correctly.

From the discussion of the *R*-matrix method, it is clear that the labelling in terms of particular electronic configurations is inherently difficult because of the different wave functions in the inner ($0 \leq r \leq a$) and external regions. Both the quantum defect (VoKy, Faucher, Zhou, Hibbert, Qu, Li and Bely-Dubau, 1998) and the QB methods (Quigley and Berrington, 1996) represent useful approaches for the identification of configurations.

4.2 Saddle-point technique

The saddle-point technique for the calculation of autoionizing states was developed by Chung and coworkers. The most important concept in this method is the explicit account of “hole” orbitals in the construction of the wave function of the multiply excited state. Formal aspects of the theory were presented by Chung (1979) who showed that a physical system with an inner-shell vacancy corresponds to the saddle-point energy solution in the Rayleigh-Ritz variation method if the vacancy is build explicitly into the wave function. Within the inner-vacancy-state picture, the method finds the best approximate solution to the stationary Schrödinger equation (Chung, 1979). The original formulation of the method was concerned with the solution of the bound-channel component of the wave function. The shortcoming of this approach is that it does not give the width of the resonance directly without including the open-channel parts of the problem. To circumvent the problem of including nonsquare-integrable components in the calculation for the description of the open-channel parts, Chung and Davis (1982) invoked the complex-scaling method to describe the continuum. Recently, the saddle-point technique was used in combination with complex scaling (Chung and Gou, 1995, 1996; Diehl, Cubaynes, Chung, Wuilleumier, Kennedy, Bizau, Journel, Blancard, VoKy, Faucher, Hibbert, Berrah, Morgan, Bozek and Schlachter, 1997; Zhang and Chung, 1998) and multichannel K -matrix theory (Fang and Chung, 2001; Chung and Fang, 2001) to calculate energies, widths and photoionization cross-sections for many triply excited states in lithium.

4.2.1 Saddle-point technique: theory

The physical observations that make the saddle-point method accurate and efficient for the evaluation of multiply excited states are (i) that the notion of an inner-shell vacancy is well-defined, no matter how complicated the resonance configuration might be, and (ii) that the continuum typically contributes very little to the energy of the resonance, and consequently its energy position can be accurately studied once the discrete part of its wave function is known. The truncated diagonalization method to be discussed in section 4.3 also makes use of this latter observation.

The starting point in the saddle-point method for triply excited Li states is to build the vacancies into the wave function. The closed-channel part of the wave function representing states with no n, l, n', l' and n'', l'' orbitals is written as

$$\Psi_b(1, 2, 3) = \mathcal{A} \left[\prod_{i=1}^3 (1 - P_{nl}(i))(1 - P_{n'l'}(i))(1 - P_{n''l''}(i)) \right] \psi(1, 2, 3), \quad (4.12)$$

with $\psi(1, 2, 3)$ a multiconfiguration wave function and \mathcal{A} the antisymmetrization operator. The projection operator for electron i ($i = 1, 2, 3$) onto the nl orbital

is

$$P_{nl}(i) = |\phi_{nl}(\mathbf{r}_i)\rangle\langle\phi_{nl}(\mathbf{r}_i)| \quad (4.13)$$

with ϕ_{nl} representing the orbital of the vacancy. The product of projection operators in equation (4.12) ensures that electron i is not in n, l , not in n', l' and not in n'', l'' . In general the vacancy orbitals are mutually orthogonal for different values of n and l and they depend non-linearly on parameters $\{q_v\}$. For example, the projection operator onto 1s for electron i is

$$P_{1s}(i) = |\phi_0(\mathbf{r}_i)\rangle\langle\phi_0(\mathbf{r}_i)|, \quad (4.14)$$

where the vacancy orbital is

$$\phi_0(\mathbf{r}) = N \exp(-q_v r). \quad (4.15)$$

Here N is a normalization constant and q_v is a 'non-linear' parameter to be optimized variationally (see below).

As an example, the choice $(1 - P_{1s}(1))(1 - P_{1s}(2))(1 - P_{1s}(3))$ for the projection operator leads to a bound state in equation (4.12), $\Psi_b(1, 2, 3)$ which describes states with configurations of the type $2l2l'nl''$. If higher-lying excited states are considered, the projection operators are changed accordingly. For example, in the calculation of the Li(3s3s3p²P^o) state (Diehl, Cubaynes, Chung, Wuilleumier, Kennedy, Bizau, Journal, Blancard, VoKy, Faucher, Hibbert, Berrah, Morgan, Bozek and Schlachter, 1997), the projection operator $\prod_{i=1}^3 (1 - P_{1s}(i))(1 - P_{2s}(i))(1 - P_{2p}(i))$ assured that the 1s, 2s and 2p vacancy states were explicitly accounted for in the construction of the resonance state wave function.

Chung (1979) proved a theorem which says that if one parameterizes the vacancy orbital ϕ_{nl} and $\Psi_b(1, 2, 3)$ (see equation (4.17) below), the discrete resonant spectrum of the Hamiltonian H can be obtained by maximizing the parameters in ϕ_{nl} and minimizing the parameters in $\psi(1, 2, 3)$ according to the variational method

$$\delta E = \delta \langle H \rangle = \delta \frac{\langle \Psi_b | H | \Psi_b \rangle}{\langle \Psi_b | \Psi_b \rangle} = 0. \quad (4.16)$$

The bound state Ψ_b is constructed from LS coupled trial functions (Chung, 1981)

$$\begin{aligned} \Psi_b(1, 2, 3) &= \mathcal{A} \sum C_{mnk}^{l_1 l_2 l_3} \\ &\times \left[\prod_{i=1}^3 (1 - P_{nl}(i))(1 - P_{n'l'}(i))(1 - P_{n''l''}(i)) \right] \psi_{mnk}^{l_1 l_2 L_{12} l_3}(1, 2, 3), \end{aligned} \quad (4.17)$$

with $l_1 l_2 l_3$ angular momenta, $C_{mnk}^{l_1 l_2 l_3}$ linear parameters and wave functions

$$\psi_{mnk}^{l_1 l_2 L_{12} l_3}(1, 2, 3) = \phi_{mnk}(r_1, r_2, r_3) Y_{l_1 l_2; L_{12}}^{l_3; LM}(\hat{\mathbf{r}}_1, \hat{\mathbf{r}}_2, \hat{\mathbf{r}}_3) \chi(1, 2, 3). \quad (4.18)$$

Here the angular component is given by

$$Y_{l_1 l_2; L_{12}}^{l_3; LM}(\hat{\mathbf{r}}_1, \hat{\mathbf{r}}_2, \hat{\mathbf{r}}_3) = \sum_{m_1 m_2 m_3 \mu} Y_{l_1 m_1}(\hat{\mathbf{r}}_1) Y_{l_2 m_2}(\hat{\mathbf{r}}_2) Y_{l_3 m_3}(\hat{\mathbf{r}}_3) \quad (4.19) \\ \times \langle l_1 l_2 m_1 m_2 | L_{12} \mu \rangle \langle L_{12} l_3 \mu m_3 | LM \rangle,$$

and the radial part by Slater type orbitals

$$\phi_{mnk}(r_1, r_2, r_3) = r_1^m r_2^n r_3^k e^{-(\alpha_i r_1 + \beta_i r_2 + \gamma_i r_3)}, \quad (4.20)$$

where α_i, β_i and γ_i are nonlinear parameters associated with the angular momentum and spin component considered. In equation (4.17) \mathcal{A} is the antisymmetrization operator and in equation (4.18) $\chi(1, 2, 3)$ is the spin wave function with total spin S . In equation (4.19) the standard notation of the Clebsch-Gordan coefficients ($\langle j_1 j_2 m_1 m_2 | jm \rangle$) is used and $Y_l m(\hat{\mathbf{r}})$ is the spherical harmonic of order l, m with polar and azimuthal angle determined by the direction of \mathbf{r} .

Inserting equation (4.17) into the variational form (4.16), the variation of E with respect to the linear parameters $C_{mnk}^{l_1 l_2 l_3}$ leads to a secular equation whose eigenvalue is a function of the nonlinear parameters $\alpha_i, \beta_i, \gamma_i$ and the non-linear parameters of the vacancy orbitals q_v . In line with the usual variational theorem, the best energy is found by minimizing it with respect to α_i, β_i and γ_i . The maximization of the parameter q_v is due to the theorem of Chung (1979). Combining these two optimizations, we see that there is a saddle-point with respect to variations in the parameters of ϕ_{nl} and $\psi_{mnk}^{l_1 l_2 l_3}$.

4.2.2 Saddle-point technique and complex scaling

The electron-electron correlations in a multiply excited atomic system cause decay into the continuum. To describe this decay the correct outgoing wave boundary conditions have to be imposed on the asymptotic wave function. In general, such boundary conditions cause numerical difficulties as they cannot *a priori* be handled within a square integrable basis. A very efficient approach for handling the electronic continuum is the method of complex scaling $r \rightarrow r e^{i\theta}$ which is based on the complex coordinate theorems of Aguilar and Combes (1971); Balslev and Combes (1971) (see, for example, the reviews by Moiseyev (1998) and Junker (1982)). In the complex scaling method, the standard problem of diagonalizing a Hermitian Hamiltonian is replaced by a problem which involves finding the eigenvalues of a non-Hermitian complex symmetric matrix. Resonance states are then described by square integrable eigenfunctions instead of a collection of continuum eigenstates of the unscaled Hamiltonian (Moiseyev, 1998).

The method of complex scaling was implemented by Chung and Davis (1982) in connection with the saddle-point technique. To obtain the width of the resonance, the total wave function is written as (Chung and Gou, 1995)

$$\Psi(1, 2, 3) = \Psi_b(1, 2, 3) + \sum_i \mathcal{A} \phi_i(1, 2) U_i(3), \quad (4.21)$$

where the bound state part $\Psi_b(1, 2, 3)$ is given by equations (4.12) and (4.17), and where $\phi_i(1, 2)$ represents a two-electron state of the Li^+ target wave function. In (4.21) the U_i 's represent the wave function of the outgoing electron and they are given by

$$U_i = \sum_n d_{i,n} r^n \exp(-\tilde{\alpha}_i r). \quad (4.22)$$

The wave functions of equation (4.22) contain linear parameters $d_{i,n}$ and nonlinear parameters $\tilde{\alpha}_i$. In the complex scaling calculation, the radial part r of U_i is complex scaled $r \rightarrow r e^{i\theta}$, with θ the complex scaling angle. When the term $\sum_i \mathcal{A}\phi_i(1, 2)U_i(3)$ is included in the calculation, the nonlinear parameters obtained from the saddle-point calculation of Ψ_b are retained, but the linear parameters are recalculated to allow for the full interaction between the open and closed-channel wave functions.

As seen from equation (4.21) the two-electron Li^+ target states $\phi_i(1, 2)$ are included in a controllable manner. For example, one could include only the $\text{Li}^+(1s1s \ ^1S^e)$ channel. In this way, the method of Chung and coworkers allows a determination of partial autoionization widths. By including many channels, one will get an estimate of the total fully coupled width. This flexibility of the saddle-point complex-rotation technique allows a detailed comparison with other theoretical results and, additionally, it is a feature which is not included in more conventional implementations of the complex rotation method which only give access to the total autoionization width of the resonance state.

4.2.3 Saddle-point technique: results on triply excited lithium

Chung (1982) applied the method to calculate the energies and wave functions for the eleven lowest triply excited lithium resonances of $^2P^o$, $^4P^e$, $^2D^e$, $^2P^e$, and $^2D^o$ symmetry. In that work the calculated resonance energy positions were compared with the resonances observed in the collision experiment by Rødbro et al. (1979) and an accurate assignment was given (see Table VII in the paper by Chung (1982)). For example, the energy of the $\text{Li}(2s2s2p \ ^2P^o)$ resonance was calculated to be 142.272 eV, which is in good agreement with more recent calculations and experiments (see table 3.2).

Following the photoabsorption experiment by Kiernan et al. (1994) and the photoion experiments by Kiernan et al. (1995) and Azuma et al. (1995), Chung and Gou (1995) reexamined nine triply excited states in lithium. These were the $2s2s2p \ ^2P^o$, $2s2p2p \ ^4P^e$, $2s2p2p \ ^2D^e$, $2s2p2p \ ^2S^e$, $2p2p2p \ ^2D^o$, $2s2p2p \ ^2P^e$, $2p2p2p \ ^2P^o$, $2s2p3p \ ^2P^e$, and $2s2p3p \ ^4P^e$ states. Compared with a previous work using the saddle-point technique (Chung, 1982), the basis set was much larger and the complex rotation technique was included to allow for a calculation of the (partial) widths of the resonances. The energies were typically improved by -0.001 to -0.003 a.u. One interesting exception was the $\text{Li}(2s2s2p \ ^2P^o)$ resonance, which was improved by -0.00994 a.u.. The term energy above the lithium ground state was reported to be 142.255 eV. Chung and Gou (1995) calculated partial, Γ_p , and total, Γ , widths for all nine resonances. Table 4.1 shows some of

Table 4.1: Energies E_0 above the lithium ground state, fully coupled widths Γ , and sum over individual partial widths $\sum \Gamma_p$ for some triply excited Li states. From Chung and Gou (1995).

Assignment	E_0 (eV)	Γ (meV)	$\sum \Gamma_p$ (meV)
$2s2s2p\ ^2P^o$	142.255	120.62	117.47
$2s2p2p\ ^2D^e$	144.762	92.63	89.99
$2s2p2p\ ^2S^e$	146.480	63.75	64.14
$2p2p2p\ ^2D^o$	146.917	81.18	81.57
$2s2p2p\ ^2P^e$	146.923	48.85	48.41
$2p2p2p\ ^2P^o$	148.729	51.84	52.14

the the intrashell results. The differences between the sum of the individual partial widths $\sum \Gamma_p$ and the fully coupled widths (including continuum–continuum couplings) are minor. The fully coupled width of the Li($2s2s2p\ ^2P^o$) resonance was reported to be $\Gamma = 117.47$ meV, substantially smaller than the value by Kiernan et al. (1994), but in better agreement with more recent experimental and theoretical values (see table 3.2.) Calculations were subsequently extended to higher members of the $^2P^o$ series (Chung and Gou, 1996).

The saddle–point complex–rotation technique was applied also for the interpretation of photoelectron spectroscopy measurements on the lowest “doubly” hollow state, the lowest state of $^2P^o$ symmetry with empty K as well as L shell. This Li($3s3s3p\ ^2P^o$) state was calculated to lie 175.12 eV above the Li($1s1s2s\ ^2S^e$) ground state. The width of the resonance was calculated to be $\Gamma \sim 282$ meV. These values were in agreement with the experimental data of $E_o(3s3s3p\ ^2P^o) = 175.165 \pm 0.050$ eV and $\Gamma = 250 \pm 50$ meV. For comparison we note that the R –matrix calculation predicted 174.90 eV for the energy position, but did not converge sufficiently to be able to give an estimate for the width. See also figure 4.1 and the accompanying discussion in section 4.1.2

In the discussion of the R –matrix method we mentioned the problem of assignment of resonances by their dominant configurations. In the saddle–point method the different space(angular)–spin components can easily be distinguished (Chung and Gou, 1996). The principal quantum numbers of the basis functions, however, are not easily extracted. In the calculations, the lowest triply excited states were identified on the basis of energy considerations. For the higher-lying resonances three factors helped with the identification. These were (i) the energy, (ii) the relative contribution to normalization of the angular–spin components, and (iii) a check of the relativistic perturbation corrections. The latter is a helpful guide to identification because a $2s2snl$ state has a higher relativistic correction than, for example, a $2s2pnl$ state, because the former is getting closer to the nucleus.

Zhang and Chung (1998) calculated even–parity states of the type $2s2l'nl''$ ($n \geq 3$), corresponding to $^2P^e$, $^2D^e$, and $^2S^e$ resonances. In table IV of that paper, the resonance energy positions and widths were compared with the R –

matrix calculations by Berrington and Nakazaki (1998) and experimental and R -matrix results by Cubaynes et al. (1996). Most of the calculated energies agreed well with those of Berrington and Nakazaki (1998). The agreement with the experiment and R -matrix results of Cubaynes et al. (1996) was less satisfactory, and there was also a disagreement in the identification. For the widths, there were found differences as large as a factor of 6 between the results of Zhang and Chung (1998) and Berrington and Nakazaki (1998). The smaller number of target states used by Berrington and Nakazaki (1998) ($1snl$, $n \leq 3$) compared with those used by Zhang and Chung (1998) ($1snl$, $n \leq 6$), suggests that the R -matrix widths are not fully converged (see also section 4.4.2).

Very recently Fang and Chung (2001); Chung and Fang (2001) combined the saddle-point technique with the K -matrix method to investigate total and partial photoionization cross-sections in the vicinity of triply excited lithium states. The convergence was checked by comparing predictions made in the different dipole forms of the photon-atom coupling. In most cases the agreement was excellent. The advantage of this method is that it combines the high accuracy of the saddle-point technique and, via the K -matrix, makes the determination of photoionization cross-sections possible. The saddle-point complex-rotation method, as discussed above, does not give information about the cross-sections, but only accounts for the structure of the system. The reader is referred to the papers by Fang and Chung (2001) and Chung and Fang (2001) and references therein for further details on the saddle-point K -matrix method.

4.3 Truncated diagonalization method

In the truncated diagonalization method, the Hamiltonian of equation (4.2) is diagonalized in a finite basis leaving out the open-channels which are built on ionization channels located energetically below the multiply excited state. This approach, which is formally based on Feshbach projection operator theory, was discussed by Lipsky and Russek (1966). A critical comparison between the saddle-point method and the Feshbach-type projection method was given by Chung (1990). By not including, for example, $1s$ orbitals in the three-electron basis, the $1s1s\ell$ continuum is effectively left out and this prevents unphysical energy shifts caused by accidental (near-)degeneracy between the resonance state and a discretized continuum. The shifts Δ_n of the bound state in the continuum due to the presence of the latter are normally small; for the lower triply excited states typically of the order of meV (Zhang and Chung, 1998). The shifts due to the interaction with the continua can subsequently be accounted for by perturbation theory.

As stated by Conneely and Lipsky (2002), the truncated diagonalization method does not yield energies as accurate as, for example, the saddle-point method (see section 4.2). The method makes it, however, possible to calculate extended Rydberg series and produce comprehensive configuration descriptions for each state. In contrast, the assignment of states in terms of dominant configurations is tedious both with the saddle-point technique and with the R -matrix

method.

4.3.1 Truncated diagonalization method: theory

A detailed account of the method was given by Ahmed and Lipsky (1975), and subsequently summarized by Conneely et al. (1992); Conneely and Lipsky (2000) and Conneely and Lipsky (2002). Following their presentation, the totally antisymmetric wave function for the three-electron system is expressed in terms of vector-coupled products of antisymmetric two-electron wave functions $\phi(1, 2 | L_j, S_j)$ constructed from two of the orbitals and multiplied by the wave function of the third electron, i.e.,

$$\Psi_i(1, 2, 3) = \sum_j a_{ij} [\phi(1, 2 | L_j, S_j) \varphi'_j(3)]^{LS} = \sum_j a_{ij} \Phi_j(1, 2; 3) \quad (4.23)$$

where $[]^{LS}$ denotes that the states are coupled to total angular momentum L and spin S , and where L_j and S_j are the intermediate angular momentum and spin of the “parent” $\phi_j(1, 2 | L_j, S_j)$. The wave function $\varphi'_j(\mathbf{r})$ is expressed as $\varphi'_j(\mathbf{r}) = R_{nl}(r) Y_{lm}(\hat{\mathbf{r}}) \chi_{1/2m}$ where $\chi_{1/2m}$ is the single-electron spin state, $Y_{lm}(\hat{\mathbf{r}})$ the spherical harmonic of order l, m and $R_{nl}(r)$ are hydrogenic functions of nuclear charge Z (in principle any set of mutually orthonormal basis functions $\{R_{nl}\}$ could be used, and in section 4.4 we shall discuss the construction of a fully numerical basis in terms of B -splines). The wave functions $\phi(1, 2 | L_j, S_j)$ are obtained by a two-electron configuration interaction calculation with an antisymmetric basis constructed straight forwardly from the φ_j 's (Ahmed and Lipsky, 1975).

The expansion coefficients a_{ij} of equation (4.23) are generalized fractional parentage coefficients, which guarantee that the linear combination (4.23) is totally antisymmetric. The way to construct these was discussed by Ahmed and Lipsky (1975). The energies and eigenstates are obtained by calculating and diagonalizing a matrix written symbolically as

$$\mathbf{H} = \mathbf{a} \mathbf{h} \mathbf{a}^T, \quad (4.24)$$

where \mathbf{a} is the matrix constructed from the a_{ij} 's and \mathbf{a}^T its transpose. The matrix \mathbf{h} has components

$$h_{ij} = \left\langle \Phi_i(1, 2; 3) \left| 3 \left(-\frac{1}{2} \nabla_{\mathbf{r}_3}^2 - \frac{Z}{r_3} + \frac{1}{r_{12}} \right) \right| \Phi_j(1, 2; 3) \right\rangle, \quad (4.25)$$

where the wave functions $\Phi_j(1, 2; 3)$ were defined in equation (4.23). From equation (4.25) it follows that the two-electron interactions can be calculated in terms of the matrix elements used in the two-electron problem

$$\left\langle \phi_i(1, 2 | n_1 l_1 n_2 l_2; L_i, S_i) \left| \frac{1}{r_{12}} \right| \phi_j(1, 2 | n'_1 l'_1 n'_2 l'_2; L_j, S_j) \right\rangle, \quad (4.26)$$

which are diagonal in L_i and S_i .

4.3.2 Truncated diagonalization method: results

Very recently Conneely and Lipsky (2002) presented a compilation of results on triply excited Li (and Be^+ , B^{++} and C^{+++}) obtained with the truncated diagonalization method. In their tables the $2,4\text{S}^{e,o}$, $2,4\text{P}^{e,o}$, $2,4\text{D}^{e,o}$ and $2,4\text{F}^{e,o}$ were considered. Energies, classifications, effective quantum numbers and configuration mixings were presented. The work also summarized the theoretical data by Conneely and Lipsky (2000). The diagonalization was performed with a basis including all configurations of the form n_1l_1, n_2l_2, n_3l_3 where $0 \leq l_i \leq l_{\max} = 5$ and $2 \leq n_i \leq n_{\max} = 20$ ($i = 1, 2, 3$) with the following restrictions. If only two of the electrons had n_i less or equal to 3, the third could be as large as n_{\max} . Otherwise the maximum value of n_i was 6. Since all the 1s orbitals were excluded, neither singly or doubly excited states were present in the basis. The data tables in Conneely and Lipsky (2002) contain the most extended Rydberg series reported in the literature with the principal quantum number of the Rydberg electron ranging up to 12.

The energy levels obtained were fitted to the Rydberg series (4.11). The thresholds were determined by diagonalizing the two-electron problem or by fitting $E_{\text{threshold}}$ to obtain a smooth behaviour of the quantum defect in the threshold region. The difference between the two threshold values is typically below 0.6% (Conneely and Lipsky, 2002).

The assignment of dominant configurations is particularly simple since the eigenstates are expanded on products of single-electron orbitals. Of particular interest for the present discussion are tables E and F of Conneely and Lipsky (2002). In table E triply excited state energies were compared with the R -matrix (Berrington and Nakazaki, 1998) and saddle-point results (Chung and Gou, 1995) as well as with the experimental data (Rødbro et al., 1979). For the $2s2p2p^4\text{P}^e$, $2p2p2p^2\text{D}^o$ and $[(2s2p)^3\text{P}^o3p]^4\text{P}^e$ resonances considered, theory agreed with experiment within errors and the differences between the theoretical predictions were typically below 0.05 eV. Table F presented the energies of the 4P^o Rydberg series of Li, and included the results of Berrington and Nakazaki (1998). Adjusting the ground state energy to -7.470976 a.u., the results were in good agreement.

In summary, the truncated diagonalization method is very suitable for the calculation of large amounts of structure data. Rydberg series are readily obtained by a single diagonalization, and — working with a quasi-complete configurational basis — the assignment of resonances is relatively straightforward.

4.4 *B*-splines approach for calculating triply excited states in lithium

To determine energies and widths of triply excited states in lithium, Hansen and Verbockhaven (Verbockhaven and Hansen, 2000*a*; Hansen and Verbockhaven, 2002, 2003) and Lambropoulos and co-workers (Madsen et al., 2000*a,b*; Madsen and Lambropoulos, 2001; Madsen, 2001) performed configuration interaction calculations with discretized basis sets constructed in terms of *B*-splines.

Hansen and Verbockhaven studied triply excited states with the truncated diagonalization method, and widths were calculated by applying Fermi's golden rule to the matrix element of the residual Coulomb interaction between the triply excited state and a set of target states in the Li^+ ion (Verbockhaven and Hansen, 2000a; Hansen and Verbockhaven, 2002, 2003). Madsen et al. performed configuration interaction calculations in combination with the method of complex rotation to determine energies and widths. The aim of these calculations was not only to consider the structure of the atom, but also to study laser-induced transitions among triply excited states. Also Bachau (1996) used a B -splines basis in investigations of non-radiative decay probabilities along the lithium isoelectronic sequence. Applications of B -splines in atomic and molecular physics was thoroughly reviewed by Bachau et al. (2001). For completeness, the next section will present some of the key formulae and highlight some of the main advantages of the method.

4.4.1 B -splines approach: theory

B -splines are piecewise polynomials designed to approximate an arbitrary function over a finite interval. The monograph by de Boor (1978) covers the properties in detail and also includes useful routines. Basically, the spirit of a B -spline calculation is to confine the system to a (large) box/sphere $[O; R]$ chosen to accommodate properly for the spatial extent of the physical system at hand. Within this box the radial function P_{nl} is expanded in terms of B -splines of order k defined on a grid $\{r_j\}$ (see equation (4.36) below). We denote such a set of N B -splines by $\{B_{i,k}\}$ ($i = 1, 2, 3, \dots, N$). Formally, the B -splines basis set is constructed inside the interval $[O; R]$ by the specification of a knot sequence $t_i (t_{i+1} > t_i)$. The B -splines of order k are defined recursively by

$$B_{i,1}(x) = \begin{cases} 1 & t_i \leq x \leq t_{i+1} \\ 0 & \text{otherwise,} \end{cases} \quad (4.27)$$

and

$$B_{i,k}(x) = \frac{x - t_i}{t_{i+k-1} - t_i} B_{i,k-1} + \frac{t_{i+k} - x}{t_{i+k} - t_{i+1}} B_{i+1,k-1}(x). \quad (4.28)$$

From these definitions, it is seen that the i th spline of order k is a polynomial of order $k - 1$, non-vanishing only for points inside the interval $[t_i, t_{i+k}]$. It is possible to define a knot sequence, allowing multiplicities of the knot points. In normal cases the endpoints are chosen to have k -multiplicity meaning $t_1 = t_2 = \dots = t_k = 0$ and $t_N = t_{N+1} = \dots = t_{N+k} = 0$, where N is the number of B -splines.

Full advantage of the properties of the B -splines is taken when evaluating integrals. Integrals involving wave functions lead to integrals containing only B -splines. For example, the integral $\int_0^R dr P_{nl}(r) q P_{n'l'}(r)$ is reduced, via the B -spline expansion (4.36), to $\sum_{i,j}^{N-1} c_i^{(nl)} c_j^{(n'l')} \langle B_i | q | B_j \rangle$ where q can be any operator. In the present context typical forms of this operator are

$q = 1, r, 1/r, d/dr, d^2/dr^2$. Computer codes for the evaluation of such matrix elements are available (de Boor, 1978). If $q(r)$ is a polynomial up to order $2k - 1$, the integrals calculated with k th order Gaussian quadrature are exact.

The specification of the knot sequence is crucial to the problem. Typical distributions are sine-like and exponential-like (see, for example, Nikolopoulos and Madsen (2003)). Depending on the problem at hand, the selection of the grid type may be essential for an accurate result. If one aims at a precise determination of the ground state of the atomic system, an exponential grid centred around the nucleus is appropriate since this provides a dense grid near the origin where the electron cloud of the ground state is centred.

Calculation of the energies of bound states is possible even in a small box, but for Rydberg states or continuum states a large box is necessary. The number of B -splines is chosen in such a way that a reasonable density of grid points is obtained. Stability of the results with respect to the magnitude of R is a criterion for convergence of the calculations.

Returning to the calculation of wave functions and energies, the starting point is the determination of one-electron orbitals. The one-electron orbitals are written as

$$\phi_{nlm}(\mathbf{r}) = \frac{1}{r} P_{nl}(r) Y_{lm}(\hat{\mathbf{r}}) \quad (4.29)$$

where $Y_{lm}(\hat{\mathbf{r}})$ is a spherical harmonic and where $P_{nl}(r)$ satisfies the one-dimensional Schrödinger equation for motion in the Coulomb field

$$\left(-\frac{1}{2} \frac{d^2}{dr^2} - \frac{Z}{r} + \frac{l(l+1)}{2r^2} \right) P_{nl}(r) = \epsilon_{nl} P_{nl}, \quad (4.30)$$

or, e.g., the one-dimensional frozen core Hartree-Fock equation

$$\left(-\frac{1}{2} \frac{d^2}{dr^2} - \frac{Z}{r} + \frac{l(l+1)}{2r^2} + V_l^{HF}(r) \right) P_{nl}(r) = \epsilon_{nl} P_{nl}(r), \quad (4.31)$$

where $V_l^{HF}(r)$ is the frozen core Hartree-Fock potential (see, for example, Chang and Kim (1986)) given by

$$\begin{aligned} V_l^{HF}(r) &= \sum_{n_c l_c}^{core} 2 \left[\frac{2l_c+1}{2l+1} \right]^{1/2} (l \| V^0(P_{n_c l_c}, P_{n_c l_c}; r) \| l) P_{nl}(r) \\ &\quad - \frac{1}{2l+1} \sum_{n_c l_c, \nu}^{core} (-1)^\nu (l \| V^\nu(P_{n_c l_c}, P_{nl}; r) \| l_c) P_{n_c l_c}(r) \\ &\quad + V_p(l, r), \end{aligned} \quad (4.32)$$

where $(l \| V^\nu(a, b; r) \| l')$ are reduced matrix elements

$$\begin{aligned} (l \| V^\nu(P_{n_a l_a}, P_{n_b l_b}; r) \| l') &= (l \| C^{[\nu]} \| l') (l_a \| C^{[\nu]} \| l_b) \\ &\quad \times \int_0^\infty dr' P_{n_a l_a}(r') P_{n_b l_b}(r') \frac{(r <)^\nu}{(r >)^{\nu+1}}, \end{aligned} \quad (4.33)$$

with $r_> = \max\{r, r'\}$ and $r_< = \min\{r, r'\}$ and where $(l\|C^{[V]}\|l')$ is proportional to a Clebsch-Gordan coefficient

$$(l\|C^{[V]}\|l') = (-1)^\nu \sqrt{(2l+1)} \langle l\nu 00 | l\nu l' 0 \rangle. \quad (4.34)$$

Finally, $V_p(l, r)$ is the core-polarization potential

$$V_p(l, r) = \frac{\alpha_l}{r^4} [1 - \exp(-(r/r_l)^6)], \quad (4.35)$$

and α_l is the static polarizability of the core and r_l are cut-off parameters.

In either case, the radial functions $P_{nl}(r)$ are expanded on a set of B -splines $\{B_{i,k}\}$ ($i = 1, 2, \dots, N$) of total number N and order k , defined on $r \in [0; R]$. The first $B_{1,k}(r)$ and last $B_{N,k}(r)$ are excluded to ensure that the boundary conditions at the interval edges are fulfilled $P_{nl}(0) = P_{nl}(R) = 0$. Accordingly, the expansion in B -splines reads

$$P_l(r) = \sum_{i=2}^{N-1} c_i^{(l)} B_{i,k}(r). \quad (4.36)$$

Inserting (4.36) into either (4.30) or (4.31) leads to a $(N-2) \times (N-2)$ generalized symmetric eigenvalue equation

$$\mathbf{A}^{(l)} \mathbf{C}^{(l)} = \epsilon_l \mathbf{B} \mathbf{C}^{(l)}, \quad \mathbf{C}^{(l)} = (c_2^{(l)}, c_3^{(l)}, \dots, c_{N-1}^{(l)}), \quad (4.37)$$

where the matrices $\mathbf{A}^{(l)}$ and $\mathbf{B}^{(l)}$ are the interaction and overlap matrices. The solution to the system of equations (4.37) gives $(N-2)$ eigenvalues and $(N-2)$ eigenvectors which through equation (4.36) correspond to the eigenstates of the system. Since the calculations are performed in a box, all eigenvalues are discrete. A finite number of states with $\epsilon_{nl} \geq 0$ correspond to continuum states. The number of bound states strongly depends on the box size and this number increases with increasing box radius.

Recently Nikolopoulos and Madsen (2003) published a computer programme which generates the one-electron orbitals as described above and includes the possibility of making a complex scaling calculation. The relevant fully antisymmetric three-electron basis states may be constructed from the one-electron orbitals and used for the final diagonalization of the (residual) electron-electron interaction.

4.4.2 B -splines: triply excited Rydberg states

Verbockhaven and Hansen used the B -splines approach in combination with configuration-interaction calculations and the truncated diagonalization method to study many triply excited resonances in Li. The results were collected in the thesis of Verbockhaven (2000) and the method is described in the review by Bachau et al. (2001).

Depending on the potential in the single-electron Hamiltonian (equations (4.30)–(4.31)) different types of single-electron basis functions can be constructed. It was shown by Verbockhaven and Hansen (1999) that the use of a Hartree–Fock instead of a hydrogenic basis has computational advantages in the calculation of the structure of the three-electron system — most importantly, the stability of the energies is higher with the Hartree–Fock basis. Explicitly, the Hartree–Fock basis gives rise to a much smaller shift of the energies obtained by the truncated diagonalization method when including the interaction with the continuum (see table II in Verbockhaven and Hansen (1999) or table 8 in Bachau et al. (2001)).

Verbockhaven and Hansen (2000a) considered the autoionization of the triply excited $\text{Li}(2s2p(^3\text{P})nl^4\text{P}^o)$ Rydberg states. The two main findings of that work were that (i) the total Auger decay rate (in the uncoupled–continuum–approximation) is remarkably constant along the series (see table 4.2) and (ii) the decay rate is dominated by the contribution from the channel leaving nl unchanged.

These two observations are signatures of the fact that the Rydberg electron remains as a spectator while the inner $2s2p$ ‘core’ electrons cause the decay. Formally, this may be seen in the participator and spectator Rydberg model which was described by Fano and Cooper (1965) and considered by Madsen (2001) in the context of triply excited Rydberg series and their doubly excited limits in hollow lithium (a similar model was later considered by Piangos and Nicolaides (2001) in a discussion of He^- resonance).

To derive a formula which describes the above observations, we express the total autoionization width as an uncoupled sum over contributions from open channels j

$$\Gamma = \sum_j \Gamma_j = \sum_j 2\pi |\langle a | V | E_j \rangle|^2, \quad (4.38)$$

where $|E_j\rangle$ are the continua states and $|a\rangle$ is the discrete part of the resonance and V the configuration interaction. The wave function for the Rydberg state $|a_n\rangle = |a\rangle$ is characterized by its spatial behaviour in an ‘outer’ and ‘inner’ region. In the outer region, the Rydberg electron is far from the nucleus and only experiences the attractive Coulomb interaction, and consequently the wave function is a Coulomb wave with a phase distortion due to the interaction with the inner region. In the inner region, the ‘core’ and the kinetic energy parts of the Hamiltonian play a larger role than the small differences in the total energy of the Rydberg states, and the wave functions $|a_n\rangle$ for different n essentially only differ by a normalization constant N_n

$$|a_n\rangle = N_n |\tilde{a}\rangle, \quad (4.39)$$

which assures a continuous transition of the wave function across the threshold when the states are normalized per unit energy, i.e., $N_n^2 \sim 1/n^{*3}$ with n^* the effective principal quantum number. A formula for the total autoionization width of the Rydberg state, Γ_n , is then derived by dividing the continuum into two different classes. In one class no electron is left in the highly excited Rydberg

Table 4.2: Total autoionization decay widths Γ_n for the lowest members of the triply excited $\text{Li}(2s2p\ ^3\text{P})nl\ ^4\text{P}^o$ Rydberg series. The first column displays the value of the principal (n) and angular momentum (l) quantum numbers of the Rydberg electron. The results are taken from Verbockhaven and Hansen (2000a) (VH) and from Berrington and Nakazaki (1998) (BN)

nl	Γ_n (meV) (VH)	Γ_n (meV) (BN)
3s	9.95	8.8
3d	9.58	4.7
4s	9.62	1.0
4d	9.44	1.1
5s	9.44	0.4
5d	9.45	0.4
6s	9.44	0.3

state (*participator* model); in the other the electron is left ‘undisturbed’ in the Rydberg state (*spectator* model). The result for the total width is (Madsen, 2001)

$$\Gamma_n = N_n^2 \tilde{\Gamma}_{part} + \Gamma_{spect}, \quad (4.40)$$

where $\tilde{\Gamma}_{part}$ corresponds to the case where the outer Rydberg electron participates in the autoionization process. In this case, the inner part of the Rydberg state determines the contribution to the configuration interaction integral, and therefore the factorization (4.39) of the wave function is valid. The second width in equation (4.40), Γ_{spect} , corresponds to the case when the Rydberg electron remains as a passive spectator. In this case, the final continuum state has one electron ionized and the Rydberg electron still left in the highly excited state. Therefore the configuration interaction integrals pick up contributions from all of space, and accordingly, the factorization of equation (4.39) does not apply. Therefore the autoionization width Γ_{spect} is independent of n as it is the interaction between the core electrons that causes the autoionization.

We now return to the results of table 4.2 which show that the widths along the $\text{Li}(2s2p\ ^3\text{P})nl\ ^4\text{P}^o$ Rydberg series are approximately independent of the principal quantum number of the Rydberg electron. This again means that the Rydberg electron remains predominantly as a spectator, and in terms of equation (4.40) this means $\tilde{\Gamma}_{part} \simeq 0$. For comparison and to illustrate the complexity of these calculations, the widths of Berrington and Nakazaki (1998) are included in table 4.2. In their R -matrix calculation, only $1snl$ target states with n up to 3 were included.

Madsen (2001) made the point that to the extent that the Rydberg electron does not participate significantly in the decay process, the total autoionization width belonging to the triply excited Rydberg state can be estimated from that of its doubly excited ionic limit. In the example considered above — the $2s2p\ ^3\text{P}^o nl\ ^4\text{P}^o$ states of lithium — this limit is the $2s2p\ ^3\text{P}^o$ state of the positive

lithium ion. The width of that particular state was calculated by Madsen (2001) using the *B*-splines approach in combination with complex rotation, and by Chung and Lin (1998) by the saddle-point complex-rotation technique. The results for the width were $\Gamma = 9.48$ meV (Madsen, 2001) and $\Gamma = 8.792$ meV (Chung and Lin, 1998). In particular the former width is close to the values of Verbockhaven and Hansen (2000*a*) as seen by table 4.2. It is of course attractive if estimates of the widths of triply excited Rydberg series can be obtained from the simpler doubly excited ionic limits.

The fact that the Rydberg electron stays as a spectator puts high demands on the representation of target states in Li^+ . Verbockhaven and Hansen (2000*a*) showed that in addition to the $1snl''$ limit it is important to include the $1s(n+1)l''$ limit, which may be more important in the decay than the $1snl''$ limit due to nonorthogonalities. This explains, for example, why the total rates of Chung and Gou (1996) for the higher terms are smaller than the ones reported by Verbockhaven and Hansen (2000*a*)

4.4.3 *B-splines and complex rotation*

Lambropoulos and co-workers have used the *B*-spline approach in combination with complex rotation in papers concerned with (i) laser-induced transitions between triply excited states (Madsen et al., 2000*a,b*) and (ii) line shapes in the photoexcitation of triply excited hollow states (Madsen and Lambropoulos, 2001). The method was similar to the one first used by Brandefelt and Lindroth (1999) in their study of $^4\text{S}^e$ resonances in He^- below the $\text{He}^+(n=1)$ threshold (see also Brandefelt and Lindroth (2002)).

The complex-rotation *B*-spline calculations provided energies and widths as well as wave functions which were used for the calculations of dipole matrix elements. The complex rotation transformation $r \rightarrow r \exp(i\theta)$ (Aguilar and Combes, 1971; Balslev and Combes, 1971) with θ the complex scaling angle gives the complex scaled three-electron Hamiltonian

$$H(\theta) = \sum_{j=1}^3 h_j(\theta) + e^{-i\theta} \sum_{j < k} \frac{1}{r_{jk}}, \quad (4.41)$$

with $r_{jk} = |\mathbf{r}_j - \mathbf{r}_k|$ and

$$h_j(\theta) = -\frac{1}{2} \nabla_{\mathbf{r}_j}^2 e^{-2i\theta} - \frac{1}{r_j} e^{-i\theta}, \quad (4.42)$$

where the indices (j, k) run over the three electrons. The complex-rotation method means that the continuum wave functions become square integrable (fall off exponentially at large distances). This in turn means that the representation of the wave functions within a box $[O; R]$ may be expected to be accurate. The complex-rotation technique reveals the triply excited states through the complex energy $E = E_0 - i\Gamma/2$, where E_0 is energy position of the resonance and Γ its

width (for reviews on complex rotation, see, for example, the works of Junker (1982) and Moiseyev (1998)).

In the calculations, the one-electron orbitals were expanded in terms of spherical harmonics as in equation (4.29) and the radial parts $P_{nl}(r)$ which fulfill

$$\left[\frac{e^{-2i\theta}}{2} \frac{d^2}{dr_j^2} + E + \frac{e^{-i\theta}}{r} - \frac{e^{-2i\theta}l(l+1)}{2r_j^r} \right] P_{nl}(r_j) = 0, \quad (4.43)$$

were subsequently expanded in terms of a number N of B -splines of order k for $r \in [O; R]$ as in equation (4.36). The box size was chosen judiciously for the problem at hand. The demand on correlation, and the fact that each electron in the triply excited state on the average feels a larger nuclear charge than if the K shell were not empty favour a rather small box and good results were obtained with $R = (15 - 25)a_0$.

Although, in principle, also other ways of implementation with B -splines can be contemplated, in practice it is essential to have the one-electron orbitals available as this allows a detailed choice of configurations for the final diagonalization and, hence, makes the problem more tractable with respect to computer memory and computational time.

From the one-electron orbitals, the fully antisymmetric three-electron basis functions were constructed by angular momentum coupling and application of the antisymmetrization operator. The complex scaling angle $\theta = 0.2$ and the basis were chosen so as to represent sufficiently accurately the triply excited states as well as the dominant decay channels. 501 three-electron basis states for the $\text{Li}(2s2s2p^2P^o)$ state and 520 states for the $\text{Li}(2s2p2p^2D^e)$ state gave $E_0 = 2.24$ au, $\Gamma = 131$ meV and $E_0 = 2.14$ au, $\Gamma = 83$ meV, in reasonable agreement with the results of Chung and Gou (1995). 200 B -splines in a box of $R = 15a_0$ were used. In table II of Madsen et al. (2000*b*) resonance parameters for a series of states were compared with parameters from other calculations.

4.4.4 B -splines: laser-induced coupling between triply excited states

Besides providing an accurate structure of the lithium atom, the work of Madsen et al. (2000*a,b*) considered the possibility of coupling different triply excited states by a near-resonant laser (see figure 4.3). This allowed a controlled investigation of new layers of structure and a scan through states of different parity. And also, the calculation of the Li^+ ion yield as a function of the detuning $\delta = E_a - E_b - \omega_2$, where E_a and E_b are the resonance positions of the two triply excited states and where ω_2 is the laser photon energy (figure 4.3), for a variety of laser intensities, pointed to a direct measure of the ac Stark splitting of the resonance line. The ac Stark splitting is directly related to the Rabi frequency Ω_{ab} between the resonance states and hence the dipole coupling matrix element D_{ab} through the relation $\Omega_{ab} = \frac{1}{2} \cdot F_0 \cdot D_{ab}$ with F_0 the field strength of the laser field given by the square root of the intensity in atomic units, $F_0 = \sqrt{I}$, and with one atomic unit of intensity equal to $I_0 = 3.51 \times 10^{16}$ W cm⁻². This

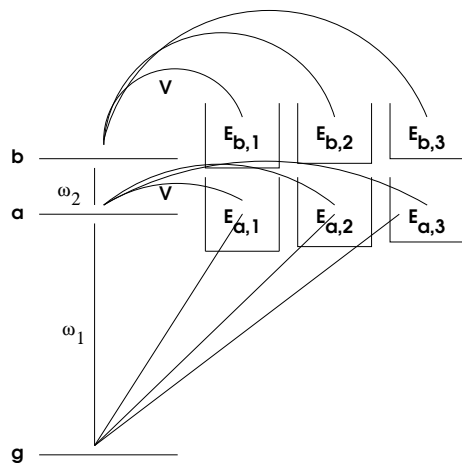


Figure 4.3: Level scheme. The $\text{Li}(1s1s2s^2S^e)$ ground state is denoted by $|g\rangle$. For the lower triply excited state, $\text{Li}(2s2s2p^2P^o)$, $|a\rangle$ denotes the discrete part and $|E_{a,j}\rangle$ ($j = 1, 2, 3, \dots$) the continuum parts. The ground state is coupled to the $\text{Li}(2s2s2p^2P^o)$ resonance by a synchrotron with angular frequency ω_1 . A laser of angular frequency ω_2 couples the $\text{Li}(2s2s2p^2P^o)$ and $\text{Li}(2s2p2p^2D^e)$ triply excited states. The latter state has discrete part $|b\rangle$ and continua $|E_{b,k}\rangle$ ($k = 1, 2, 3, \dots$). The discrete parts $|a\rangle$ and $|b\rangle$ are coupled to the continua via the configuration interaction, V , giving rise to autoionization rates Γ_a and Γ_b . Three continua are shown for each discrete state. Figure adopted from Madsen et al. (2000b)

is a direct way of studying couplings between the highly correlated manifolds of the four-body Coulomb problem.

The proposed scheme is sketched in figure 4.3. In the figure $|g\rangle$ denotes the $\text{Li}(1s1s2s^2S^e)$ ground state, $|a\rangle$ and $|E_{a,j}\rangle$ ($j = 1, 2, 3, \dots$) denote the discrete and continua parts of the $\text{Li}(2s2s2p^2P^o)$ resonance. This state is reached from $|g\rangle$ by absorption of a photon from a synchrotron radiation beam with angular frequency ω_1 . The $|b\rangle$ and $|E_{b,j}\rangle$ ($j = 1, 2, 3, \dots$) denote the discrete and continua parts of the $\text{Li}(2s2p2p^2D^e)$ triply excited state which is coupled to the $\text{Li}(2s2s2p^2P^o)$ state via a laser with an angular frequency of ω_2 tunable around the $\text{Li}(2s2s2p^2P^o) \rightarrow \text{Li}(2s2p2p^2D^e)$ resonance frequency, i.e., $\omega_2 \sim 2.5$ eV.

The processes shown in figure 4.3 were modelled by expressing the wave function of the lithium atom under the field by the state expansion

$$\begin{aligned}
 |\psi(t)\rangle &= C_g(t)|g\rangle + C_a(t)|a\rangle + C_b(t)|b\rangle \\
 &+ \sum_j \int dE_{aj} C_{E_{aj}}(t) |E_{a,j}\rangle + \sum_k \int dE_{bk} C_{E_{bk}}(t) |E_{b,k}\rangle.
 \end{aligned} \tag{4.44}$$

The Hamiltonian describing the system was written as

$$H = H_0 + V + D(t), \tag{4.45}$$

with $H_0|s\rangle = E_s|s\rangle$ ($s = g, a, b, E_{aj}E_{bk}$), V the configuration interaction and D the dipole coupling. Inserting (4.44) into the time-dependent Schrödinger equation

$$i\partial_t|\psi(t)\rangle = H|\psi(t)\rangle \quad (4.46)$$

and projecting on the individual states in the expansion (4.44) led to a set of coupled differential equations which were simplified by treating the continua as sinks (no back coupling from the continuum to the discrete parts), and by neglecting the non-energy conserving photon exchange processes which are due to the counter-rotating parts of the oscillating sinusoidal dipole interaction. The resulting equations were given explicitly in Madsen et al. (2000a) and in Madsen et al. (2000b). In section 2, the simple case of one discrete state in one continuum was considered. The physical entities that enter the coupled equations are detunings, energy positions, autoionization widths, as well as the atomic parameters describing the laser-induced couplings between the triply excited states. Also the Fano line-shape parameters (Fano, 1961) for the $|g\rangle \rightarrow |a\rangle$ and $|a\rangle \rightarrow |b\rangle$ transitions enter the equations. As detailed in the appendix of Madsen et al. (2000b), all the relevant parameters are calculated from the complex scaled wave functions. For example, the matrix element for the coupling between the $\text{Li}(1s1s2s^2S^e)$ ground state and the $\text{Li}(2s2s2p^2P^o)$ triply excited states is

$$D_{ga}^F = \bar{D}_{ga} \left(1 - \frac{i}{q_a} \right) \quad (4.47)$$

which, to make the connection to complex scaled quantities, is re-written as

$$\begin{aligned} D_{ga}^F &= \langle g| \left(D + \sum_j \int dE_{aj} \frac{D|E_{aj}\rangle \langle E_{aj}|V}{E_g + \omega_1 - E_{aj}} \right) |a\rangle \\ &= \langle g|D \left(1 + \sum_j \int dE_{aj} \frac{|E_{aj}\rangle \langle E_{aj}|V}{E_g + \omega_1 - E_{aj}} \right) |a\rangle \\ &= \langle \bar{g}_\theta | D | a_{\theta, (E_g + \omega_1)}^{(R)} \rangle \end{aligned} \quad (4.48)$$

with $|a_{\theta, (E_g + \omega_1)}^{(R)}\rangle$ the complex scaled wave function of the triply excited $2s2s2p^2P^o$ state.

Figure 4.4 shows the Li^+ photoion yield as a function of the detunings for laser intensities of $1.4 \times 10^7 \text{ Wcm}^{-2}$ (full curve), $1.4 \times 10^{10} \text{ Wcm}^{-2}$ (dot-dashed curve), $1.4 \times 10^{11} \text{ Wcm}^{-2}$ (dashed curve) and $1.4 \times 10^{12} \text{ Wcm}^{-2}$ (long-dashed curve). The intensity of the 10 ps synchrotron pulse was $4 \times 10^8 \text{ Wcm}^{-2}$. The figure shows how the line-shape changes with the increase in the intensity of the laser, and how a double-peak structure is build up. This is the double-peak structure alluded to above, and it is due to the ac Stark splitting induced by the laser which couples $|a\rangle$ and $|b\rangle$.

The requirements for the experimental observability on laser intensities and the synchrotron source should be within the range of recent and ongoing exper-

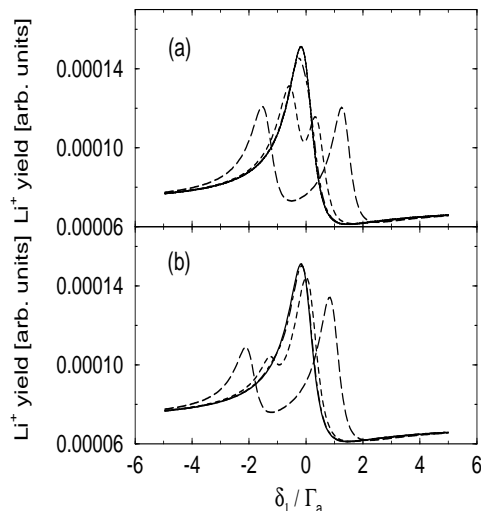


Figure 4.4: Li^+ photoion yield as a function of the detuning δ_1 for the transition between the ground state and the $\text{Li}(2s2s2p^2P^\circ)$ triply excited state. The laser which couples the $\text{Li}(2s2s2p^2P^\circ)$ and $\text{Li}(2s2p2p^2D^\epsilon)$ states is (a) on resonance and (b) detuned to the red with an amount equal to the width of the $\text{Li}(2s2s2p^2P^\circ)$ resonance. In the figure, $\Gamma_a = 131$ meV was used for the width of the $\text{Li}(2s2s2p^2P^\circ)$ triply excited state. From Madsen et al. (2000b)

iments. A very interesting prospect for the future would be to probe the triply excited states with radiation from the large-scale free-electron projects — the linac Coherent Light Source at Stanford and the TESLA project in Hamburg. The TESLA test facility has begun operation in the far-ultraviolet regime, and recently a study on the interaction of the intense soft X-rays with atom clusters was reported (Wabnitz et al., 2002).

4.4.5 *B-splines: partial widths and line shapes in photoexcitation of triply excited states*

Hansen and Verbockhaven (2002) published a work on partial widths of the $\text{Li}(2s2s2p^2P^\circ)$ triply excited state. The results were obtained with the *B-splines* approach using a Hartree-Fock wave function for the $1snl$ target state of Li^+ . The widths were compared with saddle-point complex-rotation results by Chung and Gou (1995) and with *R*-matrix calculations by Berrington and Nakazaki (1998). Table 4.3 shows some of the results. The reader should consult table 3.2 for a comparison of the total width with the experimental values. The calculations by Hansen and Verbockhaven (2002) were performed in the uncoupled continuum approximation, whereas the other approaches either included continuum coupling in the total width (Chung and Gou, 1995) or in both total and partial widths (Berrington and Nakazaki, 1998). The calculated total widths were in good agreement with each other. Chung and Gou compared

Table 4.3: Partial and total autoionization widths in meV for for the Li(2s2s2p $^2P^o$) resonance in three recent calculations. In column 1, the l -value of the continuum electron is given in parentheses. Adapted from Hansen and Verbockhaven (2002)

Channel	B -spline ^a	Saddle-point ^b	R -matrix ^c
1s2p $^3P^o$ (s)	60.40	66.02	48
1s2p $^3P^o$ (d)	7.59	6.76	9.8
1s2p $^1P^o$ (s)	17.76	20.52	11
1s2p $^1P^o$ (d)	1.07	1.25	7.4
1s2s $^3S^e$ (p)	2.61	3.65	7.4
1s2s $^1S^e$ (p)	25.34	22.41	21
1s3d $^3D^e$ (p)	0.51		
1s3s $^3S^e$ (p)	0.03	0.03	
1s3s $^1S^e$ (p)	0.01	0.08	
1s1s $^1S^e$ (p)	0.01	0.05	
Total width	115.33	117.47	123
Ratio 1s2p $^3P^o$ /1s2p $^1P^o$	3.6	3.3	3.1

^aFrom Hansen and Verbockhaven (2002, 2003). Continuum coupling not included.

^bFrom Chung and Gou (1995). Continuum coupling included for total, not for partial widths.

^cFrom Berrington and Nakazaki (1998). Continuum coupling included.

the total width including all continuum couplings (117.47 meV) and the sum of the partial widths in the uncoupled-continuum approximation (120.62 meV) which shows that the effect of continuum coupling is small. The partial widths obtained by the B -spline and the saddle-point complex-rotation methods also agree very well as seen from table 4.3. The R -matrix predictions for the partial widths, however, clearly deviate from the other theories.

Another interesting point made in the work by Hansen and Verbockhaven (2002) is the possibility of measuring partial autoionization widths in angle-resolved photoelectron spectrometry (Diehl, Cubaynes, Zhou, VoKy, Wulleumier, Kennedy, Bizau, Manson, Morgan, Blancard, Berrah and Bozek, 2000; Diehl, Cubaynes, Zhou, VoKy, Wulleumier, Kennedy, Bizau, Manson, Blancard, Berrah and Bozek, 2000). As discussed in section 3.3.3, the angular distributions of the direct photoionization electrons and the electrons coming from the autoionizing process are different. For relative cross-sections, ratios between partial cross-sections can be extracted and compared with theory. For example, the theoretical ratios of the partial widths of the 1s2p $^3P^o$ to the 1s2p $^1P^o$ were 3.6 (Hansen and Verbockhaven, 2002), 3.3 (Chung and Gou, 1995), 3.1 (Berrington and Nakazaki, 1998), whereas a ratio of ~ 4.5 was extracted by Hansen and Verbockhaven (2002) from the experimental results (Diehl, Cubaynes, Zhou, VoKy, Wulleumier, Kennedy, Bizau, Manson, Morgan, Blancard, Berrah and Bozek, 2000).

Hansen and Verbockhaven have used their method to consider other systems, and in one work (Verbockhaven and Hansen, 2001) they calculated energies and widths for autoionizing states in Li, Be⁺, and Be⁺⁺ between the 1s1s¹S^e and 1s2s³S^e ionization limits. Using a singular value decomposition scheme may speed up the computations with as much as a factor of ten (Verbockhaven and Hansen, 2000*b*).

At excitation energies greater than 151.7 eV above the Li ground state, two-step autoionization becomes possible. In this process, the triply excited state first autoionizes to a doubly excited state in Li⁺ and secondly the Li⁺⁺ state autoionizes to a state in Li⁺ (see figure 3.6). The Auger electron of the latter decay determines the decay channel and may be detected as a function of the frequency of the synchrotron radiation (Diehl, Cubaynes, Chung, Wuilleumier, Kennedy, Bizau, Journel, Blancard, VoKy, Faucher, Hibbert, Berrah, Morgan, Bozek and Schlachter, 1997; Diehl, Cubaynes, Kennedy, Wuilleumier, Bizau, Journel, VoKy, Faucher, Hibbert, Blancard, Berrah, Morgan, Bozek and Schlachter, 1997; Diehl, Cubaynes, Wuilleumier, Bizau, Journel, Kennedy, Blancard, VoKy, Faucher, Hibbert, Berrah, Morgan, Bozek and Schlachter, 1997).

This situation was analyzed in detail by Madsen and Lambropoulos (2001). Let $|g\rangle$ and $|a\rangle$ denote the ground state and a triply excited state in Li. Let $|j\rangle$ denote a particular continuum channel with a doubly excited core. Finally, let $|f\rangle$ denote the 1s ground state in the Li⁺⁺ ion located approximately 81 eV above the ground state. For triply excited states which are higher in term energy than ~ 173 eV, it becomes energetically possible to decay into the excited state Li⁺⁺($2l$), ($l = s, p$). However, this causes no difficulty in the analysis since the experiments always measured the Auger electrons which decay to the Li⁺⁺(1s) ground state from doubly excited states in Li⁺ with term energy *less* than 173 eV. The signal will be proportional to the transition rate into the final state $|f\rangle$. Clearly, how much population goes into $|f\rangle$ will depend directly upon how much goes into the doubly excited Li⁺ state $|j\rangle$. This state is fed from the triply excited state $|a\rangle$ with autoionization rate $\Gamma_{a,j}$ and with the rate $\gamma_{g,j}$ from the ground state $|g\rangle$ by direct photoionization into $|j\rangle$, and these quantities can not be separated experimentally. It turns out that information about $\Gamma_{a,j}$ can be obtained from photoionization cross-section. Indeed, for the considered process the cross-section reads (Madsen and Lambropoulos, 2001)

$$\sigma_f^j \simeq \sigma_{g,j} + \frac{\frac{1}{2}\tilde{D}_{ga}^2 E_a^r}{\delta^2 + \Gamma_a^2/4} \left(\frac{\Gamma_{a,j}}{2} - \frac{\Gamma_a}{q_a q_{a,j}} + \frac{\Gamma_{a,j}}{2q_a^2} + \frac{2\delta}{q_{a,j}} \right) \quad (4.49)$$

Here $\sigma_{g,j}$ is a contribution to the cross-section from direct photoionization from the ground state, E_a^r is the resonance position, $\delta = \omega - (E_a^r - E_g)$ is the detuning from resonance with ω the photon energy, \tilde{D}_{ga} the dipole matrix element between the ground state and the resonance, Γ_a the total autoionization width, q_a the asymmetry parameter, and $q_{a,j} = \pi V_{ja} D_{jg} / \tilde{D}_{ga}$ the partial asymmetry parameter with $V_{j,a}$ the configuration interaction and D_{jg} the dipole matrix element between $|j\rangle$ and $|g\rangle$. Calculating the resonance parameters with the

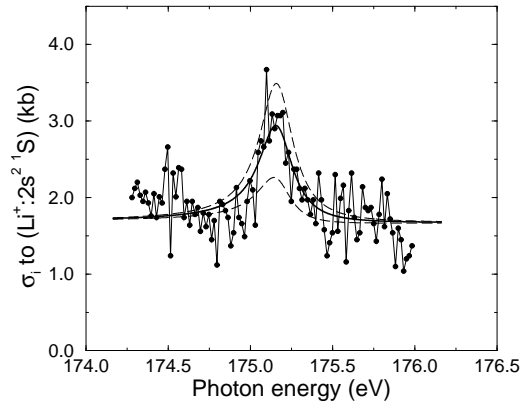


Figure 4.5: Partial cross-sections from Diehl, Cubaynes, Chung, Wuilleumier, Kennedy, Bizau, Journal, Blancard, VoKy, Faucher, Hibbert, Berrah, Morgan, Bozek and Schlachter (1997) for photoionization into the $2s2s^1S^e$ Li^+ channel vs. photon energy in the range of the $3s3s3p^2P^o$ state. The experimental points are shown by the filled dots. The thick line is a least-squares fit to the line-shape (4.49) and corresponds to a partial width of $\Gamma_{a,2s2s^1S^e} = 20$ meV. Here $a = 3s3s3p^2P^o$. The lower and upper dashed curves are for $\Gamma_{a,2s2s^1S^e} = 10$ and 30 meV, respectively. Adopted from Madsen and Lambropoulos (2001).

method described in section 4.4.4, the results so obtained agree well with values reported in the literature. For example, for the triply excited $3s3s3p^2P^o$ state, we find $E_0 = 175.12$ eV and $\Gamma = 276$ meV to be compared with the values calculated by Diehl, Cubaynes, Chung, Wuilleumier, Kennedy, Bizau, Journal, Blancard, VoKy, Faucher, Hibbert, Berrah, Morgan, Bozek and Schlachter (1997) of 175.12 eV and 271 meV for the position and the width, respectively. The measured values for the $3s3s3p^2P^o$ resonance are 175.165 ± 0.050 eV for the term energy and 0.25 ± 0.05 eV for the width (Diehl, Cubaynes, Chung, Wuilleumier, Kennedy, Bizau, Journal, Blancard, VoKy, Faucher, Hibbert, Berrah, Morgan, Bozek and Schlachter, 1997).

Figure 4.5 shows the partial cross-section (Diehl, Cubaynes, Chung, Wuilleumier, Kennedy, Bizau, Journal, Blancard, VoKy, Faucher, Hibbert, Berrah, Morgan, Bozek and Schlachter, 1997) measured for photoionization into the $2s2s^1S^e$ Li^+ ionic autoionizing state as a function of the photon energy of the synchrotron source in the energy range of the triply excited $3s3s3p^2P^o$ state. The line joining the data points (dots) gives an impression of the scattering in the data. The thick line represents a least-squares approximation of the data to the line shape of (4.49) and corresponds to a partial q -parameter of $q_{a,2s2s^1S^e} = -146$ and a partial widths of $\Gamma_{a,2s2s^1S^e} \simeq 19$ meV with $a = 3s3s3p^2P^o$. The thick curve is insensitive to changes in the partial q -values as long as these are smaller

than about -50 . The lower and upper dashed curves illustrate the sensitivity to changes in the partial widths and they are for $\Gamma_{a,2s2s^1S^e} = 10$ meV and 30 meV, respectively. The spectral resolution is about 50 meV. This leads to an uncertainty of $\simeq 20$ meV in the partial width which means that the partial widths found by fitting to the line shape is an *upper bound*, set by the experimental resolution. Accordingly, the measurement puts an upper limit of 20 meV on the partial autoionization widths of the $3s3s3p^2P^o$ triply excited state into the $2s2s^1S^e$ and $2s2p^3P^o$ Li^+ channels. This is consistent with saddle-point calculations published with the experimental data, which showed that the sum of the partial widths into these channels is smaller than 11.7 meV. An experimental resolution of 50 meV should be sufficient to estimate the autoionization width of a state like $2s3p^3P^o$ Li^+ , which has been reported to have a width of about 122.8 meV (Diehl, Cubaynes, Chung, Wuilleumier, Kennedy, Bizau, Journel, Blancard, VoKy, Faucher, Hibbert, Berrah, Morgan, Bozek and Schlachter, 1997). A higher experimental resolution would allow the determination of narrower partial widths.

4.5 Analysis of triply excited states in hyperspherical coordinates

The methods discussed so far for the calculation of triply excited states are all based on a description in terms of independent single-electron coordinates $\{\mathbf{r}_1, \mathbf{r}_2, \mathbf{r}_3\}$. The electron-electron correlations are then build in through the two-particle operator $1/r_{ij}$, $r_{ij} = |\mathbf{r}_i - \mathbf{r}_j|$. The consideration of the many-body problem with hyperspherical coordinates offers an alternative approach which introduces some correlation via collective coordinates from the outset.

The hyperspherical method was considered by Macek (1968) in a study of doubly excited states in helium. Over the years, the method proved to be very successful as a computational method and, not least, in providing a classification of doubly excited states in terms of new approximate quantum numbers (see, for example, Lin (1993) and references therein).

For triply excited states some early work with the hyperspherical approach was done by Clark and Greene (1980); Greene and Clark (1984) and by Watanabe et al. (1982). In those papers the general features concerning the grouping of hyperspherical channels into those supporting singly, doubly and triply excited states as well as strong avoided crossings among the different groups of curves were discussed. Here the focus will be on recent calculations following the experimental efforts described in section 3.3.

4.5.1 The hyperspherical method

Details of the hyperspherical method were described by Morishita and Lin (1998, 1999). From the radial distances r_1, r_2 and r_3 of the three electrons, the hyper-radius R and the hyperangles α_1 and α_2 are defined as

$$r_1 = R \sin \alpha_2 \cos \alpha_1$$

$$\begin{aligned} r_2 &= R \sin \alpha_2 \sin \alpha_1 \\ r_3 &= R \cos \alpha_2. \end{aligned} \quad (4.50)$$

Together with the spherical angles $\hat{\mathbf{r}}_i$ ($i = 1, 2, 3$), the hyperspherical coordinates for a three-electron atom are (R, Ω) where $\Omega = (\alpha_1, \alpha_2, \hat{\mathbf{r}}_1, \hat{\mathbf{r}}_2, \hat{\mathbf{r}}_3)$ denotes all the angles collectively. The hyperradius is a measure of the size of the system. It may extend to infinity, and at large R at least one electron is located far from the nucleus. One can have two, one or no electron(s) close to the nucleus corresponding to singly, doubly or triply excited states, respectively.

The wave function Ψ for the three-electron system is rescaled as $\psi = Rr_1r_2r_3\Psi$ and ψ fulfills

$$\left[-\frac{1}{2} \frac{\partial^2}{\partial R^2} + H_{ad}(\Omega; R) - E \right] \psi = 0, \quad (4.51)$$

where $H_{ad}(\Omega; R)$ is an adiabatic Hamiltonian which depends parametrically on R

$$H_{ad}(\Omega; R) = -\frac{\tilde{\Lambda}^2(\Omega)}{2R^2} + \frac{C(\Omega)}{R}. \quad (4.52)$$

Here $\tilde{\Lambda}^2$ is the square of the rescaled ‘‘grand’’ angular momentum operator

$$\begin{aligned} \tilde{\Lambda}^2(\Omega) &= -\frac{1}{\sin \alpha_2} \frac{\partial}{\partial \alpha_2} \sin \alpha_2 \frac{\partial}{\partial \alpha_2} - \frac{1}{\sin^2 \alpha_2} \frac{\partial^2}{\partial \alpha_1^2} \\ &+ \frac{\mathbf{l}_1^2}{\sin^2 \alpha_2 \cos^2 \alpha_1} + \frac{\mathbf{l}_2^2}{\sin^2 \alpha_2 \sin^2 \alpha_1} + \frac{\mathbf{l}_3^2}{\cos^2 \alpha_2}, \end{aligned} \quad (4.53)$$

and $C(\Omega)$ is the interaction

$$C(\Omega) = R \left[-Z \left(\frac{1}{r_1} + \frac{1}{r_2} + \frac{1}{r_3} \right) + \left(\frac{1}{r_{12}} + \frac{1}{r_{23}} + \frac{1}{r_{31}} \right) \right], \quad (4.54)$$

with Z the nuclear charge.

In the adiabatic approximation (Macek, 1968), the total rescaled wave function for a state with total angular momentum L , spin S and parity π is written as (Morishita and Lin, 1998)

$$\psi^{LS\pi} = \sum_{\mu} F_{\mu}^{LS\pi}(R) \left(\sum_{S_{12}} \Phi_{\mu}^{LS\pi, S_{12}}(\Omega; R) \chi_{S_{12}}^S \right), \quad (4.55)$$

where $\Phi_{\mu}^{LS\pi, S_{12}}(\Omega; R)$ is the adiabatic channel wave function, and $\chi_{S_{12}}^S$ is the total spin function with intermediate spin S_{12} . The wave function $\Phi_{\mu}^{LS\pi, S_{12}}(\Omega; R)$ and the channel potential $U_{\mu}^{LS\pi, S_{12}}(R)$ are solutions to the hyperspherical adiabatic eigenvalue problem

$$[H_{ad}(\Omega; R) - U_{\mu}^{LS\pi, S_{12}}(R)] \Phi_{\mu}^{LS\pi, S_{12}}(\Omega; R) = 0 \quad (4.56)$$

In solving (4.56) in combination with the ansatz (4.55), the Pauli exclusion principle should be fulfilled. The wave functions $F_{\mu}^{LS\pi}(R)$ in (4.55) are radial

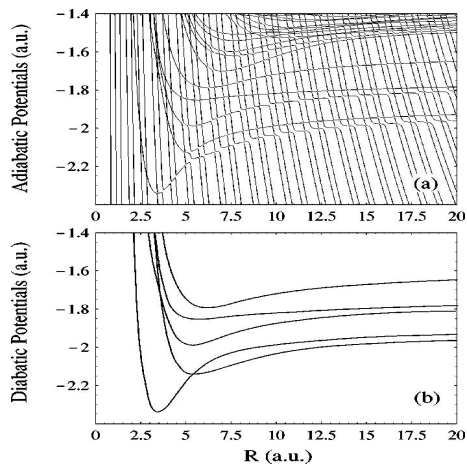


Figure 4.6: (a) Adiabatic potential curves that support triply excited states of lithium together with curves that support doubly excited states (steep curves with avoided crossings) and (b) Five potential curves that support $\text{Li}(2l2'l''^2S^e)$ triply excited states, with the couplings to the doubly excited states removed. From Morishita and Lin (1998).

functions of the hyperradius. They fulfill a system of coupled differential equations which are obtained by substituting equation (4.55) into equation (4.51) and integrating over the angular functions. The numerical implementation of the method was described by Morishita and Lin (1998).

4.5.2 Results with the hyperspherical method

In figure 4.6(a) crossings with curves supporting doubly excited states are shown. These avoided crossings give rise to autoionization. In the studies of triply excited states with the hyperspherical method these couplings have been neglected so far, and hence the studies have focused on energy levels and classification of states.

In figure 4.6(b) the couplings to the doubly excited states are removed. The five curves support $\text{Li}(^2S^e)$ triply excited states with configurations of the type $2l2'l''$. Also for other symmetries such curves have been calculated (Morishita and Lin, 1998; Yang et al., 1996*a, b*), and in general the curves with deep minima at small R correspond to intrashell resonances. For the triply excited states of $^2P^o$ symmetry, Yang et al. (1996*a*) studied the hyperspherical adiabatic potential curves and compared the resonance energies with the experimental and the multiconfiguration Dirac-Fock results of Azuma et al. (1995). In general the calculations and the experimental results agreed within ≤ 0.5 eV. The main advantage of the hyperspherical method is the classification in terms of states belonging to different potential curves.

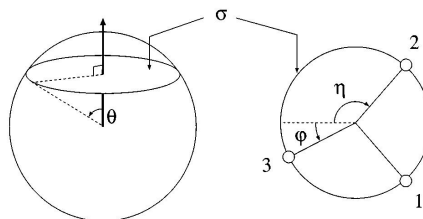


Figure 4.7: Definition of the three angles θ, ϕ, η used to describe the three electrons on a sphere. The electrons form a plane, σ . On the plane (right figure) the three electrons are confined to a circle. From Morishita et al. (1998).

In the quest for new approximate quantum numbers, Morishita and Lin (1998, 1999, 2001*a,b*) have done extensive work aiming at a clear graphical display of the wave function of the triply excited state as obtained by the hyperspherical method. As discussed, for example, by Morishita and Lin (1999), having a clear picture of the internal arrangement of the three electrons with respect to each other is essential in order to obtain an understanding of the electron correlations. The visualization of a three-electron atom is, however, not a trivial task since so many coordinates are involved. Morishita et al. (1998) studied the shape of the adiabatic channel wave function by considering the electron density after integrating out the overall rotation and summing over partial spins S_{12}

$$\rho_{LS\pi}^{\mu}(\theta, \phi, \eta; \alpha_1, \alpha_2; R) = \sum_{S_{12}} \int d\Omega_E |\Phi_{\mu}^{LS\pi, S_{12}}(\Omega; R)|^2, \quad (4.57)$$

where $d\Omega_E$ denotes the volume element of integration, and where (θ, ϕ, η) represent three independent relative angles. The studies were done for fixed $R \simeq 3a_0$ and for $r_1 = r_2 = r_3$ corresponding to the intrashell case. The angles θ, ϕ, η are defined as follows. The plane σ is defined by the three electrons. This plane makes an angle θ with respect to the nucleus, see figure 4.7. On the σ plane, the three electrons lie on a circle. The angle between electron 1 and 2 is 2η and the angle between electron 3 and the line bisecting electrons 1 and 2 is denoted by ϕ . With these definitions the ranges of the angles are $0 \leq \theta \leq \pi, 0 \leq \eta \leq \pi$ and $-\eta \leq \phi \leq \eta$. For $\phi = 0$, the electrons form an isosceles triangle. If $\phi = 0$ and $\eta = 2\pi/3$ they form an equilateral triangle. If at the same time $\theta = \pi/2$ they form a coplanar equilateral triangle with the nucleus in the centre. This latter configuration minimizes the Coulomb repulsion energy, but, as we shall discuss later, it is not allowed for all symmetries, i.e., for all sets of L, S , and π quantum numbers.

Figure 4.8 shows equidensity plots of the eight intrashell triply excited states within the $n = 2$ manifold. The surfaces clearly separate into three different groups (I, II and III). In figure 4.8(a), the maximum density occurs when the

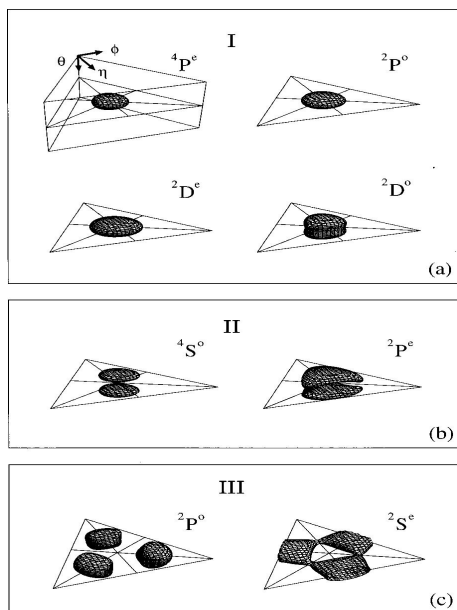


Figure 4.8: Equidensity plots for the eight $n = 2$ intrashell states at $r_1 = r_2 = r_3$. The surface represents 60% of the maximum density. From Morishita et al. (1998).

electrons form an equilateral triangle with the nucleus in the centre. This corresponds to the geometry of the BF_3 molecules. The wave function in figure 4.8(a) contains no nodes.

In figure 4.8(b) the three electrons still form an equilateral triangle, but there is a nodal surface when $\theta = \pi/2$, i.e., when the σ plane intersects the nucleus. The presence of a nodal plane implies higher excitation energy.

Finally, the last two densities in figure 4.8(c) show cases where the maxima occur for $\theta = \pi/2$, i.e., the electrons are coplanar, but the three electrons do not form an equilateral triangle (no density in the middle). The motion implied by this density is a hinge mode where the third electron is fixed, and the two other electrons are moving towards or away from each other in phase. In section 5.2, we shall discuss these findings in more detail.

Most work, so far, on triply excited states with the hyperspherical method has concentrated on the intrashell case corresponding to the situation where the three electrons are moving at equal distances from the nucleus ($r_1 = r_2 = r_3$). In one work by Morishita et al. (1997) the domain with $r_1 < r_2 < r_3$ was studied and an approximate adiabatic separability of the three-electron wave function was found. Very recently, Morishita and Lin (2003) studied radial and angular correlations for the intershell case and classified states of the type $2l2l'3l''$ by

checking for approximate quantum numbers and by studying the nature of the nodal surfaces of the states. The main findings of that work will be discussed in section 5.2.

Chapter V

Theoretical models for triply excited lithium

Going from the two- to the three-electron atom complicates matters when it comes to obtaining more physical understanding of the fundamental behaviour and dynamics of the correlated electrons in the multiply excited state, and due to the increase in the number of independent variables it is a challenge to obtain a useful classification of the states and a description in terms of approximate quantum numbers.

This is not the place to discuss in detail the progress in the understanding of doubly excited states. On the other hand it is reasonable to follow up the brief discussion in the introduction and to mention that a coherent picture has emerged over the last 3-4 decades (see, for example, Lin (1984); Herrick (1983); Mølmer and Taulbjerg (1988); Rost and Briggs (1991); Madsen and Mølmer (2001*b*) and references therein). The two excited electrons have to be treated jointly and the excitation spectrum may be understood qualitatively in terms of a “floppy” linear triatomic molecule with the two electrons on either side of the nucleus. More precisely, the geometry is approximately isomorphic with this picture. The actual motion of the electrons is very delocalized and any similarity with, for example, a true rotational spectrum is accidental (Madsen and Mølmer, 2001*b*). For doubly excited states, a set of approximate quantum numbers has been proposed (Lin, 1984), and these numbers are now widely used. The new set of quantum numbers allows the energies of the doubly excited states to be rearranged into groups displaying a higher degree of order than if classified according to their $^{2S+1}L^{\pi}$ symmetry, and a number of propensity rules have been considered (Rost and Briggs, 1991).

In an attempt to gain similar insight into the nature and systematic behaviour of triply excited states, a few models have been studied. They all single out the role played by particular geometrical arrangements of the electrons and the nucleus with respect to each other. One example is the so-called frozen- r model recently thoroughly described by Morishita and Lin (2001*b*). In this model the three electrons are confined to move at the surface of a sphere allowing a detailed investigation of angular correlations. Another recent model is the so-called symmetric rotor model by Madsen and Mølmer (2001*a*, 2002, 2003).

In this model, the electrons are assumed to be at the corners of an equilateral triangle with the (coplanar) nucleus in the center. In the following the insights obtained from these and other models will be discussed.

5.1 Three-electron ionization ladder

Following a model suggested by Watanabe and Lin (1987), which we shall discuss further below, Nicolaides and co-workers were among the first to quantify the importance of the equilateral triangle arrangement of the electrons with respect to the nucleus (Komninos et al., 1988; Nicolaides et al., 1990). Komninos et al. (1988) defined the three-electron ionization ladder (THEIL) state as the state, within a given principal quantum number manifold, with the lowest energy. Calculating the wave function in the multiconfiguration Hartree-Fock approximation, they deduced the geometrical behaviour of the triply excited THEIL state by considering the expectation values of the radii r_1, r_2 and r_3 and of the angle between any two of the electrons θ_{12} .

For the $4S^o$ states, which were the only ones considered, it was found that as n increased one reached a region where $r_1 \sim r_2 \sim r_3$, and $\theta_1 = \theta_2 = \theta_3 \sim 105^\circ$. The angle of 105° was in accordance with the later analysis by Bao (1992), and it reflects that the nucleus is not coplanar with the equilateral triangle. In fact, the $4S^o$ states have a nodal plane in the coplanar case (see, for example, Bao (1992); Morishita and Lin (2001*b*); Madsen and Mølmer (2003)). The other observation of the early calculation by Komninos et al. (1988), that $r_1 \sim r_2 \sim r_3$, lends support to the frozen- r model which will be discussed further below.

In another work Nicolaides et al. (1990) considered the THEIL states from the point of view of a rotating oblate symmetric top and used this analogy to suggest a spectral formula which was used for the prediction of the energy positions of some triply excited states. Later Nicolaides et al. (1993) made calculations of triply excited states in more detail, and recently extensive calculations were performed to determine triply excited states of He^- within the $n = 3$ manifold (Nicolaides and Piangos, 2001).

5.2 Normal mode analysis of triply excited states

Previous sections have documented the successes of *ab initio* theories in determining the spectrum of triply excited states and the ability of these methods to calculate accurate photoionization spectra. The progress in obtaining an appropriate classification scheme has in a sense been more slowly, and only in the last few years a more detailed picture of the modes of correlated electronic motion has emerged.

Watanabe and Lin (1987) were the first to study the motion of the electrons in a triply excited state from a molecular point of view. They studied the symmetries of the problem and made calculations in the r -frozen model. These studies were later followed by Bao (1992) who studied $4S^o$ triply excited states

and showed that there is a nodal plane for these states when the nucleus is coplanar with the plane spanned by the three electrons. The r -frozen model was justified by the calculations of Komninos et al. (1988) showing strong radial confinement (see section 5.1).

Bao et al. (1994) considered the lowest energy states of $^{2S+1}L^\pi$ symmetry and predicted an ordering of the states based on geometry and symmetry constraints. Bao et al. (1997) followed up on these studies and described the symmetry properties of the wave functions. The nodal surfaces for the wave functions were identified, and from these various normal modes were inferred. The question of how to classify the states was, however, not addressed.

Morishita and Lin (2001*a,b*) have reported detailed investigations on the visualization and identification of collective normal modes of intrashell triply excited states with the frozen- r model. The reader is referred to Morishita and Lin (2001*b*) for details and an extensive list of references. Here the method and main findings will be discussed.

In the r -frozen model the radial degrees of freedom are frozen and the Hamiltonian reads (Morishita and Lin, 2001*b*)

$$H = \frac{1}{2r_0^2} \sum_{i=1}^3 \hat{\mathbf{l}}_i^2 + \frac{1}{r_0} \sum_{i>j} \frac{1}{|\hat{\mathbf{r}}_i - \hat{\mathbf{r}}_j|} - \frac{3Z}{r_0}, \quad (5.1)$$

where Z is the effective nuclear charge, $\hat{\mathbf{l}}_i$ the angular momentum operator of the i th electron with respect to the nucleus, $\hat{\mathbf{r}}_i$ is the unit vector pointing from the nucleus to the i th electron, and r_0 is the radius of the sphere on which the electrons are confined. Morishita and Lin (2001*b*) used $Z = 1.423$ and $r_0 = 6.326a_0$ to simulate the $n = 3$ shell of intrashell states in He^- . The effective charge, however, only enters through the constant electron-nucleus interaction term, $-3Z/r_0$, which just adds to the total energy and does not affect the relative order of the energy levels. The choice of r_0 is not expected to change this ordering either, and, hence, the predictions of the model should be independent of the exact values used when it comes to a classification of states. Accordingly, the results should apply to triply excited He^- as well as, for example, to triply excited lithium. The multiconfiguration Hartree-Fock calculations by Komninos et al. (1988) as well as calculations using the hyperspherical method (Morishita and Lin, 1999) showed a localization in the radial coordinates and hence provide quantitative justification of the r -frozen model.

The total antisymmetric wave function is expressed by

$$\psi = \sum_{S_{12}} \Phi_{LM}^{SS_{12}}(\hat{\mathbf{r}}_1, \hat{\mathbf{r}}_2, \hat{\mathbf{r}}_3) \chi_{S_{12}}^S, \quad (5.2)$$

where $\chi_{S_{12}}^S = \left[\{\chi(1)\chi(2)\}^{S_{12}} \chi(3) \right]^S$ is the coupled spin function of the three electrons with intermediate spin S_{12} and total spin S . The spatial wave function $\Phi_{LM}^{SS_{12}}(\hat{\mathbf{r}}_1, \hat{\mathbf{r}}_2, \hat{\mathbf{r}}_3)$ is obtained on the r_0 -sphere by diagonalization in a basis

of coupled spherical harmonics $\left[\{Y_{l_1 m_1}(\hat{\mathbf{r}}_1) Y_{l_2 m_2}(\hat{\mathbf{r}}_2)\}^{L_{12} M_{12}} Y_{l_3 m_3}(\hat{\mathbf{r}}_3) \right]^{LM}$ with total angular momentum L and projection M , intermediate quantum numbers L_{12} and M_{12} , and individual orbital and magnetic quantum numbers $\{l_i, m_i\}$ ($i = 1, 2, 3$). Besides total spin S and total angular momentum L , parity π is a good number.

When the 64 eigenenergies within the $n = 3$ shell of the model atom are calculated and ordered according to $^{2S+1}L^\pi$ symmetries an erratic picture emerges. Based on a consideration of symmetries and normal modes the states may be rearranged into groups displaying a higher degree of order. The accompanying analysis of the wave function was done (Morishita and Lin, 2001b) in the body-fixed frame defined by

$$\begin{aligned} \mathbf{S}_z &= \mathbf{r}_1 \times \mathbf{r}_2 + \mathbf{r}_2 \times \mathbf{r}_3 + \mathbf{r}_3 \times \mathbf{r}_1 \\ \mathbf{S}_y &= \frac{\sqrt{3}}{2}(\mathbf{r}_1 - \mathbf{r}_2) \\ \mathbf{S}_x &= \mathbf{S}_y \times \mathbf{S}_z. \end{aligned} \quad (5.3)$$

The three electrons span a plane σ and in the body-fixed frame the z axis, S_z , is perpendicular to σ — and it goes through the nucleus as well.

Each wave function $\Phi_{LM}^{SS_{12}}(\hat{\mathbf{r}}_1, \hat{\mathbf{r}}_2, \hat{\mathbf{r}}_3)$ (which is in the laboratory coordinates) is expanded in body-fixed wave functions $\phi_{LM_I}^{SS_{12}}(\Omega_I)$ through a rotation

$$\Phi_{LM}^{SS_{12}}(\hat{\mathbf{r}}_1, \hat{\mathbf{r}}_2, \hat{\mathbf{r}}_3) = \sum_{M_I=-L}^L \phi_{LM_I}^{SS_{12}}(\Omega_I) \mathcal{D}_{M_I M}^L(\omega), \quad (5.4)$$

where $\mathcal{D}_{M_I M}^L(\omega) = \langle LM_I | e^{-i\alpha \hat{L}_z} e^{-i\beta \hat{L}_y} e^{-i\gamma \hat{L}_z} | LM \rangle$ is an element of the Wigner rotation matrix (Brink and Satchler, 1975), ω is the set of Euler angles $\omega = (\alpha, \beta, \gamma)$ defining the orientation of the body-fixed frame with respect to the laboratory fixed frame, M_I is the projection of $\hat{\mathbf{L}}$ on the body-fixed z axis, and $\Omega_I = (\theta, \eta, \phi)$ is the set of three internal angles used to describe the internal relative positions of the electrons. These angles were discussed in section 4.5 and defined in figure 4.7. From equations (5.4) and (5.2), the density distribution for each rotational component $T = |M_I|$ is defined

$$\rho_T(\Omega_I) = \begin{cases} \sum_{S_{12}} |\phi_{LM_I}^{SS_{12}}(\Omega_I)|^2 & (T = 0) \\ \sum_{S_{12}} \left(|\phi_{LM_I}^{SS_{12}}(\Omega_I)|^2 + |\phi_{L-M_I}^{SS_{12}}(\Omega_I)|^2 \right) & (T \neq 0) \end{cases} \quad (5.5)$$

and the purity of each rotational component is calculated by

$$A_T = \int d\Omega_I \rho_T(\Omega_I). \quad (5.6)$$

When A_T is close to unity, T is considered to be an approximate good quantum number and may be used to label the state. Note that if the three electrons in

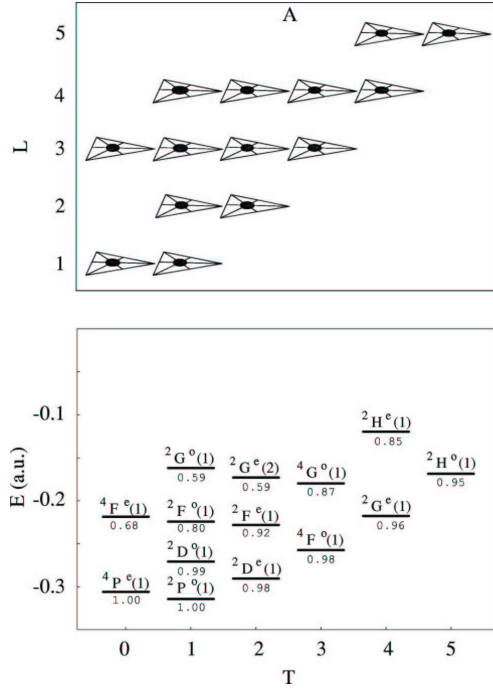


Figure 5.1: Rotational levels and contour surface plots of the electronic density distribution for the $3l3l'3l''$ triply excited states that form the group A characterized by the absence of nodal planes. In the lower panel each state is denoted by L, S and π and the number n indicates the n th state of that symmetry, starting from 1. The number below each level indicates the rotational purity A_T of equation (5.6). The plots in the upper frame give the density of the corresponding T components of the states in the lower frame. Each surface represents the equidensity surface at 60% of the maximum. From Morishita and Lin (2001b).

their correlated motion act as a rigid symmetric top T would be a good quantum number.

Density plots for the model atom similar to the ones considered in section 4.5 allows one to access the nodal surfaces, which are subsequently used to identify the normal modes. As an example, we consider the coplanar geometry with the nucleus in the σ -plane of the equilateral triangle. Since, in this case, a rotation of π radians around S_z ($e^{-i\pi M_I} = (-1)^{M_I}$) is equivalent to the parity operation, we see that the parity equals $\pi = (-1)^{M_I}$. If this condition is not satisfied, i.e., if $\pi(-1)^{M_I} = -1$, this particular $T = |M_I|$ component of the wave function vanishes, and there will be a nodal plane in the coplanar geometry at $\theta = \pi/2$. This nodal surface is associated with a mode where the plane of the electrons oscillate with respect to the nucleus. Likewise, the nodal surface at $\phi = 0$ may be associated with a swing mode where two electrons are fixed and the third

electron is swinging up and down such that when the three electrons form an isosceles triangle, the wave function vanishes. A nodal surface orthogonal to the $\phi = 0$ plane at $\eta = 2\pi/3$ gives rise to a mode having one electron fixed and the other two electrons performing the motion of a hinge, moving towards or away from each other. Morishita and Lin (2001*b*) grouped the different states into classes depending on the nodal pattern. Figure 5.1 shows, for example, the nodeless states designated by A. In the $n = 2$ manifold, this group is spanned by the states labelled by I in figure 4.8.

The upper part of the figure shows the contour surface plots. Each plot exhibits a maximum at the center ($\theta = \pi/2, \eta = 2\pi/3, \phi = 0$) meaning that the preferred geometry is the equilateral coplanar triangle. Each surface is plotted at 60% of the maximum density. In general, the size of the surface measures the floppiness of the state. The larger the surface, the floppier a state. For the lower states in each group, the rotational purity is quite close to unity. As the higher-lying states are considered, the purity decreases, which may be interpreted to be a consequence of centrifugal distortion. The geometry of the states in figure 5.1 is the coplanar equilateral triangle configuration that minimizes the Coulomb repulsion energy. Due to constraints imposed by the ${}^{2S+1}L^\pi$ symmetry, this geometry, however, is only allowed for the 14 states shown. The remaining 50 triply excited states of the $n = 3$ manifold have other nodal surfaces and belong to different groups.

For the considered states the most well-localized ones have a shape similar to a symmetric top molecule. For the oblate symmetric top, the rotational energy levels are given by

$$E(L, T) = \frac{1}{2I} [2L(L+1) - T^2], \quad (5.7)$$

with I the moment of inertia. The qualitative predictions of the formula are consistent with the results in figure 5.1 in the sense that for fixed L the higher T -states have lower energy and that for fixed T the states with higher L have higher energy. In two respects the results in the figure deviate from the prediction of the formula. Firstly, the difference in energy between two L -component for fixed T is not independent of T as predicted by equation (5.7). This discrepancy is due to the fact that the three electrons do not form a rigid oblate symmetric top. Secondly, the ‘‘rotational’’ series in figure 5.1 terminate which as a consequence of the existence of a maximum total angular momentum of $L_{\max} = 5$ within the third principal shell ($L_{\max} = 6$ is Pauli-forbidden).

Based on the analysis sketched above, Morishita and Lin (2001*b*) classified all the 64 states within the $n = 3$ shell. The results were compared with *ab initio* results on N^{+4} and N^{+2} by Vaeck and Hansen (1992) and on He^- by Nicolaides and Piangos (2001). In the N^{2+} and He^- cases complete agreement with respect to the ordering of the states was observed. For N^{4+} there were two cases where the results of Vaeck and Hansen (1992) gave a different ordering between successive L -states for fixed T . The ordering of the states from Vaeck and Hansen (1992) is consistent with a simple application of Hund’s rule.

In conclusion, a classification scheme has emerged for the intrashell case

which group states according to specific bending, vibrational modes of a XY_3 molecule. The scheme rearrange the symmetries ($^{2S+1}L^\pi$) into T -dependent rotationallike series. Even though the system shows isomorphic correlation patterns with the oblate symmetric top molecule, the analogy should be used with caution. For example the fitting of the spectra with a formula like (5.7) is meaningless. We shall discuss these aspects further in our presentation of the symmetric rotor model.

For the intershell case, Morishita and Lin (2003) studied $2l2l'3l''$ states with the hyperspherical method. As in the intrashell case, the level positions appeared rather erratic when ordered according to $^{2S+1}L^\pi$ symmetry, and again the objective was to regroup these levels into different classes such that the energy levels exhibit a more regular pattern. The classification was done in a way similar to the intrashell case, i.e., in terms of the approximate quantum number T which, by calculating the purity of the rotational component (equation (5.6)), was shown to be fairly accurate in many cases. The dominant T components were subsequently analyzed in a body-fixed frame, and the nodal surfaces were identified. Compared with the intrashell case where all three electrons are at approximately equal distances from the nucleus, in the intershell case, one electron is further away, and this opens for the possibility of a stretch mode of the outer electron with respect to the two inner electrons, and this results in many more classification groups (Morishita and Lin, 2003).

5.3 Symmetric rotor model

In a series of papers Madsen and Mølmer have considered an analytical ansatz for triply excited states in lithium or lithiumlike ions (Madsen and Mølmer, 2001a, 2002, 2003). The explicit construction of the wave function is based on the propensity, discussed in sections 4.5.2 and 5.2, for the three excited electrons to arrange themselves in the corners of an equilateral triangle with the nucleus in the center. This arrangement minimizes the electron repulsion, and it was suggested more than 25 years ago to play an important role in the three-electron-ejection Wannier problem (Klar and Schlecht, 1976; Grujić, 1983; Kuchiev and Ostrovsky, 1998; Ostrovsky, 2001) (see also Grujić (1999) for a semiclassical treatment based on the same geometry). Madsen and Mølmer were the first to develop a quantum mechanical description which invoked this physical picture to provide an explicit construction of the wave function of triply excited states below threshold. It was suggested, and verified by a quantitative comparison with *ab initio* calculations, that hollow three-electron atoms which have no electrons in the inner Bohr orbital can be accurately described by a simple analytical product wave function with a spatial arrangement of the three electrons in a coplanar equilateral triangle (Madsen and Mølmer, 2001a, 2002, 2003).

Hollow states for the case of three electrons moving in the Coulomb field of a point-like nucleus of charge Z are, in the non-relativistic case, described by the Hamiltonian of equation (4.2). In the theoretical descriptions above, electron-

electron correlations are accounted for in terms of linear combinations of angular momentum and spin–multiplet wave functions which cannot be factorized into a product of single–particle states. In the symmetric rotor model, the electron–electron interaction will be taken care of by a simple product of three carefully chosen single–particle states. Entanglement is subsequently enforced by spin, exchange and rotational symmetry.

5.3.1 Construction of the symmetric rotor states

In the coplanar equilateral triangle geometry, the interaction between any single electron and the two others is approximately represented by a repulsive field along the direction of the single electron under concern with respect to the nucleus. For the pure Coulomb potential, the spherical and polarized Stark bases both span the degenerate n^2 –dimensional eigenspace for a given principal shell, n . In addition to solving the pure Coulomb problem, the Stark states are eigenstates of the hydrogenic Hamiltonian perturbed by a weak external electric field causing only intrashell transitions (Schiff, 1955). Hence, the interelectronic interaction tends to stabilize the electrons consistently in individual Stark states along three different directions. The Stark states are maximally polarized and will be denoted by $|n, k = n - 1, m = 0\rangle$, with k the parabolic quantum number and m the magnetic quantum number. The Stark basis is related to the spherical $|n l m\rangle$ basis via a unitary transformation (see, for example, Schiff (1955); Burgdörfer (1983))). Choosing for convenience the rotor to be in the xy plane, the ansatz for the spatial part of the intrinsic rotor is given by

$$|\Psi_R\rangle = |n n - 1 0\rangle_0 |n n - 1 0\rangle_{2\pi/3} |n n - 1 0\rangle_{-2\pi/3}, \quad (5.8)$$

where the subscripts $0, \pm 2\pi/3$ denote one electron after the x axis and the two other electrons rotated $\pm 2\pi/3$ in the xy plane.

Figure 5.2 shows the column probability density, i.e., the electron density integrated over the z coordinate as a function of x and y in the one–electron state $|n n - 1 0\rangle_0$ and in the three–electron state of equation (5.8). Figures 5.2(a), 5.2(c) and 5.2(e) show the electron density in the one–electron Stark state polarized along the x axis for $n = 2, 3$ and 4. The peak around the atomic nucleus at $(x, y) = (0, 0)$ is a feature in the single–electron Stark states reflecting the attraction between the electron and the nucleus. Figures 5.2(b), 5.2(d) and 5.2(f) show the total electron density in the three–electron state (5.8). This density reflects the threefold symmetry of the state, and it splits up into a three–pointed star for $n = 3$ and $n = 4$. The accumulated electron density can be expanded on spherical harmonics with the maximal angular momentum and azimuthal quantum numbers equal to twice the maximal electronic angular momentum in the given principal shell. For $n = 2$ (figure 5.2(b)), this restricts the azimuthal dependence to a combination of a constant, $\exp(\pm i\phi)$ and $\exp(\pm 2i\phi)$, and only the constant term is compatible with the threefold rotational symmetry. Thus the density in figure 5.2(b) shows full rotational symmetry, although the individual electrons in the $n = 2$ shell are split at an angle of $2\pi/3$ radians in the

xy plane.

The state $|\Psi_R\rangle$ is an intrinsically anisotropic state which breaks the spatial rotational symmetry, and as a consequence it is not an eigenstate of \hat{L}^2 and \hat{L}_z . To obtain such a state, we perform the rotational average

$$|\Psi_{R,M_I}^{LM}\rangle = \mathcal{N} \int d\omega \mathcal{D}_{MM_I}^L(\omega)^* |\Psi_R\rangle_\omega, \quad (5.9)$$

where \mathcal{N} is a normalization constant, $\omega = (\alpha, \beta, \gamma)$ is a set of Euler angles, $\int d\omega$ is shorthand for $\int d\omega = \int_0^{2\pi} d\alpha \int_0^{2\pi} d\gamma \int_0^\pi d\beta \sin\beta$ and $\mathcal{D}_{MM_I}^L(\omega)$ is an element of the Wigner rotation matrix (Brink and Satchler, 1975). On the right-hand side of equation (5.9), the state $|\Psi_R\rangle_\omega$ refers to the direction specified by ω . Finally, the quantum number M_I fixes the projection of the angular momentum of the intrinsic rotor with respect to the z axis, and its norm corresponds to the T quantum number introduced by Lin and co-workers (see section 5.2). Expanding the intrinsic rotor in a set of angular-momentum eigenstates, it is readily seen that (5.9) is an eigenstate of \hat{L}^2 and \hat{L}_z (Madsen and Mølmer, 2001b, 2002). The argument goes as follows. Firstly, $|\Psi_R\rangle$ is expanded in a set of angular momentum eigenstates,

$$|\Psi_R\rangle = \sum_{L',M_I'} C_{L',M_I'} |L'M_I'\rangle. \quad (5.10)$$

Secondly, the state after direction ω is expressed as

$$|\Psi_R\rangle_\omega = \sum_{L',M_I',M'} C_{L',M_I'} \mathcal{D}_{M',M_I'}^{L'}(\omega) |L'M'\rangle, \quad (5.11)$$

which is substituted into equation (5.9). The orthogonality properties of the Wigner functions (Brink and Satchler, 1975)

$$\int d\omega \mathcal{D}_{MM'}^I(\omega)^* \mathcal{D}_{NN'}^J(\omega) = \frac{8\pi}{2I+1} \delta_{M,N} \delta_{M',N'} \delta_{I,J}. \quad (5.12)$$

then gives

$$|\Psi_{R,M_I}^{LM}\rangle = \mathcal{N} \frac{8\pi^2}{2L+1} C_{LM} |LM\rangle, \quad (5.13)$$

which shows that the state in equation (5.9) is indeed an eigenstate of \hat{L}^2 and \hat{L}_z .

The function in (5.9) has to be supplemented by the spin function $|\chi_{M_S}^S\rangle$ with S the total spin and M_S its projection, and the total wave function has to be properly antisymmetrized by the three-electron antisymmetrization operator

$$\mathcal{A} = \frac{1}{\sqrt{6}} (1 + C + C^2 - P_{12} - P_{23} - P_{13}), \quad (5.14)$$

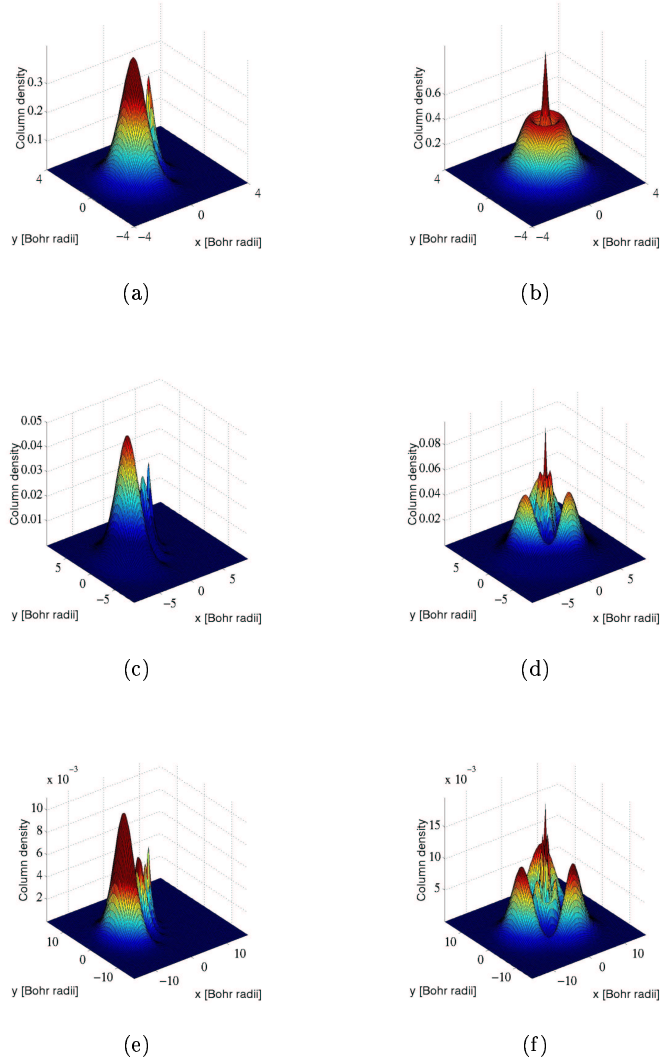


Figure 5.2: Panels (a), (c) and (e): column probability density in the xy plane for Stark states within $n = 2, 3$ and 4 principal shells and maximally polarized along the x axis. Panels (b), (d) and (f): electron charge column density added over the three electrons in the rotor state of equation (5.8). Adopted from Madsen and Mølmer (2002).

where C is a cyclic permutation and where P_{ij} is the operator that interchanges electron i and j . The total ansatz for the symmetric rotor then reads

$$\left| \Psi_{R, M_I}^{LM, SM_S} \right\rangle = \mathcal{N} \int d\omega \mathcal{D}_{M M_I}^L(\omega)^* \mathcal{A} \left[\left| \Psi_{R, M_I}^{LM}, \chi_{M_S}^S \right\rangle_\omega \right]. \quad (5.15)$$

The quartet spin states are determined by maximal single-electron spin projections and step up and down operators. This accounts for four spin states. The doublet spin states are constructed in a way similar to spin waves in solids (Kittel, 1963) to circumvent the specification of the intermediate spin of any two of the electrons. The papers by Madsen and Mølmer (2002, 2003) contain complete listings of all eight spin states. For example, the doublet spin states $|SM_S\rangle$ with projection $M_S = 1/2$ are given by

$$\left| \frac{1}{2} \frac{1}{2} \right\rangle_{\pm} = \frac{1}{\sqrt{3}} \left[|\uparrow\uparrow\downarrow\rangle + |\downarrow\uparrow\uparrow\rangle e^{\pm 2\pi i/3} + |\uparrow\downarrow\uparrow\rangle e^{\pm 2\pi i/3} \right], \quad (5.16)$$

where the notation $|\uparrow (\downarrow)\rangle$ means single-electron projection $|m_s = \frac{1}{2} (m_s = -\frac{1}{2})\rangle$.

5.3.2 Classification scheme and configuration mixing

The quartet states are all fully symmetric, meaning that the antisymmetrization only concerns the spatial parts. For doublet states, the spin and spatial degrees of freedom mix and a more careful investigation of the effect of \mathcal{A} is required. Madsen and Mølmer (2003) have discussed the details. The symmetry of the ansatz (5.15) together with the antisymmetrization gives rise to a classification of states and an identification of a quantum number.

First it is noted as is well-known from molecular theory that for a planar symmetric top, M_I is the parity quantum number (Herzberg, 1945). This property was shown explicitly by Madsen and Mølmer (2003) for the wave function ansatz (5.15), i.e.,: $|\Psi_{R, M_I}^{LM, SM_S}\rangle$ is even under parity if M_I is even; $|\Psi_{R, M_I}^{LM, SM_S}\rangle$ is odd under parity if M_I is odd.

Madsen and Mølmer (2003) also considered the effect of the antisymmetrization operator explicitly by letting it operate directly on the intrinsic rotor. Confining the rotor to the xy plane, the antisymmetrization operator may be expressed in terms of rotations around the z and y axes

$$\mathcal{A} = \frac{1}{\sqrt{6}} (1 + D_z + D_z^2 - (D_z + D_y D_y D_z^2 + D_z^2 D_y D_z)). \quad (5.17)$$

Here $D_z \equiv D_z(2\pi/3)$ is a $2\pi/3$ rotation around the z axis, and $D_y \equiv D_y(\pi)$ is a π rotation around the y axis. Expanding the rotor in angular momentum eigenstates, the effect of \mathcal{A} may then be calculated. For the quartet states one finds

$$\left| \Psi_{R, M_I}^{LM, \frac{1}{2} M_S} \right\rangle = \mathcal{N} \sum_{q=-1}^1 e^{i \frac{2\pi}{3} M_I q} \left(\left| \Psi_{R, M_I}^{LM}; \chi_{M_S}^{3/2} \right\rangle \right) \quad (5.18)$$

Table 5.1: Configurational versus symmetric rotor mixing fractions for some triply excited states in Li. The first column gives antisymmetrized LS states, the second is for the symmetric rotor, $|\Psi_{R,M_I}^{LM,S M_S}\rangle$. The last columns present values from the literature. The following abbreviations have been used: multiconfiguration Dirac-Fock (MCDF), saddle-point complex rotation (SPCR), configuration interaction (CI).

LS state	$ \Psi_{R,M_I=-1}^{L=1,S=1/2}\rangle$	MCDF	SPCR	CI
$2s2s2p (^2P^o)$	88.89	74 ^a	83.4 ^c	
$2p^3 (^2P^o)$	11.11	12 ^a	13.8 ^c	
$2s2p3s (^2P^o)$		8 ^a		
$3s3s3p (^2P^o)$	67.44	61.8 ^b		64.0 ^d
$3p^3 (^2P^o)$	18.97	20.0 ^b		19.5 ^d
$3s3p3d (^2P^o)$	11.80	13.5 ^b		13.2 ^d
$3p3d3d (^2P^o)$	1.79	3.3 ^b		
$3p3p3p (^4P^e)$	94.6			90.06 ^d
$3p3p3d (^4P^e)$	5.37			5.2 ^d
$3s3p3d (^2D^o)$	54.99			57.45 ^d
$3p3p3p (^2D^o)$	41.24			37.45 ^d
$3p3d3d (^2D^o)$	3.77			

^aFrom Azuma et al. (1995).

^bFrom Azuma et al. (1997).

^cFrom Chung and Gou (1998). Only total ssp and ppp fractions, irrespectively of n , are given.

^dFrom Vaeck and Hansen (1992). Results are for N^{4+} .

$$- (-1)^{L+M_I} \left| \Psi_{R,-M_I}^{LM} ; \chi_{M_s}^{3/2} \right\rangle,$$

and for the doublet states one finds

$$\begin{aligned} \left| \Psi_{R,M_I}^{LM, \frac{1}{2}M_s} \right\rangle &= \mathcal{N} \sum_{q=-1}^1 e^{i\frac{2\pi}{3}(M_I \mp 1)q} \left(\left| \Psi_{R,M_I}^{LM} ; \frac{1}{2} \frac{1}{2}_{\pm} \right\rangle \right. \\ &\quad \left. - (-1)^{L+M_I} \times \left| \Psi_{R,-M_I}^{LM} ; \frac{1}{2} \frac{1}{2}_{\pm} \right\rangle \right). \end{aligned} \quad (5.19)$$

The prefactors $\left(1 + e^{-i\frac{2\pi}{3}M_I} + e^{i\frac{2\pi}{3}M_I}\right)$ and $\left(1 + e^{-i\frac{2\pi}{3}(M_I \mp 1)} + e^{i\frac{2\pi}{3}(M_I \mp 1)}\right)$ show that only quartet states with $|M_I| = 0$ modulo 3 and doublet states with $|M_I| = \{1, 2\}$ modulo 3 are allowed. From these observations and equations (5.18) and (5.19), the maximally polarized symmetric rotor states are now seen to give rise to the following states. For quartet states, the $M_I = 0$ case gives

$${}^4P^e, {}^4F^e, {}^4H^e, \dots \quad (5.20)$$

In particular the ${}^4S^e$ state is forbidden for the maximally correlated rotor, a result which is consistent with the discussion in section 5.2. If $M_I \neq 0$ both

Table 5.2: Symmetric rotor mixing fractions for the lowest $\text{Li}(4s4s4p^2P^o)$ state. The labels $ll'l''$ are shorthand for antisymmetric $|4l4l'4l''(^2P^o)\rangle$ states.

ssp	ppp	spd	pdd	sdf	ppf	pff	ddf	fff
52.9	21.4	18.5	5.62	0.461	0.957	0.0345	0.0769	0.00312

even and odd values are allowed for $L \geq |M_I|$. For example, for $M_I = 3$ the series will be ordered as

$${}^4F^o, {}^4G^o, {}^4H^o, \dots \quad (5.21)$$

and the states are degenerate with respect to $\pm|M_I|$. For the doublet state with $|M_I| \bmod 3 = \{1, 2\}$ it is seen from equation (5.19) that both even and odd values of L are allowed. For $|M_I| = 1$, the series

$${}^2P^o, {}^2D^o, {}^2F^o, {}^2G^o, \dots \quad (5.22)$$

emerges. For $|M_I| = 2$ the following series is found

$${}^2D^e, {}^2F^e, {}^2G^e, {}^2H^e, \dots \quad (5.23)$$

The above results are consistent with the results of Bao et al. (1994) and also with the classification scheme of Morishita and Lin (2001b) where the states considered here correspond to the group of states labelled by A (see figure 5.1).

To address the quality of the symmetric rotor ansatz, Madsen and Mølmer (2001a, 2002) calculated configuration mixing coefficients and compared them with *ab initio* results. The mixing coefficient are the amplitudes on the individual independent-electron configurations making up the basis, and the mixing fractions are the modulus square of these amplitudes.

Table 5.1 shows a comparison between configurational and symmetric rotor mixing fractions for some triply excited states in the second and third principal shells. The symmetric rotor predicts the general trend in the mixing fractions for both cases. The configuration calculations of Vaeck and Hansen (1992) are for lithiumlike N^{4+} ions. The comparison with these results shows the Z independence of the configuration mixing fractions in the symmetric rotor model. For cases where the prediction for the mixing fraction based on the symmetric rotor is 100%, also the configuration–interaction calculations give predictions very close to 100% (Vaeck and Hansen, 1992).

Compared with the $n = 2$ and $n = 3$, the $n = 4$ results of table 5.2 show an increase in the *ppp* and *spd* portions at the cost of a decrease in the *ssp* portion (Madsen and Mølmer, 2002).

5.3.3 Distribution over l quantum numbers

Recently, Madsen and Mølmer (2003) considered the distribution over individual angular momentum quantum numbers, l , in triply excited states. The successful prediction of configuration mixing coefficients by the symmetric rotor model

implies that the model should also produce reliable predictions for this purpose. The interest in the l distributions dates back to the discussion by Fano (1974) who pointed out that electron–electron correlation in the vicinity of the double electron escape threshold leads to the population of high angular momentum states. Fano’s qualitative arguments were based on Wannier theory. Drukarev (1982) derived a formula for the l distribution assuming one electron to be strongly polarized in a Stark state $|n, k = n - 1, m = 0\rangle$ along the direction of the second electron. As discussed in section 5.3.1, the Stark states are related to the spherical basis states by a unitary matrix whose elements are Clebsch–Gordon coefficients. The probability, according to Drukarev, that the electron is found with a particular value of its angular momentum is

$$P_d(l) = |\langle j j j - j | l 0 \rangle|^2, \quad (5.24)$$

where j in the Clebsch–Gordon coefficient is given by $j = (n - 1)/2$. This analysis does not take into account the conserved quantum numbers, i.e., the total angular momentum, spin and parity. For doubly excited states this shortcoming was fixed by Rau (1984) who exploited the SO(4) symmetry of the pure Coulomb problem and the approximate analytical diagonalization within the doubly–excited symmetry basis (DESB) (Wulfman, 1973; Sinanoğlu and Herrick, 1975; Herrick and Sinanoğlu, 1975). Later, Themelis and Nicolaides (1995) compared the DESB predictions for doubly excited states with *ab initio* calculations, and in general good agreements were found. Note in passing that the DESB states continue to find applications. For example in the interpretation of photodetachment data of He^- in the vicinity of the double electron escape threshold (Petrunin et al., 2003)). In that case, the DESB theory express the highly correlated doubly state $(nn' {}^4L)$ in terms of a linear combination of $|nl n' l'\rangle$ configurations, $|nn' {}^4L\rangle = \sum_{ll'} C_{nl n' l'}^{L \pi} |nl n' l'\rangle$. The expansion coefficients are proportional to a 9-j symbol and can easily be evaluated¹. The DESB model qualitatively explained certain aspects of the observations such as the population in the $\text{He}({}^3\text{P}^o)$ channels and the lack of population in the $\text{He}(1sns {}^3\text{S}^e)$ Rydberg states (Petrunin et al., 2003).

The detailed evaluation of the l distribution $P(l)$ in triply excited states including the appropriate symmetry is quite involved, and the reader is referred to the work of Madsen and Mølmer (2003) for details. Figures 5.3 and 5.4 show examples where the symmetric rotor predictions for the l distributions are compared with the predictions from equation (5.24). In general, different l distributions are obtained for each LS term. In the limit of high n where the effect of antisymmetrization is expected to be small, the symmetric rotor probability may be expressed as

$$P(l) = P_d(l)F(L, M_I, l), \quad (5.25)$$

which is a product of the distribution given by Drukarev and a factor $F(L, M_I, l)$ which depends on the weighted rotational average of the Wigner function $\mathcal{D}_{00}^l(\omega)$,

¹For example, using the CERNLIB Program Library, <http://wwwinfo.cern.ch/asd/cernlib/>

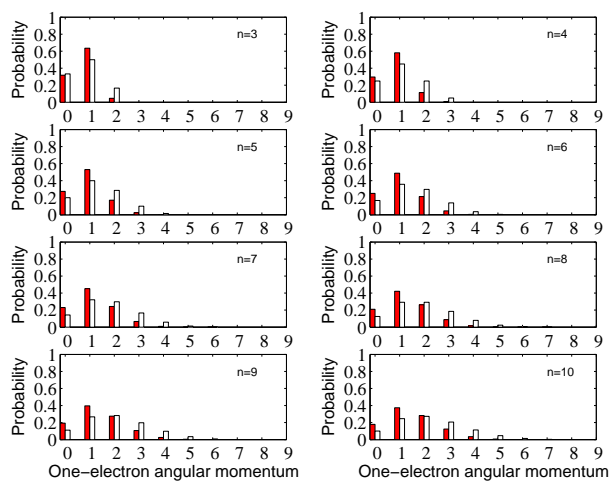


Figure 5.3: l distribution for intrashell $|M_I| = 0$, $4P^e$ states in $n = 3, 4, 5, \dots, 10$ manifolds. Filled columns are symmetric rotor results. Open columns are the probabilities from equation (5.24). The latter are symmetry (L, S, π) independent, and consequently the same in figures 5.3 and 5.4.

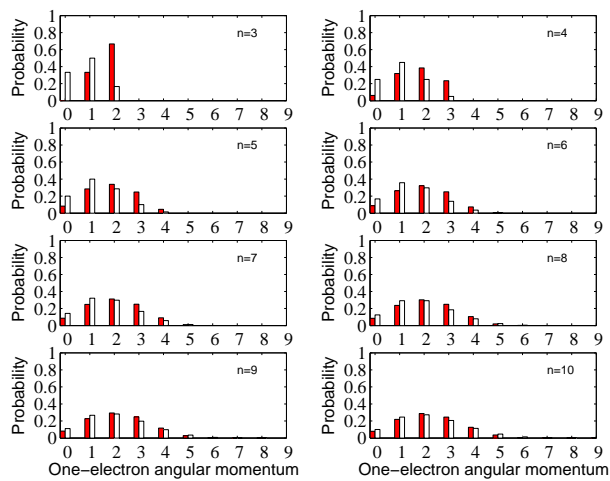


Figure 5.4: As figure 5.3 but for intrashell $|M_I| = 1$, $2G^o$ states.

Table 5.3: Energies of $n = 2$ intrashell states according to L and T values, $E(L, T)$. Energies are from Chung and Gou (1995).

$E(1, 1)$ [au]	$E(1, 0)$ [au]	$E(2, 2)$ [au]	$E(2, 1)$ [au]
-2.2502755	-2.2393792	-2.1581752	-2.0790325

multiplied by overlap functions between Stark states oriented along different directions. Based on the explicit form of the factor $F(L, M_I, l)$ and the plotted data in figures 5.3 and 5.4, Madsen and Mølmer (2003) concluded that for high n the enforcement of rotational symmetry (specific L) leads to a correction but not to an altogether different distribution than suggested by Drukarev. For the lower n -values the Hilbert space may be so small that certain l values are forbidden due to symmetry as, for example, in the $n = 3$ case in figure 5.4.

5.3.4 Rotational structure in the spectrum of triply excited states?

The formalism which was employed for the derivation of equation (5.25) will be discussed below and it was extensively used by Madsen and Mølmer (2001*b*, 2002) in their analysis of energy spectra. The question considered was whether one could or could not expect rotational structure in the spectra of triply excited states once the latter had been properly classified. The fact that the coplanar equilateral triangle geometry is similar to that of an oblate symmetric top molecule did inspire a search for rotorlike structure in triply excited states (Morishita et al., 1998). Also the identification of rotorlike structure in the energy spectra of doubly excited atoms (Kellman and Herrick, 1978) was a motivating reason. The spectrum of an oblate symmetric top is of the form of equation (5.7) with $T = |M_I|$, I the moment of inertia and L the angular momentum.

Vaeck and Hansen (1992) presented a quantitative analysis of the energy spectra of lithiumlike N^{4+} calculated by a configuration interaction approach and grouped the states according to the scheme developed by Lin and co-workers (Watanabe and Lin, 1987; Bao et al., 1997; Morishita and Lin, 2001*b*). From a close examination of the ordering and the distance of the levels, it was concluded that “there is no evidence of specific prolate or oblate structure”. Although there is no quantitative justification of such structure, the mere fact that, for example, all 64 triply excited states within the $n = 3$ manifold (except two states) follow qualitatively the classification and ordering suggested by the normal modes model (section 5.2) and the symmetric rotor model (section 5.3.2), suggests that the triply excited states share correlation patterns isomorphic to those of symmetric top molecules.

Madsen and Mølmer (2002) analyzed the benchmark calculations by Chung and Gou (1995) of the $n = 2$ intrashell states, using the labelling of Watanabe and Lin (1987). Denoting the energy $E(L, T)$, table 5.3 lists the energies of relevance. The three energy differences, $E(L, T) - E(L', T')$ where either $L \neq L'$ or $T \neq T'$ were calculated and the pertaining values of the moments of inertia

Table 5.4: Energy difference between states with isomorphic correlation patterns and associated values of the moment of inertia from equation (5.7).

(L, T)	(L', T')	$E(L, T) - E(L', T')$ [au]	I [au]
(1,0)	(1,1)	0.0108963	45.89
(2,1)	(1,1)	0.171243	23.36
(2,1)	(2,2)	0.0791427	18.95

determined. Table 5.4 shows the energy differences and the assigned values of the moment of inertia. Clearly, a variation from ~ 19 to ~ 46 in I proves to be insufficient ground to conclude that the spectrum is that of a rigid rotor.

Apart from these fluctuations of the rotational constant, also the mean radii indicate that the atomic system is too small to account for even the smallest value of I in table 5.4. This is seen by relating the moment of inertia to the distance of the electrons to the nucleus by $I = 3\langle r^2 \rangle$, requiring root-mean-square values of r between $2.5 a_0$ and $4.85 a_0$. For a hydrogenic system with $Z = 3$, the root-mean-square radius of a 2s electron from the center is $2.16 a_0$ and the root-mean-square radius of the maximally polarized Stark state is only $2 a_0$.

Finally, the rigid rotor model gives the wrong scaling of the energies. The moment of inertia scales with r^2 . Consequently, the energies should scale as Z^2 according to (5.7). For the intrashell case considered here, however, energies scale linearly with Z since

$$E_{nLM_I} = \frac{\langle \psi_{R,M_I}^{LMSM_S} | H | \psi_{R,M_I}^{LMSM_S} \rangle}{\langle \psi_{R,M_I}^{LMSM_S} | \psi_{R,M_I}^{LMSM_S} \rangle}, \quad (5.26)$$

leads to

$$E_{nLM_I} = 3E_N + ZE_{nLM_I}^{\text{corr}}, \quad (5.27)$$

since matrix elements of $1/r_i$ and $1/r_{ij}$ scale linearly with Z . Here E_n is the Bohr energy in the n shell for charge Z .

The preceding discussion has shown that the picture of the three electrons oriented around the nucleus with an angle of $2\pi/3$ radians between them is the correct one for a class of triply excited states. But the discussion also showed that the relating rigid body picture is misleading when it comes to quantitative predictions of the energy levels. This problem was analyzed formally by Madsen and Mølmer (2002) by an extension of the work by Peierls and Yoccoz (1957). In short, the symmetric rotor is written as $|\Psi_{R,M_I}^{LM,SMS}\rangle = \mathcal{N} \int d\omega \mathcal{D}_{MM_I}^L(\omega)^* |\Phi_R\rangle_\omega$ with $|\phi_R\rangle = \mathcal{A} [|\Psi_R, \chi_{M_S}^S\rangle]$, and this ansatz is used to calculate the expectation energy of the Hamiltonian (4.2). As detailed by Madsen and Mølmer (2001b, 2002), the energy is

$$E = \frac{\int \int d\omega d\omega' \mathcal{D}_{MM_I}^L(\omega)^* \mathcal{D}_{MM_I}^L(\omega') h(\Omega)}{\int \int d\omega d\omega' \mathcal{D}_{MM_I}^L(\omega)^* \mathcal{D}_{MM_I}^L(\omega') n(\Omega)}, \quad (5.28)$$

with

$$h(\Omega) = {}_{\omega'} \langle \Phi_R | H | \Phi_R \rangle_{\omega}, \quad (5.29)$$

$$n(\Omega) = {}_{\omega'} \langle \Phi_R | \Phi_R \rangle_{\omega}, \quad (5.30)$$

and where Ω is the resultant of first applying the rotation operator $\hat{D}(\omega)$ and then the operator $\hat{D}^+(\omega')$. The overlaps of equations (5.29) and (5.30) are expanded in the complete set of Wigner rotation matrices.

$$h(\Omega) = \sum_{l,m,m'} h_{m,m'}^l \mathcal{D}_{mm'}^l(\Omega), \quad (5.31)$$

$$n(\Omega) = \sum_{l,m,m'} n_{m,m'}^l \mathcal{D}_{mm'}^l(\Omega), \quad (5.32)$$

with coefficients defined by

$$k_{mm'}^l = \frac{2l+1}{8\pi} \int d\Omega k(\Omega), \mathcal{D}_{mm'}^l(\Omega)^* \quad (5.33)$$

for $k(\Omega) = h(\Omega), n(\Omega)$. The energy (5.28) may then be expressed directly in terms of the expansion coefficients

$$E = \frac{h_{MM_I}^L}{n_{MM_I}^L}. \quad (5.34)$$

The point now is that *if* the state $|\Phi_R\rangle$ were very anisotropic, as it would be for a quasirigid body, the overlaps of equations (5.29) and (5.30) would vanish for small values of Ω in the calculation of the $h_{MM_I}^L$ and $n_{MM_I}^L$ in (5.33). In such a case the $\mathcal{D}_{MM_I}^L(\Omega)$ function could be Taylor expanded, and indeed if this is done consistently to second order in the Euler angles Ω , one obtains the energy

$$E = E_0 + B_y L(L+1) - (B_y - 2B_z) M_I^2 \quad (5.35)$$

with a constant term E_0 and rotational constants B_y and B_z . Equation (5.35) has exactly the form of the spectrum of the symmetric top given in equation (5.7). Nevertheless, there are some important differences in the physics. For classical rigid rotors the rotational energy is purely kinetic. For the ‘‘quantum rotor’’ a rotational spectrum shows up irrespective of the nature of the Hamiltonian, as long as a symmetry broken ansatz is a valid approximation for the physical state $|\Psi_{R,M_I}^{LM,SM_s}\rangle$, *and* the overlap functions fall off sufficiently fast. The reason why no rotational spectrum is observed in the case of triply excited states is precisely that the overlap functions $h(\Omega)$ and $n(\Omega)$ do not fall off sufficiently fast to justify the Taylor expansion needed.

Chapter VI

Conclusions and outlook

Following the first photoabsorption experiment on triply excited resonances (Kiernan et al., 1994) a lot of effort has been put into the detailed investigation of the layers of structure in these systems. Here, recent work has been reviewed and some main results have been presented.

Experiments were discussed in chapter 3. Both the electron-scattering and the photoabsorption approach were considered. In view of the latest developments, special focus was put on the latter. The photoion and photoelectron measurement techniques were compared with respect to accuracy and information. As pointed out by Hansen and Verbockhaven (2002) experiments measuring angle resolved photoelectron spectra allow a more detailed comparison with theory. As such, more angle resolved studies would be highly desirable for future calibration of theoretical techniques.

Following the overview of experimental results, different theoretical approaches were discussed. The theories may be divided into two main categories. Firstly, there are the various calculational techniques aiming at an *ab initio* prediction of energy levels, widths and ionization spectra (chapter 4). Secondly, there are the models which are concerned with obtaining more physical insight into the correlated motion of triply excited states in terms of normal modes, classification schemes and wave functions (chapter 5). The methods reviewed in chapter 4 have been extensively applied to lithium. Here the *R*-matrix approach is outstanding for the calculation of photoelectron cross-sections and in a broader perspective, the detailed experiments on lithium provide data that can be used to test and develop the *R*-matrix codes which may then be applied with even greater confidence in, for example, the OPACITY project. The saddle-point method is a very accurate method, but it is well-suited only for the calculations of a few states. Results obtained by the saddle-point method have served as benchmarks for other theoretical calculations.

The other methods discussed in chapter 4 were the truncated diagonalization method and the *B*-splines approach. These methods are good at providing data on a lot of states and at giving predictions for extended Rydberg series. One great advantage of the *B*-spline method is that it operates with a fully nu-

merical basis. This means, for example, that the effective potentials describing the particle–particle interactions may be easily changed without adding to the complexity of the calculation. Also discussed in that part of this work was the investigations of the signatures of introducing a laser which could induce transitions directly among the triply excited states. This seems to be an interesting proposal for future experimental work as such studies would (i) provide data on the laser dipole coupling between the highly correlated states and (ii) allow a controlled investigation of various symmetries (L , S , π eigenstates) which cannot be reached by photon excitation from the lithium ground state. Also work relating to the line shape in photoexcitation of multiply excited states was discussed. Finally, it was described how information of the autoionization process of triply excited Rydberg states can be derived from the study of their doubly excited limits.

In the chapter on theoretical models (chapter 5), the work on identification of normal modes of the correlated three–electron motion and the visualization and classification of triply excited states was reviewed. Also the construction of an analytical ansatz for some triply excited states was discussed. These investigations supplement each other and suggest an ordering of states after an intrinsic quantum number $T = |M_I|$ which is the projection of the angular momentum operator on the body fixed axis perpendicular to the plane spanned by the three electrons. Also these models explain qualitatively the ordering of states within a given T –manifold. It is noteworthy that these models, in agreement with *ab initio* calculations, predict increasing energy with increasing angular momentum quantum number. Just the opposite of the behaviour in singly–excited configurations (Hund’s rule).

Besides the future prospects discussed above, there is every reason to believe that advances in bright coherent radiation sources will stimulate the field further. Synchrotron based facilities as the advanced light source in Berkeley is becoming increasingly intense. Other interesting developments are the large–scale intense free–electron laser projects — the TESLA project in Hamburg and the linac Coherent Light Source at Stanford. The TESLA test facility has begun operation in the far–ultraviolet regime and recently a study on the interaction of intense soft X–rays with atom clusters was reported (Wabnitz et al., 2002). The clusters absorbed energy much more effectively than anticipated on the grounds of existing models, and thus the question of absorption of light by such small objects will have to be reexamined. The study of three–electron atoms subject to an intense free–electron laser beam is an interesting possibility for the future.

Chapter VII

Dansk resumé

I denne afhandling beskrives teori og eksperimenter for lithium og lithium-lignende ioner i tilfælde, hvor alle tre elektroner har hovedkvantetal større end eller lig to. Disse tilstande kaldes tripelexciterede tilstande eller "hule" atomer. I energispektret ligger tilstandene over tærsklen for dobbelt-ionisation. De lavestliggende tripelexciterede tilstande i lithium ligger cirka 140 eV over grundtilstanden. De tripelexciterede tilstande er diskrete tilstande i kontinuetsområdet og ud over energipositionen er de karakteriseret ved en henfaldsbredde som følge af autoionisation fra Coulombfrastødningen mellem elektronerne. Elektronerne i disse tilstande er meget afhængige af hinanden – de er stærkt korrelerede. Det betyder, at sædvanlige middelfeltsmetoder er utilstrækkelige og en stor del af dette arbejde handler om at udvikle alternative teoretiske metoder, som giver en tilfredsstillende beskrivelse af elektron-elektron korrelationen. Det er fremskridt i de eksperimentelle teknikker og specielt i udviklingen af intense synkrotronstrålingskilder, som har sat skub i de seneste års teoretiske udvikling.

I kapitel 1 gives en kort introduktion til emnet og der relateres til to-elektron problemet. Man forstår nu dette problem forholdvis godt og i fremtiden vil mange af udfordringerne ligge i at opnå en større indsigt i det fundamentale 4-legeme Coulombproblem, hvor tre elektroner bevæger sig omkring atomkernen.

I kapitel 2 beskrives en simpel teori for excitation og henfald af autoioniserende tilstande. Her introduceres energier og henfaldsbredder og den typiske signatur af en autoioniserende tilstand, den såkaldte Fanoprofil, udledes.

Herefter følger i kapitel 3 en gennemgang af de forskellige eksperimenter, der er foretaget med henblik på at studere tripelexciterede tilstande. Først gennemgås resultater fra kollisionseksperimenter og dernæst studeres de nyere fotoexcitationseksperimenter og der gives en sammenlignende diskussion af kollision- og foton eksperimenterne. I fotoexcitationseksperimenterne har man, som funktion af de indkomne fotoners energi, dels målt, hvor mange fotoner, der absorberes (fotoabsorption), hvor mange ioner, der bliver produceret (photoion) og endelig har man målt de elektroner, der frigives til kontinuetsområdet, når fotonerne ioniserer atomerne (fotoelektron).

I kapitel 4 beskrives forskellige teoretiske metoder til beregning af energier

og henfaldsbreder af de tripelexciterede tilstande. Specielt omtales R -matrix, saddelpunkts- og diagonaliseringsmetoden. R -matrix metoden er meget generel og god til at forudsige fotoionisationstværsnit, mens saddelpunktsmetoden er meget nøjagtig, men den er bedst egnet til at studere nogle få specifikke tilstande med henblik på beregning af energier og henfaldsbreder. Diagonaliseringsmetoden, eventuelt i kombination med numeriske B -spline basisfunktioner, er mere fleksibel end saddelpunktsmetoden. Med en enkelt diagonalisering kan man beregne mange tilstande til en præcision, der kan sammenlignes med, hvad der kan opnås med saddelpunktsmetoden. Endvidere diskuteres den hypersfæriske metode, som tager udgangspunkt i et sæt af kollektive koordinater og er specielt velegnet til at få indblik i elektronernes korrelerede bevægelse.

I kapitel 4 er det afgørende bidrag fra forfatteren udvikling af en teoretisk metode, der kombinerer B -spline- og kompleksrotationsmetoden. Disse metoder er tidligere hver for sig blevet anvendt med stor succes til at studere atomare og molekylære systemer. Det enestående ved den nye metode er, at den bibeholder B -spline basissetets fleksibilitet og samtidig muliggør en forholdvis simpel udregning af henfaldsbreder v.h.a. kompleksrotation. Metoden er blevet anvendt til at studere laserinducerede koblinger mellem forskellige tripelexciterede tilstande med henblik på et systematisk og kontrolleret studie af de exciterede tilstande via dipoludvalgsregler. I dette afsnit er der endvidere bidrag, der fremmer forståelsen af lineprofiler. Endelig bliver det påpeget, at man kan lære meget om Rydbergtilstande i tripelexciterede tilstande ved at studere, hvordan tilstandene i deres dobbeltexciterede grænse i den tilhørende ion opfører sig. Relationen mellem tripelexciterede Rydbergtilstande og deres dobbeltexciterede grænse introducerer naturlige grænser for, hvilke værdier henfaldsbrederne for Rydbergtilstandene kan antage og muliggør simple beregninger.

I kapitel 5 diskuteres teoretiske modeller med det formål at opnå en bedre forståelse af elektronernes korrelerede bevægelse. Efter en kort introduktion beskrives modelberegninger, der viser, at de tre elektroner foretrækker at orientere sig i et plan i en ligesidet trekant i tilfælde, hvor de har samme hovedkvantetal. Hvis symmetrien af tilstanden tillader det, foretrækkes det endvidere, at kernen er i samme plan som elektronerne og i centrum af trekanten. Denne rumlige konfiguration minimerer Coulombfrastødningen mellem de tre elektroner og er derfor naturlig ud fra den klassiske fysiks love. Samtidig minder dette billede om den indbyrdes orientering af de individuelle atomer i symmetriske top molekyler. Med udgangspunkt i dette quasimolekylære billede beskrives, hvordan de tre elektroners bevægelse kan karakteriseres v.h.a. molekylære egen-svingninger og i den forbindelse introduceres et approksimativt kvantetal, der giver projektionen af impulsmomentet vinkelret på elektronplanet i det elektron- og kernefikserede koordinatsystem. Kapitel 5 afsluttes med en beskrivelse af et andet af forfatterens hovedbidrag. Det diskuteres, hvordan en kvantemekanisk analytisk model, der er konstrueret v.h.a. et geometrisk billede af de tre elektroner i en ligesidet trekant, beskriver elektron-elektron korrelationerne meget præcist. Modellen giver gode forudsigelser for konfigurationsblanding og den giver det samme approksimative kvantetal, som blev udledt i den molekylære

model. Endvidere er det muligt med modellen at forudsige de enkelte elektroners impulsmomentfordeling og ikke mindst løser modellen et udestående problem vedrørende rotationelle strukturer i spektret.

Bibliography

- Agentoft M, Andersen T and Chung K T 1984 *J. Phys. B: At. Mol. Phys.* **17**, L433.
- Aguilar J and Combes J M 1971 *Commun. Math. Phys.* **22**, 269.
- Ahmed M and Lipsky L 1975 *Phys. Rev. A* **12**, 1176.
- Azuma Y, Hasegawa S, Koike F, Kutluk G, Nagata T, Shigemasa E, Yagishita A and Sellin I A 1995 *Phys. Rev. Lett.* **74**, 3768.
- Azuma Y, Koike F, Cooper J W, Nagata T, Kutluk G, Shigemasa E, Wehlitz R and Sellin I A 1997 *Phys. Rev. Lett.* **79**, 2419.
- Bachau H 1996 *J. Phys. B: At. Mol. Opt. Phys.* **29**, 4365.
- Bachau H, Cormier E, Decleva P, Hansen J E and Martín F 2001 *Rep. Prog. Phys.* **64**, 1815.
- Balslev E and Combes J M 1971 *Commun. Math. Phys.* **22**, 280.
- Bao C G 1992 *J. Phys. B: At. Mol. Opt. Phys.* **25**, 3725.
- Bao C G, Xie W F and Lin C D 1994 *J. Phys. B: At. Mol. Opt. Phys.* **27**, L193.
- Bao C G, Yang X and Lin C D 1997 *Phys. Rev. A* **55**, 4168.
- Berrington K and Nakazaki S 1998 *J. Phys. B: At. Mol. Opt. Phys.* **31**, 313.
- Bloch C 1957 *Nucl. Phys.* **4**, 503.
- Bohr N 1913 *Phil. Mag.* **26**, 1.
- Brandefelt N and Lindroth E 1999 *Phys. Rev. A* **59**, 2691.
- Brandefelt N and Lindroth E 2002 *Phys. Rev. A* **65**, 032503.
- Brink D M and Satchler G R 1975 *Angular Momentum* Clarendon Press, Oxford.
- Bruch R, Paul G, Andrä J and Lipsky L 1975 *Phys. Rev. A* **12**, 1808.
- Burgdörfer J 1983 *Z. Phys. A* **309**, 285.

- Burke P G and Berrington K A, eds 1993 *Atomic and Molecular Processes: an R-matrix approach* (Bristol: IOP Publishing).
- Burke P G and Taylor K T 1975 *J. Phys. B: At. Mol. Phys.* **8**, 2620.
- Buttle P J A 1967 *Phys. Rev.* **160**, 719.
- Chang T N and Kim Y S 1986 *Phys. Rev. A* **34**, 2609.
- Chung K T 1979 *Phys. Rev. A* **20**, 1743.
- Chung K T 1981 *Phys. Rev. A* **23**, 2957.
- Chung K T 1982 *Phys. Rev. A* **25**, 1596.
- Chung K T 1990 *Phys. Rev. A* **42**, 5726.
- Chung K T and Davis B F 1982 *Phys. Rev. A* **26**, 3278.
- Chung K T and Fang T K 2001 *Phys. Rev. A* **63**, 062716.
- Chung K T and Gou B C 1995 *Phys. Rev. A* **52**, 3669.
- Chung K T and Gou B C 1996 *Phys. Rev. A* **53**, 2186.
- Chung K T and Gou B C 1998 *Chin. Phys. Lett.* **15**, 332.
- Chung K T and Lin C D 1998 *At. Nuc. Data Tables* **69**, 101.
- Clark C W and Greene C H 1980 *Phys. Rev. A* **21**, 1786.
- Conneely M J and Lipsky L 2002 *Atomic Data and Nuclear Data Tables* **82**, 115.
- Conneely M J, Lipsky L and Russek A 1992 *Phys. Rev. A* **46**, 4012.
- Conneely M and Lipsky L 2000 *Phys. Rev. A* **61**, 032506.
- Cooper J W, Fano U and Prats F 1963 *Phys. Rev. Lett.* **10**, 518.
- Cubaynes D, Diehl S, Journel L, Rouvellou B, Bizau J M, Moussalami S A, Willeumier F J, Berrah N, VoKy L, Faucher P, Hibbert A, Blancard C, Kennedy E T, Morgan T J, Bozek J and Schlachter A S 1996 *Phys. Rev. Lett.* **77**, 2194.
- de Boor C 1978 *A Practical Guide to Splines* Springer, New York.
- Diehl S, Cubaynes D, Bizau J M, Journel L, Rouvellou B, Moussalami S A, Willeumier F J, Kennedy E T, Berrah N, Blancard C, Morgan T J, Bozek J, Schlachter A S, VoKy L, Faucher P and Hibbert A 1996 *Phys. Rev. Lett.* **76**, 3915.

- Diehl S, Cubaynes D, Chung K T, Wuilleumier F J, Kennedy E T, Bizau J M, Journal L, Blancard C, VoKy L, Faucher P, Hibbert A, Berrah N, Morgan T J, Bozek J and Schlachter A S 1997 *Phys. Rev. A* **56**, R1071.
- Diehl S, Cubaynes D, Kennedy E T, Wuilleumier F J, Bizau J M, Journal L, VoKy L, Faucher P, Hibbert A, Blancard C, Berrah N, Morgan T J, Bozek J and Schlachter A S 1997 *J. Phys. B: At. Mol. Opt. Phys.* **30**, L595.
- Diehl S, Cubaynes D, Wuilleumier F J, Bizau J M, Journal L, Kennedy E T, Blancard C, VoKy L, Faucher P, Hibbert A, Berrah N, Morgan T J, Bozek J and Schlachter A S 1997 *Phys. Rev. Lett.* **79**, 1241.
- Diehl S, Cubaynes D, Zhou H L, VoKy L, Wuilleumier F J, Kennedy E T, Bizau J M, Manson S T, Morgan T J, Blancard C, Berrah N and Bozek J 2000 *Phys. Rev. Lett.* **84**, 1677.
- Diehl S, Cubaynes D, Zhou H S, VoKy L, Wuilleumier F J, Kennedy E T, Bizau J M, Manson S T, Blancard C, Berrah N and Bozek J 2000 *J. Phys. B: At. Mol. Opt. Phys.* **33**, L487.
- Drukarev G F 1982 *Sov. Phys. -JETP* **56**, 532.
- Fang T K and Chung K T 2001 *Phys. Rev. A* **63**, 020702(R).
- Fano U 1961 *Phys. Rev.* **124**, 1866.
- Fano U 1974 *J. Phys. B: At. Mol. Phys.* **7**, L401.
- Fano U and Cooper J W 1965 *Phys. Rev. A* **137**, 1364.
- Feagin J M and Briggs J S 1986 *Phys. Rev. Lett.* **57**, 984.
- Feagin J M and Briggs J S 1988 *Phys. Rev. A* **37**, 4599.
- Fock V 1930 *Z. Physik* **61**, 126.
- Greene C H and Clark C W 1984 *Phys. Rev. A* **30**, 2161.
- Grujić P 1983 *J. Phys. B: At. Mol. Phys.* **16**, 2567.
- Grujić P 1999 *Eur. Phys. J. D.* **6**, 441.
- Hansen J E 1975 *J. Phys. B: At. Mol. Phys.* **8**, L403.
- Hansen J E and Verbockhaven G 2002 *J. Phys. B: At. Mol. Opt. Phys.* **35**, L265.
- Hansen J E and Verbockhaven G 2003. in preparation.
- Hartree D R 1928 *Proc. Cambridge Phil Soc.* **26**, 89.
- Heisenberg W 1925 *Z. Physik.* **33**, 879.

- Herrick D R 1983 *Adv. Chem. Phys.* **52**, 1.
- Herrick D R and Sinanoğlu O 1975 *Phys. Rev. A* **11**, 97.
- Herzberg G 1945 *Molecular Spectra and Molecular Structure, II Infrared and Raman Spectra of Polyatomic Molecules* (Princeton, New Jersey: Van Nostrand).
- Journel L, Cubaynes D, Bizau J M, Moussalami S A, Rouvellou B, Wuilleumier F J, VoKy L, Faucher P and Hibbert A 1996 *Phys. Rev. Lett.* **76**, 30.
- Junker B 1982 *Adv. At. Mol. Phys.* **18**, 207.
- Kellman M E and Herrick D R 1978 *J. Phys. B: At. Mol. Phys.* **11**, L755.
- Kennedy E T 2001 *Physica Scripta* **T95**, 32.
- Kiernan L M, Kennedy E T, Mosnier J P, Costello J T and Sonntag B F 1994 *Phys. Rev. Lett.* **72**, 2359.
- Kiernan L M, Lee M K, Sonntag B F, Sladeczek P, Zimmermann P, Kennedy E T, Mosnier J P and Costello J T 1995 *J. Phys. B: At. Mol. Opt. Phys.* **28**, L161.
- Kittel C 1963 *Quantum Theory of Solids* (New York: Wiley).
- Klar H and Schlecht W 1976 *J. Phys. B: At. Mol. Phys.* **9**, 1699.
- Komninos Y, Chryros M and Nicolaides C A 1988 *Phys. Rev. A* **38**, 3182.
- Kuchiev M Y and Ostrovsky V N 1998 *Phys. Rev. A* **58**, 321.
- Lambropoulos P and Zoller P 1981 *Phys. Rev. A* **24**, 379.
- Li J M, VoKy L, Qu Y Z, Yan J, Zhang P H, Zhou H L and Faucher P 1997 *Phys. Rev. A* **55**, 3239.
- Li J M, VoKy L, Yan J and Qu Y Z 1996 *Chin. Phys. Lett.* **13**, 902.
- Lin C D 1984 *Phys. Rev. A* **29**, 1019.
- Lin C D 1986 *Adv. At. Mol. Opt. Phys.* **22**, 77.
- Lin C D 1993 in C. D Lin, ed., 'Review of Fundamental Processes and Applications of Atoms and Ions' World Scientific, Singapore p. 357.
- Lipsky L and Russek A 1966 *Phys. Rev.* **142**, 59.
- Lisitsa V S and Yakovlenko S I 1974 *Sov. Phys. JETP* **39**, 975.
- Macek J 1968 *J. Phys. B: At. Mol. Phys.* **1**, 831.
- Madden R P and Codling K 1963 *Phys. Rev. Lett.* **10**, 516.

- Madsen L B 2001 *J. Phys. B: At. Mol. Opt. Phys.* **34**, 2137.
- Madsen L B 2002 *Phys. Rev. A* **65**, 053417.
- Madsen L B and Lambropoulos P 2001 *J. Phys. B: At. Mol. Opt. Phys.* **34**, 1855.
- Madsen L B and Mølmer K 2001a *Phys. Rev. Lett.* **87**, 133002.
- Madsen L B and Mølmer K 2001b *Phys. Rev. A* **64**, 060501(R).
- Madsen L B and Mølmer K 2002 *Phys. Rev. A* **65**, 022506.
- Madsen L B and Mølmer K 2003 *J. Phys. B: At. Mol. Opt. Phys.* **36**, 769.
- Madsen L B, Schlagheck P and Lambropoulos P 2000a *Phys. Rev. Lett.* **85**, 42.
- Madsen L B, Schlagheck P and Lambropoulos P 2000b *Phys. Rev. A* **62**, 062719.
- Mannervik S, Short R T, Sonnek D, Träbert E, Möller G, Lodwig V, Heckmann P H, Blanke J H and Brand K 1989 *Phys. Rev. A* **39**, 3964.
- Manson S T and Starace A F 1982 *Rev. Mod. Phys.* **54**, 389.
- Martinson I and Gaupp A 1974 *Phys. Rep.* **15**, 113.
- Mehlman G, Cooper J W and Saloman E B 1982 *Phys. Rev. A* **25**, 2113.
- Moiseyev N 1998 *Phys. Rep.* **302**, 211.
- Mølmer K and Taulbjerg K 1988 *J. Phys. B: At. Mol. Opt. Phys.* **21**, 1739.
- Morishita T, Li Y and Lin C D 1998 *Phys. Rev. A* **58**, 4214.
- Morishita T and Lin C D 1998 *Phys. Rev. A* **57**, 4268.
- Morishita T and Lin C D 1999 *Phys. Rev. A* **59**, 1835.
- Morishita T and Lin C D 2001a *J. Phys. B: At. Mol. Opt. Phys.* **34**, L105.
- Morishita T and Lin C D 2001b *Phys. Rev. A* **64**, 052502.
- Morishita T and Lin C D 2003 *Phys. Rev. A* **67**, 022511.
- Morishita T, Tolstikhin O I, Watanabe S, and Matsuzawa M 1997 *Phys. Rev. A* **56**, 3559.
- Müller A, Hofmann G, Weissbecker B, Stenke M, Tinschert K, Wagner M and Salzborn E 1989 *Phys. Rev. Lett.* **63**, 758.
- Nicolaidis C A and Beck D R 1977 *J. Chem. Phys.* **66**, 1982.
- Nicolaidis C A, Chrysos M and Komninos Y 1990 *Phys. Rev. A* **41**, R5244.
- Nicolaidis C A and Piangos N A 2001 *J. Phys. B: At. Mol. Opt. Phys.* **34**, 99.

- Nicolaides C A, Piangos N A and Komninos Y 1993 *Phys. Rev. A* **48**, 3578.
- Nikolopoulos L A A and Madsen L B 2003 *Comput. Phys. Commun.* **151**, 47.
- Ostrovsky V N 2001 *Phys. Rev. A* **64**, 022715.
- Peierls R E and Yoccoz J 1957 *Proc. Phys. Soc., London, Sect. A*) **70**, 381.
- Petrinin V V, Jacobsen M H, Madsen L B, Aseyev S A and Andersen T 2003 *Phys. Rev. Lett.* **90**, 013002.
- Piangos N A and Nicolaides C A 2001 *J. Phys. B: At. Mol. Opt. Phys.* **34**, L633.
- Quigley L and Berrington K 1996 *J. Phys. B: At. Mol. Opt. Phys.* **29**, 4529.
- Rau A R P 1984 *J. Phys. B: At. Mol. Phys.* **17**, L75.
- Rau A R P 1990 *Rep. Prog. Phys.* **53**, 181.
- Rødbro M, Bruch R and Bisgaard P 1979 *J. Phys. B: At. Mol. Phys.* **12**, 2413.
- Rost J M and Briggs J S 1991 *J. Phys. B: At. Mol. Phys.* **24**, 4293.
- Safronova U I and Senashenko V S 1978 *J. Phys. B: At. Mol. Phys.* **11**, 2623.
- Schiff L I 1955 *Quantum Mechanics* (Singapore: McGraw-Hill).
- Schrödinger E 1926 *Ann. Physik* **79**, 361.
- Seaton M J 1983 *Rep. Prog. Phys.* **46**, 167.
- Simons R L, Kelly H P and Bruch R 1979 *Phys. Rev. A* **19**, 682.
- Sinanoglu O and Herrick D R 1975 *Journ. Chem. Phys.* **62**, 886.
- Tanner G, Richter K and Rost J M 2000 *Rev. Mod. Phys.* **72**, 497.
- Themelis S I and Nicolaides C A 1995 *J. Phys. B: At. Mol. Opt. Phys.* **28**, L379.
- Vaeck N and Hansen J E 1992 *J. Phys. B: At. Mol. Opt. Phys.* **25**, 883.
- Verbockhaven G C 2000 Study of strongly correlated systems by means of *B*-splines PhD thesis University of Amsterdam, Van der Waals-Zeeman Institute.
- Verbockhaven G and Hansen J E 1999 *Phys. Scr.* **T80**, 476.
- Verbockhaven G and Hansen J E 2000a *Phys. Rev. Lett* **84**, 2810.
- Verbockhaven G and Hansen J E 2000b *Mol. Phys.* **98**, 1117.
- Verbockhaven G and Hansen J E 2001 *J. Phys. B: At. Mol. Opt. Phys.* **34**, 2337.

- VoKy L, Faucher P, Hibbert A, Li J M, Qu Y Z, Yan J, Chang J C and Bely-Dubau F 1998 *Phys. Rev. A* **57**, 1045.
- VoKy L, Faucher P, Zhou H L, Hibbert A, Qu Y Z, Li J M and Bely-Dubau F 1998 *Phys. Rev. A* **58**, 3688.
- Wabnitz H, Bittner L, de Castro A R B, Döhrmann R, Gürtler P, Laarmann T, Laasch W, Schultz J, Swiderski A, von Haefen K, Möller T, Faatz B, Fateev A, Feldhaus J, Gerth C, Hahn U, Saldin E, Schneidmiller E, Sytchev K, Tiedtke K, Treusch R and Yurkov M 2002 *Nature (London)* **420**, 482.
- Watanabe S, Dourneuf M L and Pelamourgues L 1982 *J. Phys. (Paris) Colloq.* **43**, C2-223.
- Watanabe S and Lin C D 1987 *Phys. Rev A* **36**, 511.
- Wehlitz R, Huang M T, Berrington K A, Nakazaki S and Azuma Y 1999 *Phys. Rev. A* **60**, R17.
- Winter H P and Aumayr F 1999 *J. Phys. B: At. Mol. Opt. Phys.* **32**, R39.
- Wuilleumier F J, Diehl S, Cubaynes D, Bizau J M and Kennedy E T 1998 *J. Electron Spectrosc.* **88**, 41.
- Wuilleumier J F 2000 *Physics Essays* **13**, 230.
- Wulfman C E 1973 *Chem. Phys. Lett.* **23**, 370.
- Yang X, Bao C G and Lin C D 1996a *Phys. Rev. Lett.* **76**, 3096.
- Yang X, Bao C G and Lin C D 1996b *Phys. Rev. A* **53**, 3934.
- Zatsarinny O and Fischer C F 2000 *J. Phys. B: At. Mol. Opt. Phys.* **33**, 313.
- Zhang Y and Chung K T 1998 *Phys. Rev. A* **58**, 1098.